

Strain-based Topology Optimization of a 2D Morphing Transitional Surface

Shawn Madison Parsons

Thesis submitted to the faculty of the Virginia Polytechnic Institute and State University in  
partial fulfillment of the requirements for the degree of

Master of Science

In

Aerospace Engineering

Michael K. Philen, Chair  
Robert A. Canfield  
Pradeep Raj  
Pablo A. Tarazaga

May 4, 2018  
Blacksburg, VA

Keywords: Morphing, Trailing Edge, Topology, Optimization

Copyright 2018, Shawn Madison Parsons

# Strain-based Topology Optimization of a 2D Morphing Transitional Surface

Shawn Madison Parsons

## ABSTRACT

Changing the wing shape and configuration of an aircraft can optimize performance for the wide variety of conditions experienced during a typical flight. While the idea of applying morphology, changing wing shape or geometry, is as old as aviation itself, back to the Wright Flyer, implementations of it have been slow to develop due to many associated challenges, such as overcoming materials and manufacturing limits. Designing morphing structures, as they are commonly referred to, requires a structure that can withstand the applied loads but also change shape. Smart materials can provide a potential solution, with shape changing capabilities, but also add the challenge of added weight and energy requirements for the actuation devices. One such morphing application that has not yet been extensively explored is creating a continuous trailing edge to eliminate discontinuities, or gaps, created by flight control actuation. Structural optimization is widely employed to design optimum structures for the applied load conditions and solve challenges such as these. Topology optimization is a widely used structural optimization technique that modifies the material layout to decrease the objective function, which is typically a function of the displacement. However, topology optimization has not been widely explored for morphing structures. Additionally, topology structures are often considered theoretical and impractical due to the complexity and irregular material layouts of many of the resultant optimum structures. A solution to this problem could be the growing trend of additive manufacturing. Additive manufacturing methods, such as 3D printing, has grown in popularity and has been used as a solution to producing theoretical structures with the ability to freely place material in any configuration. This provides to motivation to explore topology optimization for a morphing structure problem with the possibility to realize the structure with multi-material additive manufacturing. This work evaluates the implementation of several strain based objective functions in topology optimization and finds strain-based objective functions to be easily implementable and effective in place of strain energy minimization for standard benchmark problems in structural optimization. After verifying the use of strain as an objective function in topology optimization, the approach is applied to a 2D morphing problem design to simulate the problem of interest, an actuated flight control of a fixed-large displacement boundary condition problem. The resultant optimization and the suitability of topology optimization for designing morphing structures is discussed and found to be valid for linear, low shear, problems but future work will require non-linear analysis.

## Strain-based Topology Optimization of a 2D Morphing Transitional Surface

Shawn Madison Parsons

### **GENERAL AUDIENCE ABSTRACT**

Morphing aircraft offer many benefits. However, the design of stiff yet flexible structures still provides many obstacles to fully exploring and realizing morphing structures. Due to this, many morphing challenges remain open. Topology optimization is a type of structural optimization that optimizes the material layout of a structure based on imposed boundary conditions and load paths. This type of optimization is promising for solving morphing design challenges but many of the optimized structures are not suited for traditional manufacturing and material arrangements. Multi-material additive manufacturing is an emerging technology that can produce a single structure with many different materials integrated in custom geometries. This could be the solution to realizing topology optimized structures. Despite the rich amount of current research in morphing aircraft, many challenges still remain open and topology of morphing structures could provide the solution to these morphing challenges.

# ACKNOWLEDGEMENTS

I would like to thank first my advisor, Dr. Philen, for his guidance these past two years. He allowed me to be a part of an exciting lab filled, literally, with exciting projects and ideas. Thank you for helping me use my time wisely these two years and guiding my research to get to this point. My advisor and lab mates, Brady and Carson, have set a high standard for the quality of work produced in our lab group. I would like to thank Brady, who has since become Dr. Doepke and become a NASA engineer, for being my guide into Grad School when I first got here. I would like to thank Carson for engaging in my constant chatter and also being interested in airplanes, succulents, 3D Printing, and hot wings. My two years spent in the lab were filled with good role models, good conversation, and bang snaps.

I would like to thank my Department for allowing me to thrive here in the past two years. While many faculty impacted my time here, I would especially like to thank Dr. Raj and Dr. Artis. Being a Teaching Assistant to you two taught me more than I ever contributed to the courses I was able to assist you in. Dr. Raj is a model of professionalism and experience that I will consider myself fortunate if I achieve half as much of. Dr. Artis is a model of engagement both professionally and in his community. He knows literally everyone, and I aspire to be as well rooted in my community and well connected as he is.

I would like to thank my boyfriend, Kevin, for his continual support, both in the procurement of ice cream and his help in Matlab debugging. I couldn't have gotten to this point without you. Finally, I would like to thank my parents. They model hard work every day and have raised me to have the strength and integrity to successfully complete my education and enter the real world.

# TABLE OF CONTENTS

ABSTRACT.....	ii
GENERAL AUDIENCE ABSTRACT.....	iii
ACKNOWLEDGEMENTS.....	iv
TABLE OF CONTENTS.....	v
LIST OF FIGURES.....	viii
LIST OF TABLES.....	x
CHAPTER 1: INTRODUCTION AND LITERATURE REVIEW.....	1
1.1 History of Morphing Aircraft.....	3
1.2 Current Morphing Research.....	8
1.3 Morphing Aircraft Skins.....	10
1.4 Structural Optimization.....	12
1.5 Additive Manufacturing: A Solution for Design Challenges.....	13
1.6 Motivation.....	16
1.7 Thesis Overview.....	18
CHAPTER 2: FINITE ELEMENT ANALYSIS.....	19
2.1 Governing Global Equation.....	19
2.2 Element Stiffness Derivation.....	21
2.3 Mesh Generation.....	24
2.4 Global Assembly.....	25
2.5 Boundary Conditions and Solution.....	25
2.6 Stress and Strain.....	26
2.7 Matlab Implementation.....	27
2.8 Validation.....	28

CHAPTER 3: TOPOLOGY OPTIMIZATION .....	29
3.1 A 99 line topology optimization code written in Matlab .....	29
3.1.1 Numerical Derivation .....	29
3.1.2 General Matlab Overview .....	32
3.2 Strain Based Objective Function.....	34
3.2.1 Strain Objective Function Variations .....	36
3.2.2 Results of Strain Variation Implementation .....	39
3.3 Discussion of Results of Strain Variation Implementation.....	43
CHAPTER 4: PROBLEM OF INTEREST AND CORRESPONDING SOLUTION .....	44
4.1 Application of Strain Based Topology to Problem of Interest-Single Load Case .....	45
4.1.1 Strain Implementation Variance-Load Case 1 .....	46
4.1.2 Strain Implementation Variance-Load Case 3.....	50
4.1.3 Strain Implementation Variance-Load Case 4.....	53
4.1.4 Conclusions from Single Load Case Implementation .....	57
4.2 Volume Fraction Effect.....	58
4.3 Various Material Starting Configuration Effects .....	59
4.4 Varying Aspect Ratio Effect on Optimization Result.....	60
4.5 Application of Strain Based Topology to Problem of Interest-Multiple Load Case.....	63
4.5.1 Multi Load Optimization for X & Y Displacement Problem .....	63
4.5.2 Multi Load Optimization for Y Only Displacement Problem .....	66
4.5.3 Discussion of Multiple Load Case Implementation .....	67
4.6 Evaluation of Optimized Solutions for Various Load Cases .....	68
4.6.1 Results of Material Solutions Evaluation .....	68
4.6.2 Discussion of Material Solutions Evaluation.....	70
4.7 Comments on Strain Based Topology Optimization of Problem of Interest .....	71

CHAPTER 5: CONCLUSIONS AND FUTURE WORK.....	73
Thesis Overview and Summary of Conclusions.....	73
Future Work and Conclusion.....	74
BIBLIOGRAPHY .....	76
Appendix.....	82
Appendix A-Finite Element Code.....	82
Main FEM Code .....	82
Function: Element Shape Functions .....	85
Function: Element Stiffness.....	85
Function: Gauss Quadrature .....	86
FEM-Initial Processing and Mesh Generation.....	87
Appendix B-Topology Optimization .....	91
Single Load Case Topology Optimization.....	92
Multiple Load Case Topology Optimization .....	99

# LIST OF FIGURES

Figure 1 Clement Ader’s proposed morphing aircraft [1] .....	3
Figure 2 The Wright Flyer [1].....	4
Figure 3 High –lift trailing-edge flap configurations compared to a basic airfoil section [18] .	5
Figure 4 Variable Sweep Examples (a) (c) (left) P-1101 drawings, (b) (d) (right) Bell X-5 In Flight and on the ground [16] .....	6
Figure 5 Grumman F-14 Tomcat [24].....	7
Figure 6 FlexSys and AFRL Adaptive Compliant Trailing Edge [3] .....	9
Figure 7 NASA Variable Camber Continuous Trailing Edge Flap Concept [5] .....	9
Figure 8 Various Morphing Wing Skin Concepts [4].....	11
Figure 9 Topology Optimization of a Cantilevered Beam [4] .....	13
Figure 10 Working Principles of Additive Manufacturing Processes [64].....	15
Figure 11 Airplane with Flight Control [2].....	17
Figure 12 Detail A- Proposed Transitional Surface.....	17
Figure 13 General Steps and Simple Example of the Galerkin Method for FEM .....	20
Figure 14 Basic four-node rectangular element.....	21
Figure 15 Mesh Generation Example .....	25
Figure 16 Local to Global Stiffness Matrix Assembly .....	25
Figure 17 Example Boundary Condition Implementation and Solution.....	26
Figure 18 Matlab Implementation Finite Element Flowchart.....	27
Figure 19 FEM Validation Example .....	28
Figure 20 Topology Optimization Algorithm Flow Chart.....	32
Figure 21 MBB Beam .....	33
Figure 22 Low Element Count Topology Optimization of MBB Beam.....	33
Figure 23 Increasing Element Number Solution of MBB Beam .....	34
Figure 24 Gauss and Nodal Points .....	37
Figure 25 Benchmark Problem Material Layout Solutions for Various Strain Implementations .....	40

Figure 26 Strain Objective Function Effect on other Objective Functions.....	41
Figure 27 Benchmark Problem Objective Function Convergence .....	41
Figure 28 Average Strain Results for the Strain Objective Functions-MBB Problem .....	42
Figure 29 Defined Problem of Interest.....	45
Figure 30 Summary of Load Cases .....	46
Figure 31 Load Case 1 Material Layout Solutions for Various Strain Implementations.....	47
Figure 32 Strain Variation Effect on Objective Functions-Load Case 1 .....	47
Figure 33 Average Strains for the Strain Objective Functions - Load Case 1 .....	48
Figure 34 Strain Plots for Load Case 1 Optimization Result.....	49
Figure 35 Load Case 3- Material Layout Solutions for Various Strain Implementations .....	50
Figure 36 Strain Variation Effect on Objective Functions-Load Case 3 .....	51
Figure 37 Average Strains for the Strain Objective Functions - Load Case 3.....	51
Figure 38 Strain Plots for Load Case 3 Optimization Result.....	52
Figure 39 Load Case 4- Material Layout Solutions for Various Strain Implementations .....	54
Figure 40 Strain Variation Effect on Objective Functions-Load Case 4 .....	54
Figure 41 Average Strains for the Strain Objective Functions - Load Case 4.....	55
Figure 42 Strain Plots for Load Case 4 Optimization .....	56
Figure 43 Effect of Volume Fraction on Resultant Solution .....	59
Figure 44 Effect of Material Starting Configurations and Resultant Solution.....	60
Figure 45 Effect of Varying Aspect and Displacement Ratios on Resultant Solution .....	62
Figure 46 Material Solutions for Multi-Load Case Optimization.....	64
Figure 47 Average Strains for Multi-Load Optimization- Load Case 1 & 2 .....	64
Figure 48 Material Layout Solutions for Multiple Load Case Optimization.....	66
Figure 49 Average Strains for Multi-Load Optimization- Load Case 4 & 5 .....	67
Figure 50 Material Layouts being evaluated.....	68
Figure 51 Load Case 1 Strain Comparison .....	69
Figure 52 Load Case 2 Strain Comparison .....	69
Figure 53 Load Case 3 Strain Comparison .....	70
Figure 54 Load Case 4 Strain Comparison .....	70

# LIST OF TABLES

Table 1 Summary of Strain Based Objective Functions .....	36
---	----

# CHAPTER 1: INTRODUCTION AND LITERATURE REVIEW

Since the first flying machines of the early 20th century, aircraft designs have constantly evolved and improved. Many designers have been inspired by nature, particularly the way birds continuously adapt to their environment via different wing shapes and configurations. Changing the wing shape and configuration of an aircraft can optimize performance for the wide variety of conditions experienced during a typical flight [6]. While the idea of applying morphology, changing wing shape or geometry, is as old as aviation itself, back to the Wright Flyer, implementations of it have been slow to develop due to many associated challenges, such as overcoming materials and manufacturing limits. Designing morphing structures, as they are commonly referred to, requires a structure that can withstand the applied loads but also change shape [7]. Smart materials can provide a potential solution, with shape changing capabilities, but also add the challenge of added weight and energy requirements for the actuation devices. Despite challenges, morphing structures have been implemented and researched [8].

While a wide number of morphing applications have been successfully pursued, such as changing sweep, span, and camber, there are still many design spaces that have not yet been solved. [9] One such morphing application that has not been extensively explored is creating a continuous trailing edge to eliminate discontinuities, or gaps, created by flight control actuation. Continuous trailing edge concepts have been explored, such as the Flexsys and NASA/Boeing Designs concepts [10, 11]. However, both of these concepts employ new designs modifying the entire trailing edge. There exists opportunity to explore the design of transitional structures that could be implemented with a fixed trailing edge and traditional flight control systems.

Creation of such a solution will require the design of a structure both flexible and stiff, allowing for both shape change and robustness for handling aerodynamic loads. A solution to this problem could be the growing trend of additive manufacturing. Additive manufacturing methods, such as 3D printing, has grown in popularity and has been used as a solution to producing theoretical structures with the ability to freely place material in any configuration. Furthermore, multi-material additive manufacturing has grown in popularity with the ability to use several different materials to manufacture the structure in unique combinations [12]. These types of multi-material

structures are different from typical multi-material structures, such as composites, due to the manufacturing design freedom of combining the materials in any configuration [13].

This advancement in manufacturing can accelerate the realization of optimized theoretical structures. Many optimized structures, such as topology optimization, are optimized as a mesh of elements with different volume fractions which can be interpreted as either different volume fill fractions of the same material or as different materials with fractions of a specified Young's Modulus. Traditional manufacturing makes the realization of optimized structures difficult but additive manufacturing can overcome these limitations [14]. If combined, the motivation of overcoming design and manufacturing challenges of morphing structures and the pursuit of additive manufacturing in realization of optimized structures could result in a solution that expands the design space for aerospace challenges and is the focus of this thesis.

## 1.1 History of Morphing Aircraft

The idea of morphing was envisioned even before heavier than air flight was achieved. In 1890, Clement Ader proposed an idea for a morphing aircraft capable of wing extension, as seen below in Figure 1. While his idea had little technical merit and never successfully flew, it shows the early recognition of morphing as tool to expand flight capabilities. Ader saw morphing as a warfare advantage “The airplanes of the line will be somewhere between scouts and bombers. They will benefit as much as possible from the speed of the former and the strength and the armament of the latter.” [15] The Wright Brothers became the first to successfully demonstrate wing warping in flight with the Wright Flyer in 1903. From their patent description describing wing warping “... owing to the varying conditions to be met there are numerous disturbing forces which tend to shift the machine from the position which it should occupy to obtain the desired results. It is the chief object of our invention to provide means for remedying this difficulty...” it can be seen that changing wing shape and geometry was recognized early on as a solution for active control.



**Figure 1 Clement Ader’s proposed morphing aircraft [1]**

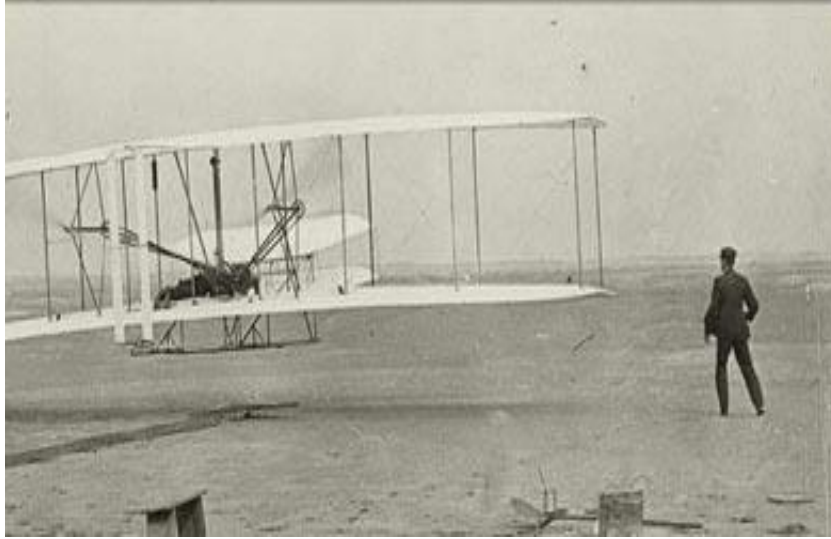


**Figure 2 The Wright Flyer [1]**

The onset of World War I shortly after the birth of aviation led to further advancements in aviation and in morphing by replacing wing warping with articulated control surfaces. Following World War I, the first major conflict to widely employ aviation use, biplanes were in favor, due higher strength to weight ratios and greater maneuverability than monoplanes of that time. During this time, wing leading edge and trailing edge flap and slat research took off. This development would eventually benefit lift enhancement on high speed monoplanes while biplanes fell out favour as higher aircraft speeds became possible with propulsion advancements. Flaps, or high lift devices, alter wing camber to safely allow aircraft to fly lower speeds, particularly during takeoff and landing. Three well known examples of this technology development for leading edge flaps occurred between 1917 and 1919 alone, with Gustav Lachmann from Germany[16], Mader for the Junkers Aircraft Manufacturing Company also in Germany, and Frederick Handley in Britain[17]. Orville Wright, continuing the Wright Brothers aviation legacy, developed the split flap with J.M.H. Jacobs in 1920. The Fowler Flap, still used in modern aircraft was awarded its patent to Harlan D. Fowler in 1928, seen below in Figure 3 [18].

While these articulated control surfaces were the most widely implemented and practical developments from this time period, some inventors of this time period had early insight into the possibilities of compliant, variable camber designs. In 1920, Parker patented a device for a compliant morphing wing arrangement. This design was intended to be implemented on the upper wing of a biplane as a means of increasing lift on low-speed biplanes without flap deflection [19]. Another patent in 1933 by Vincent Burnelli proposed a means of changing both wing area and

camber [20]. While it is evident that interest in these morphing technologies went back to the 1920s, material and manufacturing limitations kept this idea from being pursued until the late 1970s.

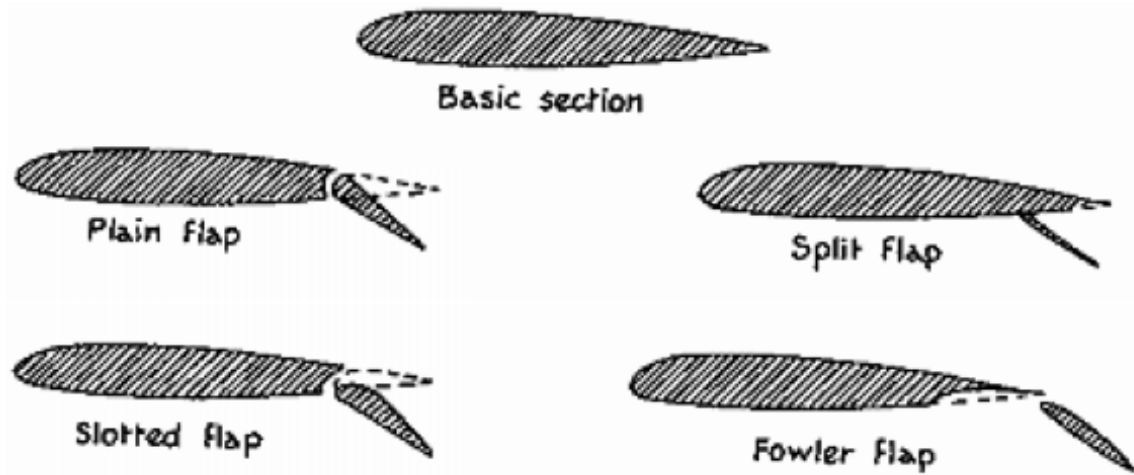


**Figure 3 High –lift trailing-edge flap configurations compared to a basic airfoil section [18]**

Another example of early aircraft morphing technology is the concept of “wing swing” or variable sweep. Advantages of variable sweep are improved longitudinal and directional stability. Early patents, that were never realized, date back as far as 1904 with Clement Ader and his hydrofoil vehicle design [15], and Edson Gallaudet in 1914 with the concept of sweeping back wingtips for banking improvement [21]. However, most credit Alexander Lippisch of Germany, who filed for a patent in 1924, as being the founder of the modern variable sweep concept [22]. While he lost interest in pursuing the concept, Woldemar Voigt, of the German aircraft company Messerschmitt, took the concept and developed it into plans for the P-1101. The P-1101 was built in 1944 but never flown and changed sweep on the ground, not in flight. Following World War II, engineers at the American aircraft company, Bell Aircraft Corporation, used the P-1101 plans as the basis for the Bell X-5. The Bell X-5 took flight in 1951 and was the first aircraft capable of changing sweep in flight. Both aircraft can be seen in Figure 4 below [16].

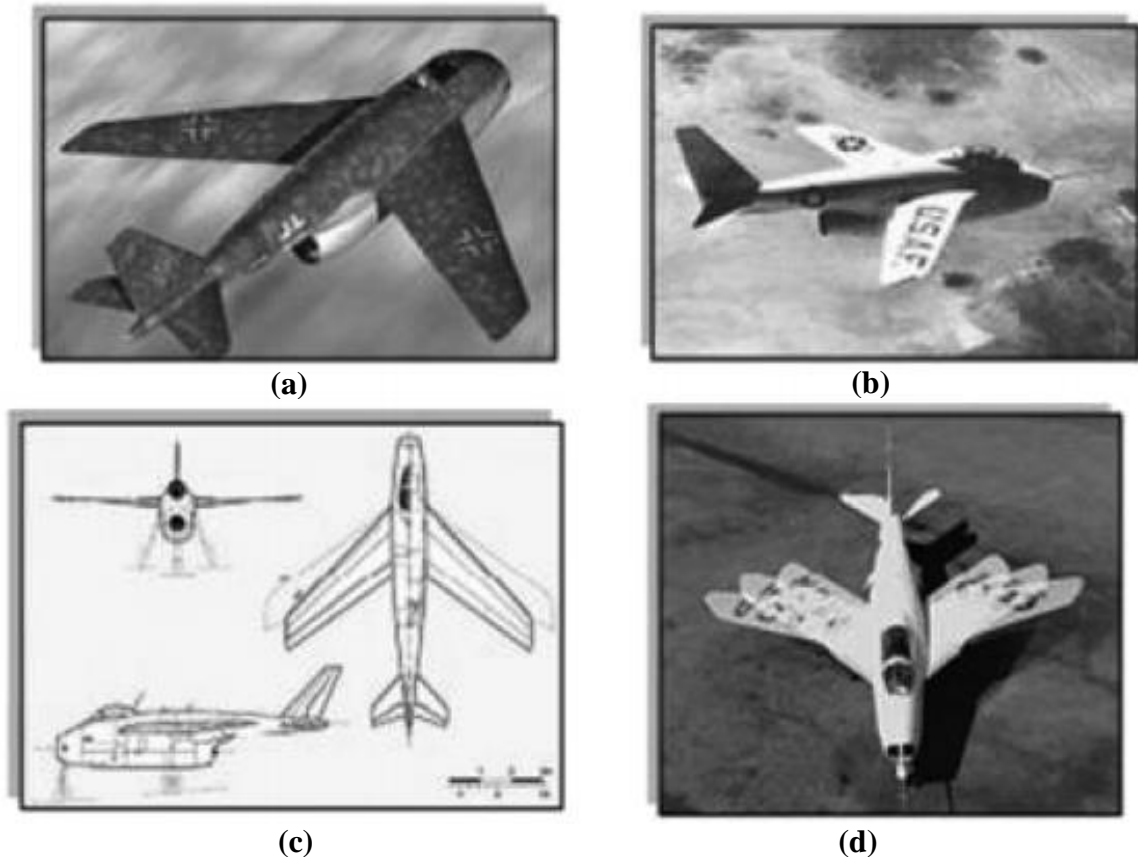


**Figure 4 Variable Sweep Examples (a) (c) (left) P-1101 drawings, (b) (d) (right) Bell X-5 In Flight and on the ground [16]**

The Bell X-5 was an excellent example of the changing requirements and capabilities for military aircraft that arose in the 1950s and 1960s, many of which drove the interest in pursuing morphing capabilities. The Cold War, following World War II, shifted missions towards long range and long endurance flights, supersonic speed, and ability to takeoff from short runways, such as aircraft carriers. These mission requirements led to renewed interest in morphing technologies during that time period and the following decades. The Grumman F-14 Tomcat introduced in the 1970s is the most successful variable sweep American military aircraft and a direct result of the mission requirements and an example of the morphing development that resulted. Another example is the US Air Force Mission Adaptive Wing project from the 1970s that renewed interest in realizing compliant variable camber. The program modified an F-111 and successfully demonstrated improved flight performance from the morphing characteristics [23].



**Figure 5 Grumman F-14 Tomcat [24]**

The following decades proved that morphing aircraft interest has multidisciplinary appeal. In the 1990s, the NASA Aircraft Morphing Program emerged whose title many consider the origin of the phrase "morphing aircraft." The main focus of the program was to advance research in the related areas of smart materials, adaptive structures, and microflow control and produce technologies focused on multipoint efficiency [25]. The U.S. Department of Defense during this period also pursued smart material and smart structures research with the many DARPA (Defense Advanced Research Projects Agency) projects aimed at advancing smart structure applications. The DARPA Smart Rotor Program and Smart Wing Programs started in the 1990s and aimed at aerodynamic control for noise and vibration reduction. These programs opened the way for the DARPA Morphing Aircraft Structures Program which began in 2002 and ended in 2007. The objective of the program is an answer to the Defense Technology Objective released in 2003: "Morphing is a capability to provide superior and/or new vehicle system performance ... while in flight by tailoring the vehicle's state ... to adapt to the external operational environment and

multivariable mission roles ... in the context of this DTO, morphing aircraft are multirole aircraft that change their external shape substantially to adapt to a changing mission environment during flight" [26]. The program was an unmanned aerial vehicle demonstration of the new system capabilities and advantages that morphing has to offer. Programs like these provide a rich legacy and motivation for current morphing research.

## **1.2 Current Morphing Research**

Increasing performance demands and mission capabilities for the current and future aviation industry have ensured that morphing aircraft research remains today. Current advances in not only materials and manufacturing, a historic challenge in morphing, but also computational capabilities are empowering current morphing research. Many research initiatives are arising to use these advances. The NOVEMO, NOvel Air VEhicle Configurations, project in 2014 was focused on investigating novel air vehicle configurations with new lifting concepts and finding morphing wing solutions to improve cost-effectiveness in air transport [27]. The Air Force Research Lab (AFRL) started a collaboration with FlexSys in 1998 to develop a wing leading and trailing edge morphing solutions. In 2015, the collaborators, with the help of the NASA Armstrong Flight Research Center, successfully completed initial flight tests of a new morphing wing technology, the Adaptive Compliant Trailing Edge (ACTE), seen in Figure 6. The ACTE flight control surface has the potential to reduce aircraft structural weight and reduce noise [3]. This is not the only industry and research partnership to explore this concept, Boeing and NASA partnered in 2012 to advance work on the Variable Camber Continuous Trailing Edge Flap (VCCTEF) concept, seen in Figure 7. The VCCTEF concept is an adaptive aeroelastic wing shaping control technology aimed at improving both vehicle control and performance [5].



**Figure 6 FlexSys and AFRL Adaptive Compliant Trailing Edge [3]**

Beyond large research collaborations, the academic community is contributing largely to morphing concepts, both large and small. A concept for a telescopic morphing aircraft with flight controls driven by asymmetrical morphing was published in 2017 [28]. Also in 2017, the design of morphing unmanned aerial vehicles was proposed using a combination of smart materials, piezoelectrics and shape memory alloys [29]. Other recent smart material concepts include the use of pressurized honeycomb for a morphing wingtip structure [30], variable stiffness fluidic flexible matrix composite tubes for morphing wing structures [31], and corrugated structures for artificial wing flapping [32].

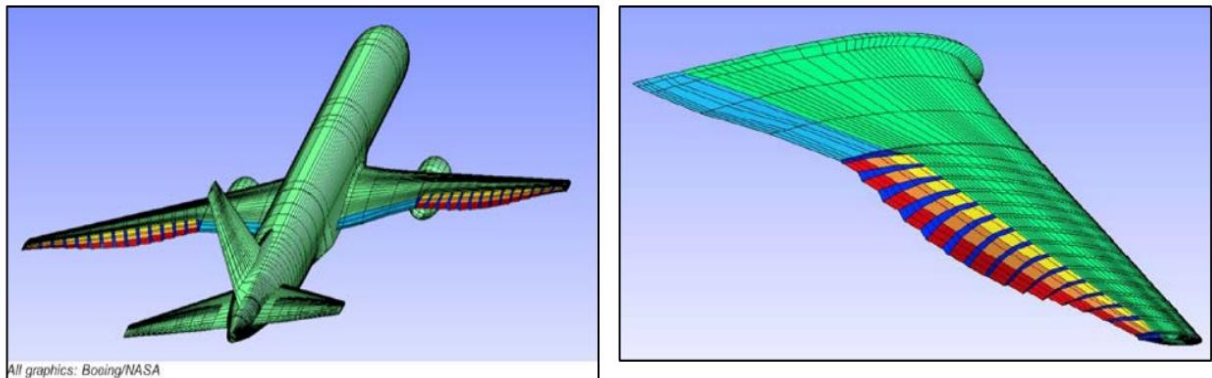


**Figure 7 NASA Variable Camber Continuous Trailing Edge Flap Concept [5]**

### 1.3 Morphing Aircraft Skins

One area critical to the realization of proposed morphing structures is the design of a skin stiff enough to withstand aerodynamic loads and sufficiently flexible for large deformations. Additionally, an added complexity to wing skin structures is the need for a seamless aerodynamic surface. Most of today's aircraft use metallic materials or composite materials for aircraft skins, which provide high strength but not flexibility. Solutions to this challenge include both active and passive designs. Active designs adapt to the environment and loads via actuation. Passive designs have their fixed topology, geometry, and material defined during the design process.

Current active morphing skin work includes the use of artificial muscles or smart material actuation, such as Shape Memory Alloys. Examples of artificial muscle implementation are embedded pressurized pneumatic muscle fibers (PMF) for variable stiffness skin regulated by changing the internal air pressure [33, 34] and the use of carbon fiber and polyurethane elastomeric composite actuated by rubber muscle actuators (RMAs) [35]. Examples of smart material actuation use include the use SMAs (Shape Memory Alloys) to actuate flexible skins [36] and as actuators for structural members as a means of using SMAs as active rods used as truss elements in a compliant rib structure [37].

Passive morphing skins fall generally into two categories: mesostructures and elastomeric structures. Mesostructures, where "meso" means intermediate, define structures that contain structural elements located between other structural elements. Elastomeric designs are structures reliant on the elastomeric properties of the material itself. Popular mesostructures for morphing concepts include the use of honeycomb and corrugated structures. Honeycomb, and other cellular structures, have the properties of low in plane stiffness and high aerodynamic pressures when sandwiched between flexible face sheets. The use of these structures as compliant morphing skins has been extensively investigated [38-40] with investigations into both honeycomb and cellular geometry and material choice for achieving the large deflection and high material strain requirements of the morphing problem. Experimental honeycomb design of zero Poisson's ratio have been explored as a way of eliminating the transverse strain. Similarly, corrugated structures have been explored as the internal mesostructure due to their high stiffness in the longitudinal direction and compliance in the transverse direction [41-48]. Elastomeric morphing skin solutions have, to date, largely focused on design of woven fiber materials for in plane compliance and out

of plane stiffness [49-52]. Figure 8 shows several morphing wing skin concepts including both honeycomb and corrugated designs.

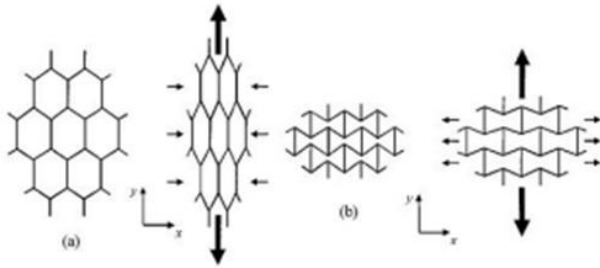


Figure 4. (a) Positive Poisson's ratio honeycomb and (b) auxetic honeycomb<sup>(83)</sup>.

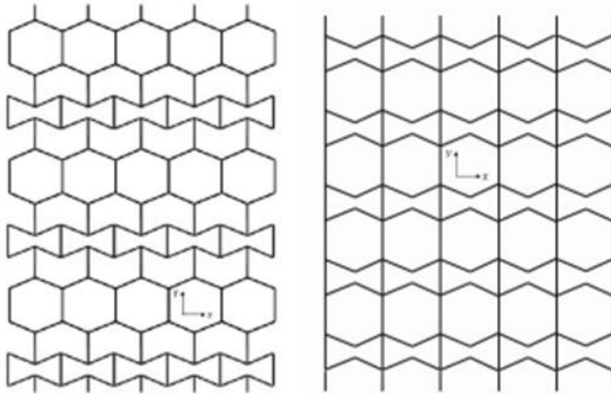


Figure 5. Hybrid (left) and accordion (right) cellular structures<sup>(83)</sup>.

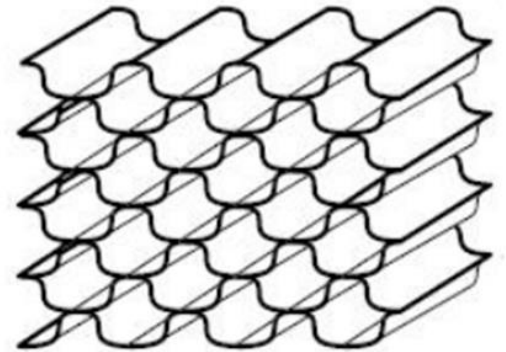


Figure 6. Schematic of Flex-Core® by Hexcel<sup>(89)</sup>.

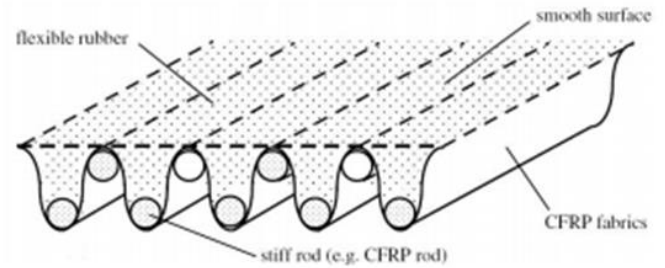


Figure 10. Reinforced corrugated structure with elastomeric surface<sup>(78)</sup>.

### Figure 8 Various Morphing Wing Skin Concepts [4]

## 1.4 Structural Optimization

To meet the morphing aircraft design challenges, design optimization techniques have been applied to the morphing structure problem. Sizing, shape, and topology optimization are the most widely practiced structural optimization types. Size optimization changes and finds the optimum size of structural members. Shape optimization modifies predetermined structural boundaries. Topology optimization gives the optimum material layout for the applied loading paths and boundary conditions. While shape and size optimization are widely explored for aircraft design [53-59], topology optimization is the most promising for morphing structures with the key advantage of no specified starting configuration.

Topology optimization is referred to as layout optimization and has been widely explored in both research and practical applications [61]. Topology can be considered an intermediate binary problem where discretized elements take on the form of values from 0 to 1 representing the material layout and density fill of the individual elements. Figure 9 represents this concept where the initial layout and optimized solution can be seen. The optimized solution has elements in black, representing a material layout value of 1 or full volume, white, with an empty or 0 value, and gray elements that have values in between. The optimized layout of the elements in topology is solved with various approaches. One method is the homogenous approach which assumes a continuous linearly elastic structure filled with infinite microscale voids that can be optimized to find the optimum porosity of the medium. High porosity results in a high material layout in that area and conversely low porosity results in less material layout in the specified discretized area. Another method is the Evolutionary Structural Optimization (ESO) which slowly removes inefficient material from a continuum and the resulting solution is the evolved optimum solution. SIMP, Solid Isotropic Material Penalization, exponentially penalizes the discretized material density variables such that smaller material densities are exponentially driven towards 0, or no material, and higher densities are exponentially driven towards 1, or full material [62].

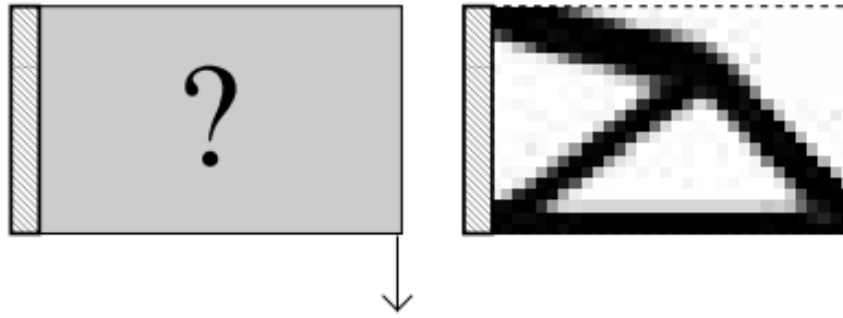


**Figure 9 Topology Optimization of a Cantilevered Beam [4]**

## **1.5 Additive Manufacturing: A Solution for Design Challenges**

Additive manufacturing is today a popular and widely implemented method for rapid prototyping. The ASTM F42 Technical Committee defines additive manufacturing (AM) as the “process of joining materials to make objects from three-dimensional (3D) model data, usually layer upon layer, as opposed to subtractive manufacturing methodologies” [63]. This modern type of manufacturing allows for complex and custom geometries and material layouts. Additive manufacturing is currently being implemented in both industry and research areas. Many industries are exploring and utilizing this technology ranging from aerospace to biomedical to many other fields [64]. Many well-known companies are acknowledging the value of additive manufacturing and creating new business units enable its development. Boeing has announced plans to develop and additive manufacturing standard and General Electric has recently created GE Additive, to name a few [65, 66].

Since its origins almost 30 years ago, additive manufacturing has involved to include many different types of processes and material types, as can be seen in Figure 10. The most common types of additive manufacturing are stereolithography (SLA), Direct Metal Laser Sintering (DMLS), Fusion Deposition Modeling (FDM), PolyJet, and Laminated Object Manufacturing (LOM). Due to the rich variety of additive manufacturing processes, there exists a wide variety of materials for additive manufacturing processes. Ranging from flexible elastomers, such as flexible elastomer filament for FDM Printer, NinjaFlex<sup>®</sup>, to high strength space rated materials, Ultem<sup>®</sup>, additive manufacturing offers a large design space for producing structures. With the popularity

of additive manufacturing, new materials, from high strength to conductive inks, are being created and entering the market every year.

Beyond the wide range of materials available, and becoming available, the exciting aspect of additive manufacturing lies in the potential for multi-functional material, or a single structure with many different materials integrated in custom geometries. While very few additive manufacturing process systems are able to achieve this, many are excited about the potential it offers. The aerospace sector in particular is interested in this development for the potential for custom high strength, light weight parts and overcome design challenges associated with aviation and spacecraft. Recently, the Air Force Research Lab has announced its work in creating platforms to allow this. "The stabilized processes have freed engineers from design limitations they previously ran up against with traditional manufacturing." Other aerospace companies are interested in this recent development as a solution to previous design challenges."Applying additive manufacturing to create multi-functional materials would allow engineers to tailor design requirements and optimize the parts' material accordingly", said Zach Loftus, an additive manufacturing fellow at Lockheed [67].

**Table 1** Working principles of AM processes

State of starting material	Process	Material preparation	Layer creation technique	Phase change	Typical materials	Applications
Liquid	SLA	Liquid resin in a vat	Laser scanning/light projection	Photopoly-merization	UV curable resin, ceramic suspension	Prototypes, casting patterns, soft tooling
	MJM	Liquid polymer in jet	Ink-jet printing	Cooling & photopoly-merization	UV curable acrylic plastic, wax	Prototypes, casting patterns
	RFP	Liquid droplet in nozzle	On-demand droplet deposition	Solidification by freezing	Water	Prototypes, casting patterns
Filament/ Paste	FDM	Filament melted in nozzle	Continuous extrusion and deposition	Solidification by cooling	Thermoplastics, waxes	Prototypes, casting patterns
	Robocasting	Paste in nozzle	Continuous extrusion	–	Ceramic paste	Functional parts
	FEF	Paste in nozzle	Continuous extrusion	Solidification by freezing	Ceramic paste	Functional parts
Powder	SLS	Powder in bed	Laser scanning	Partial melting	Thermoplastics, waxes, metal powder, ceramic powder	Prototypes, casting patterns, metal and ceramic preforms (to be sintered and infiltrated)
	SLM	Powder in bed	Laser scanning	Full melting	Metal	Tooling, functional parts
	EBM	Powder in bed	Electron beam scanning	Full melting	Metal	Tooling, functional parts
	LMD	Powder injection through nozzle	On-demand powder injection and melted by laser	Full melting	Metal	Tooling, metal part repair, functional parts
	3DP	Powder in bed	Drop-on-demand binder printing	–	Polymer, Metal, ceramic, other powders	Prototypes, casting shells, tooling
Solid sheet	LOM	Laser cutting	Feeding and binding of sheets with adhesives	–	Paper, plastic, metal	Prototypes, casting models

**Figure 10 Working Principles of Additive Manufacturing Processes [64]**

## 1.6 Motivation

Morphing aircraft offer many benefits. However, the design challenge of stiff yet flexible structures still provides many obstacles to a large set of morphing applications. Current morphing skin structures further the challenge for morphing actuation and fall into two categories: active or passive. Active materials typically have high energy or weight requirements for actuation. Passive solutions may require larger structures than feasible for many areas, such as honeycomb structures. Elastomeric woven fiber materials may require less volume but still may not meet the design requirements of large displacement yet robust to aerodynamic buckling. Due to these limitations, many morphing challenges remain open for research exploration.

Topology optimization is promising for aerospace design and morphing structures with the freedom to converge to unconstrained optimum designs. However, the disadvantage is that traditionally many of the resulting optimum designs are not suited for traditional manufacturing and material arrangements. Due to this, topology optimization of large displacement morphing structures has not been explored. However, multi-material additive manufacturing could provide the solution to the realization of topology optimized structures. Multi-material additive manufacturing can be a solution to the wide range of material properties needed and challenging integration of many materials created by topology solutions.

One of the morphing challenges open for exploration is that of a trailing edge transitional surface. When a flight control is actuated, a gap is created from the edge of the fixed trailing edge to the edge of the deflected flight control. These gaps are known to be significant sources of drag and aeroacoustic noise. (\*Insert appropriate reference). Elimination of this gap could provide aeroacoustics and aerodynamic benefits. Since a surface eliminating this gap would need to be able to transition from states at rest to deflected, or morph, this is a good candidate for a morphing solution. However, the trailing edge of a typical aircraft is narrow, limiting material volume and integration of actuation, driving the solution towards an elastomeric passive surface. Due to these challenges, solutions in this area are slow to emerge. Once a solution that has emerged has been provided by Flexsys, seen in Figure 6. It is of interest to see if designing a structure to meet this morphing challenge looks like the Flexsys corrugated solution. Topology optimization of a surface for this area could provide a structure that would meet the lightweight, limited material and

integration design drivers. Multi-material additive manufacturing could provide the realization of the proposed solution.

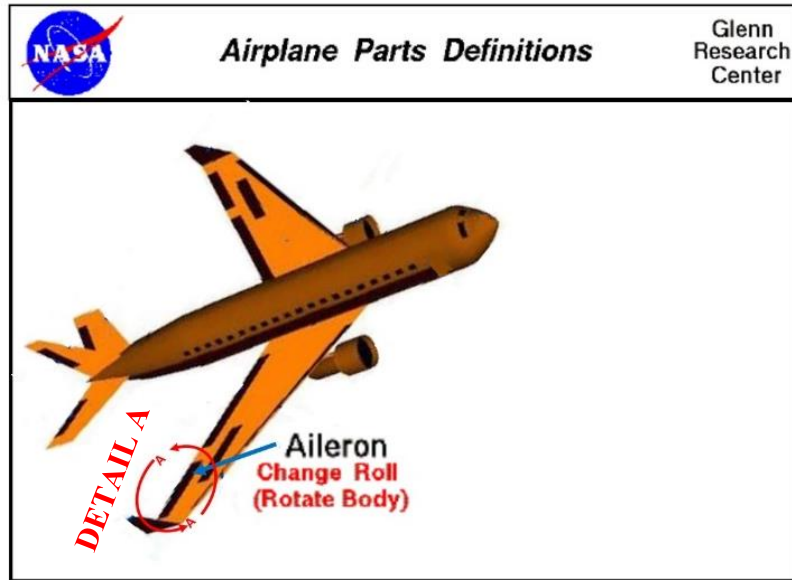


Figure 11 Airplane with Flight Control [2]

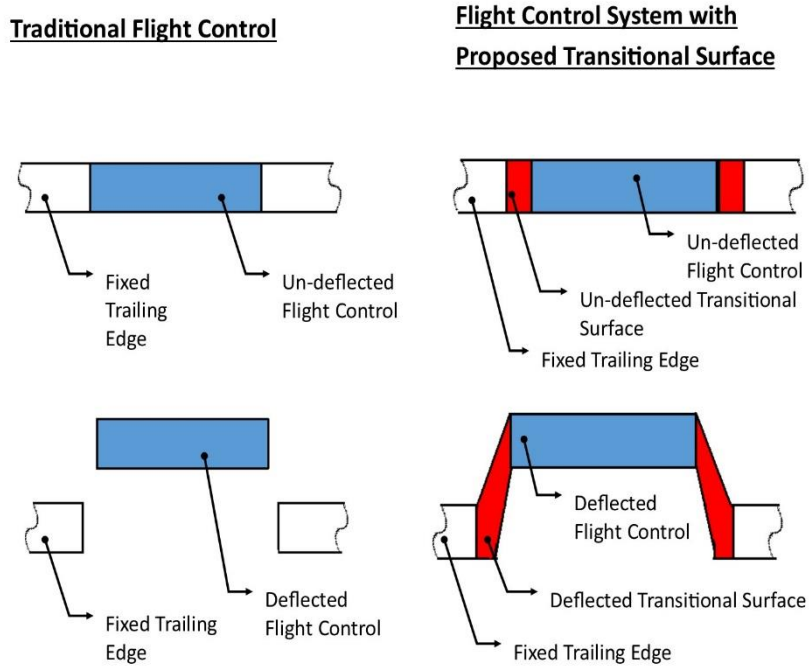


Figure 12 Detail A- Proposed Transitional Surface

## 1.7 Thesis Overview

This focus of this chapter, Chapter 1, is to present the reader with the current challenges associated with morphing aircraft and the promising technologies and techniques that can be used to overcome these design challenges. The motivation to demonstrate this possibility of these techniques to expand the design space for aerospace applications is the driving force behind this research.

Chapter 2 details the derivation, implementation and validation of the Finite Element Analysis code used.

Chapter 3 details the selection of the Topology Optimization Code as the 99 Line Topology Code by O. Sigmund [68]. Chapter 3 also details the implementation of the author's finite element code and validation of that implementation in the topology program. The chapter also demonstrates the change of the optimization problem from displacement minimization to strain minimization.

Chapter 4 applies the previously demonstrated optimization algorithm to the modeled problem of interest, a 2-D surface with transverse and axial displacement boundary conditions. The solution is shown as well as examining several other material distributions for the problem of interest and isolated transverse and axial displacement boundary condition cases for both single load cases and multiple load case optimization.

Chapter 5 is the final chapter that discusses the conclusions and future work.

## CHAPTER 2: FINITE ELEMENT ANALYSIS

Topology optimization utilizes finite element analysis (FEA) to determine displacement, strain, and other required variables. A finite element analysis program was developed and coded via Matlab for integration into the topology optimization code. The finite element program utilizes four noded rectangular elements. This chapter derives the finite element analysis implemented and details validation of the program against benchmark problems. Section 2.1 describes the derivation of the governing equation for the finite element method. Section 2.2 derives the element stiffness formulation. Section 2.3 details the creation of the mesh based on input parameters. Section 2.4 describes the global assembly process. Section 2.5 details the incorporation of the boundary conditions and the solution to the finite element problem. Section 2.6 gives the stress and strain calculations. Section 2.7 details the Matlab implementation of the finite element program. Section 2.8 validates the finite element analysis using benchmark problems.

### 2.1 Governing Global Equation

The finite element method is a numerical method for solving engineering and physics problems. In the method, a continuum structure is broken into very small discretized elements, called finite elements, which are interconnected at points, or nodes. Once discretized, an influence coefficient matrix, which for the finite element problem is the stiffness matrix, is computed and the basic equation of the finite element method is solved.

Mathematically speaking, the finite element method is based on three main ideas. The partial differential (PDE) of the governing equation of motion is written in weak or variational form. The Galerkin method is applied to convert the continuous problem into one that can be solved on a finite-dimensional subspace. A basis of piecewise polynomials is chosen for the finite-dimensional subspace to determine the shape functions for the element where the shape functions approximate values across the element based on the discrete values obtained at the nodes. Figure 13 gives an overview of the general steps of the finite element approximation techniques.

<u>General Steps</u>	<u>Simple Example of the Displacement of an Elastic Rod</u>
1. Begin with the Governing PDE ('Strong Form')	$m \frac{\partial^2 u(x,t)}{\partial t^2} - EA \frac{\partial^2 u(x,t)}{\partial x^2} = 0$
2. Apply Trial Function	$\int_0^L v(x) \left[ m \frac{\partial^2 u(x,t)}{\partial t^2} - EA \frac{\partial^2 u(x,t)}{\partial x^2} \right] dx = 0$
3. Integrate by Parts	$= \int_0^L \left( m \frac{\partial^2 u(x,t)}{\partial t^2} v(x) \right) dx - \left( EA \frac{\partial u(x,t)}{\partial x} v(x) \right) \Big _0^L + \int_0^L \left( EA \frac{\partial u(x,t)}{\partial x} \frac{\partial v(x,t)}{\partial x} \right) dx = 0$
4. Apply Boundary Conditions to get "Weak Form"	$v(0) = 0 \quad v(L) = 0$ $= \int_0^L \left( m \frac{\partial^2 u(x,t)}{\partial t^2} v(x) + EA \frac{\partial u(x,t)}{\partial x} \frac{\partial v(x,t)}{\partial x} \right) dx = 0$
5. Apply Galerkin technique to approximate the functions at the discrete points	$u(x,t) = \sum_{i=1}^n \phi_i(x) q_i(t)$ $v(x) = \sum_{j=1}^n \phi_j(x)$
6. Substitution of Galerkin approximations yields approximate solutions	$\left( \int_0^L m \sum_{i=1}^n \sum_{j=1}^n \phi_i(x) \phi_j(x) dx \right) \dot{q}_i + \left( \int_0^L EA \sum_{i=1}^n \sum_{j=1}^n \phi_{i,x}(x) \phi_{j,x}(x) dx \right) q_i = 0$ <div style="border: 1px solid red; padding: 5px; width: fit-content; margin-left: auto; margin-right: auto;"> <p style="font-size: small; margin: 0;">Analogous to the Governing FEM Equation</p> <p style="margin: 0;"><math>[K]\{u\} = \{f\}</math></p> </div>

**Figure 13 General Steps and Simple Example of the Galerkin Method for FEM**

Based on these concepts, the resultant governing equation for the global system of the finite element method is given as:

$$[K]\{u\} = \{F\} \tag{0.1}$$

where  $[K]$  represents the stiffness matrix.  $\{u\}$  represents the displacement vector containing an x displacement ( $u$ ) and y displacement ( $v$ ) for each node in the global system, and  $\{F\}$  represents the force vector containing an x force and y force for each node in the global system.

## 2.2 Element Stiffness Derivation

The element type chosen is the basic four-node rectangular element with nodal degrees of freedom shown in Figure 14.

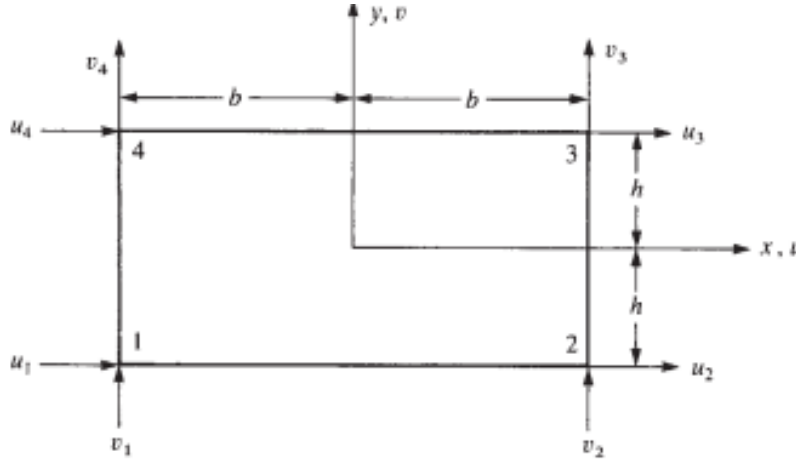


**Figure 14 Basic four-node rectangular element**

For elements with constant thickness, the element stiffness matrix,  $[k]$ , can be written as:

$$[k] = \iint_A [B]^T [D] [B] dx dy \quad (0.2)$$

$$[k_{el}] = \begin{bmatrix} k_{11} & k_{12} & k_{13} & k_{14} & k_{15} & k_{16} & k_{17} & k_{18} \\ k_{21} & k_{22} & k_{23} & k_{24} & k_{25} & k_{26} & k_{27} & k_{28} \\ k_{31} & k_{32} & k_{33} & k_{34} & k_{35} & k_{36} & k_{37} & k_{38} \\ k_{41} & k_{42} & k_{43} & k_{44} & k_{45} & k_{46} & k_{47} & k_{48} \\ k_{51} & k_{52} & k_{53} & k_{54} & k_{55} & k_{56} & k_{57} & k_{58} \\ k_{61} & k_{62} & k_{63} & k_{64} & k_{65} & k_{66} & k_{67} & k_{68} \\ k_{71} & k_{72} & k_{73} & k_{74} & k_{75} & k_{76} & k_{77} & k_{78} \\ k_{81} & k_{82} & k_{83} & k_{84} & k_{85} & k_{86} & k_{87} & k_{88} \end{bmatrix} \quad (0.3)$$

$$[D] = \frac{E}{1-\nu^2} \begin{pmatrix} 1 & \nu & 0 \\ \nu & 1 & 0 \\ 0 & 0 & \frac{1-\nu}{2} \end{pmatrix} \quad (0.4)$$

$$[B] = \begin{bmatrix} \frac{dN_1(x,y)}{dx} & 0 & \frac{dN_2(x,y)}{dx} & 0 & \frac{dN_3(x,y)}{dx} & 0 & \frac{dN_4(x,y)}{dx} & 0 \\ 0 & \frac{dN_1(x,y)}{dy} & 0 & \frac{dN_2(x,y)}{dy} & 0 & \frac{dN_3(x,y)}{dy} & 0 & \frac{dN_4(x,y)}{dy} \\ \frac{dN_1(x,y)}{dx} & \frac{dN_1(x,y)}{dy} & \frac{dN_2(x,y)}{dx} & \frac{dN_2(x,y)}{dy} & \frac{dN_3(x,y)}{dx} & \frac{dN_3(x,y)}{dy} & \frac{dN_4(x,y)}{dx} & \frac{dN_4(x,y)}{dy} \end{bmatrix} \quad (0.5)$$

$$\begin{aligned} N_1 &= \frac{(x-x_2)(y-y_4)}{(x_1-x_2)(y_1-y_4)} \\ N_2 &= \frac{(x-x_1)(y-y_3)}{(x_2-x_1)(y_2-y_3)} \\ N_3 &= \frac{(x-x_4)(y-y_2)}{(x_3-x_4)(y_3-y_2)} \\ N_4 &= \frac{(x-x_3)(y-y_1)}{(x_4-x_3)(y_4-y_1)} \end{aligned} \quad (0.6)$$

where  $D$  is the stress-strain material matrix,  $E$  is Young's Modulus and  $\nu$  is Poisson's ratio. This work assumes plane stress and uses the stress-strain material matrix for plane stress given in Eq. (0.4).  $B$  is the strain-displacement matrix for the element. Strains are defined in terms of the derivatives of the displacements with respect to the  $x$  and  $y$  coordinates, and the strain-displacement matrix is represented by the interpolating shape functions ( $N_1, N_2, N_3, N_4$ ) with respect to the  $x$  and  $y$  coordinates.

For the selected 4 node rectangular element, the element stiffness matrix is of the size [8X8] and given in Eq. (0.3). The shape functions,  $(N_1, N_2, N_3, N_4)$ , of  $x$  and  $y$  for the 4-node rectangular element are derived using Lagrange Polynomial technique, given in Eq. (2.7).

$$\begin{aligned}
 U(x, y) &= \sum_{j=1}^{n=4} U_j \prod_{k=1; k \neq j}^{n=4} \frac{(x - x_k)}{(x_j - x_k)} \prod_{l=1; l \neq k}^{n=4} \frac{(y - y_l)}{(y_j - y_l)} = \\
 &\frac{(x - x_2)(y - y_4)}{(x_1 - x_2)(y_1 - y_4)} U(x_1, y_1) + \frac{(x - x_1)(y - y_3)}{(x_2 - x_1)(y_2 - y_3)} U(x_2, y_2) + \dots \\
 &\frac{(x - x_4)(y - y_2)}{(x_3 - x_4)(y_3 - y_2)} U(x_3, y_3) + \frac{(x - x_3)(y - y_1)}{(x_4 - x_3)(y_4 - y_1)} U(x_4, y_4) \quad (0.7) \\
 &= N_1 U(x_1, y_1) + N_2 U(x_2, y_2) + N_3 U(x_3, y_3) + N_4 U(x_4, y_4)
 \end{aligned}$$

where the desired degrees of freedom,  $u$  ( $x$  displacement) and  $v$  ( $y$  displacement), can be written as:

$$u(x, y) = \begin{bmatrix} N_1 & 0 & N_2 & 0 & N_3 & 0 & N_4 & 0 \end{bmatrix} \left\{ \begin{array}{l} u_1(t) \\ v_1(t) \\ u_2(t) \\ v_2(t) \\ u_3(t) \\ v_3(t) \\ u_4(t) \\ v_4(t) \end{array} \right\} \quad (0.8)$$

$$v(x, y) = \begin{bmatrix} 0 & N_1 & 0 & N_2 & 0 & N_3 & 0 & N_4 \end{bmatrix} \left\{ \begin{array}{l} u_1(t) \\ v_1(t) \\ u_2(t) \\ v_2(t) \\ u_3(t) \\ v_3(t) \\ u_4(t) \\ v_4(t) \end{array} \right\} \quad (0.9)$$

## 2.3 Mesh Generation

An essential part of the finite element analysis solution is the discretization of the structure into a grid of finite elements. The grid significantly impacts rate of convergence, solution accuracy, and computation time. Several factors that go into the grid quality include grid density, type of element, and variability of size and shape throughout structure. Due to the desired simplicity of the model, the mesh generation for this work operations under the following assumptions:

- Uniform Structured Grid
- 2D
- 4 Noded Rectangular Elements
- Location in Global System Represented by Node Numbers
- Input Structure is of Rectangular Shape

The mesh generation implemented in this work takes the dimensions of the structure, divides the structure into elements, and creates a Local to Global Mapping Matrix (*LtGMM*) to assign local values into the global position. Figure 15 demonstrates an example discretization of a structure into elements and the forming of the local to global mapping matrix.

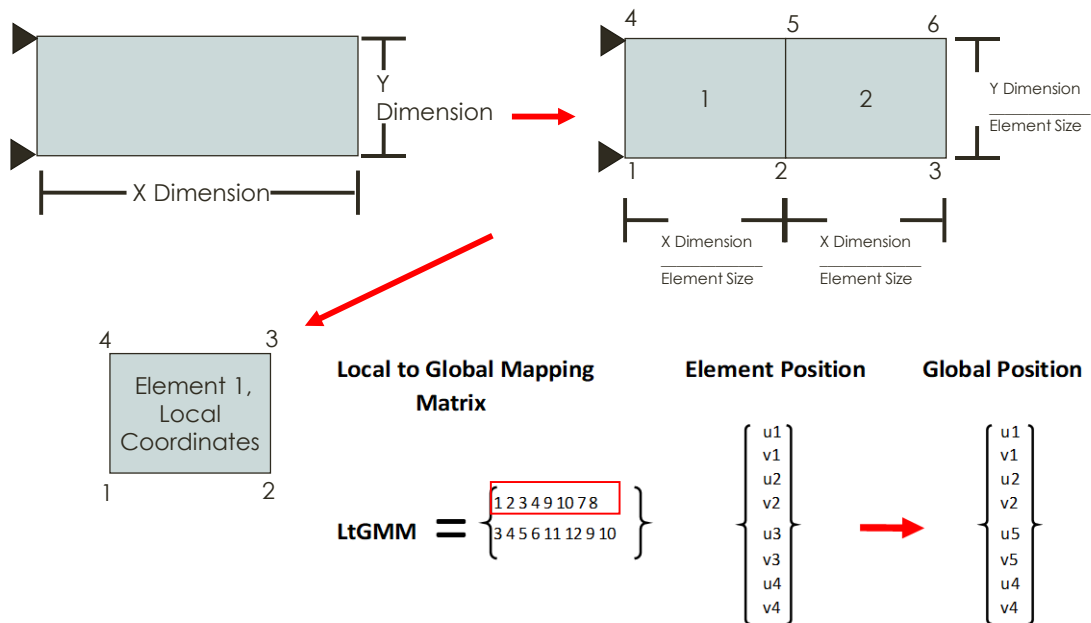


Figure 15 Mesh Generation Example

## 2.4 Global Assembly

The assembly process is one of the most complicated steps in the finite element program. The assembly process is highly dependent on the mesh generation technique and likewise dependent on the grid density, type of element, and variability of size and shape throughout the structure. The simplicity of the mesh generation technique chosen for this work simplifies the global assembly by virtue of elements of the same type. Global assembly is the process of taking the individual element stiffness matrices and adding them in to appropriate global position in the Global Stiffness Matrix which is used in the finite element governing equation. Figure 16 gives an example of element stiffness matrices being assembled into the global stiffness matrix.

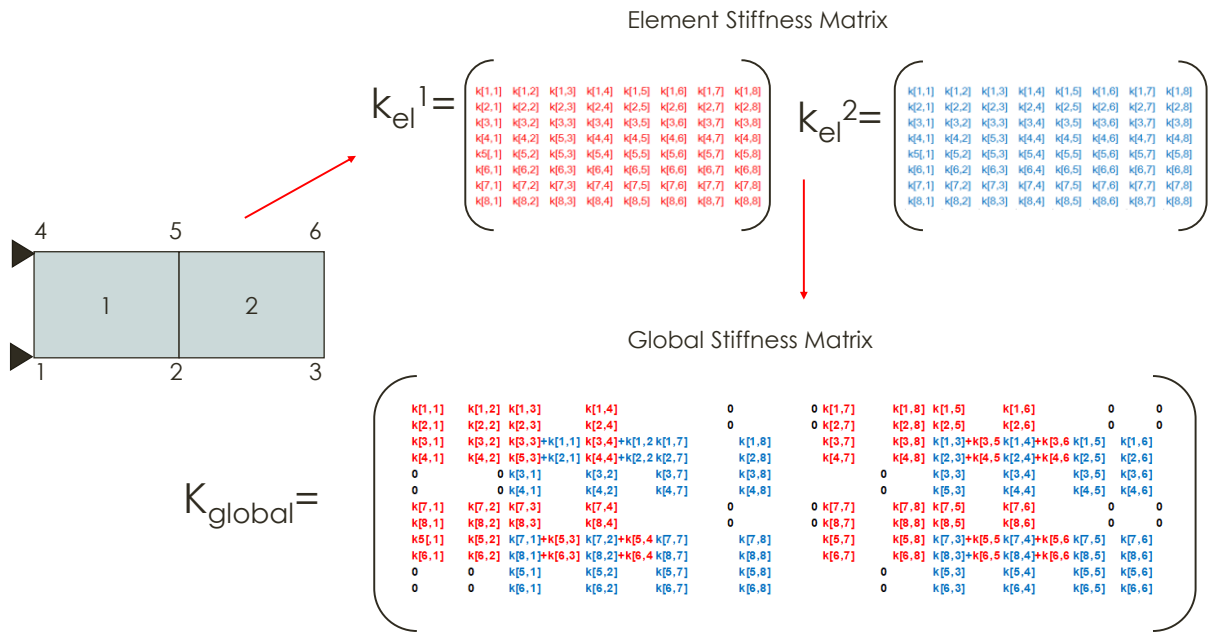
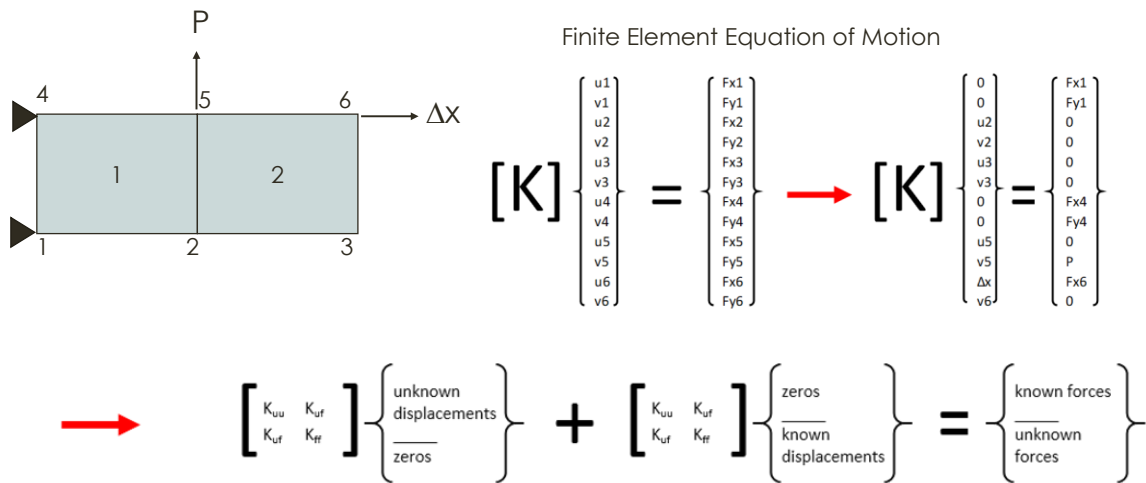


Figure 16 Local to Global Stiffness Matrix Assembly

## 2.5 Boundary Conditions and Solution

The final step in the finite element process is adding in the boundary conditions to the finite element governing equation and solving for the desired unknowns. Once the force and

displacement boundary conditions are added to the appropriate position in the global system, the remaining unknowns can be solved via matrix operations. In the matrix solution, the global system is rearranged and sorted into the displacement and force boundary conditions, respectively. Once sorted, the respective unknowns, force or displacement, are solved for and assembled back into the global position. Figure 17 demonstrates an example implementation of force and displacement boundary conditions and the resultant matrix operations for the solution.



**Figure 17 Example Boundary Condition Implementation and Solution**

## 2.6 Stress and Strain

Stress and Strain can be calculated at any point in the element using the solved for nodal displacements and equations given below.

$$\{\epsilon^{el}(x, y)\} = \begin{Bmatrix} \epsilon_{xx} \\ \epsilon_{yy} \\ \gamma_{xy} \end{Bmatrix} = [B]^{el} \{u^{el}\} \quad (0.10)$$

$$\{\sigma^{el}(x, y)\} = \begin{Bmatrix} \sigma_{xx} \\ \sigma_{yy} \\ \tau_{xy} \end{Bmatrix} = [D]^{el} [B]^{el} \{u^{el}\} \quad (0.11)$$

## 2.7 Matlab Implementation

Figure 18 contains the process for the Finite Element program developed by the author. Appendix A contains the Matlab implementation of the finite element code.

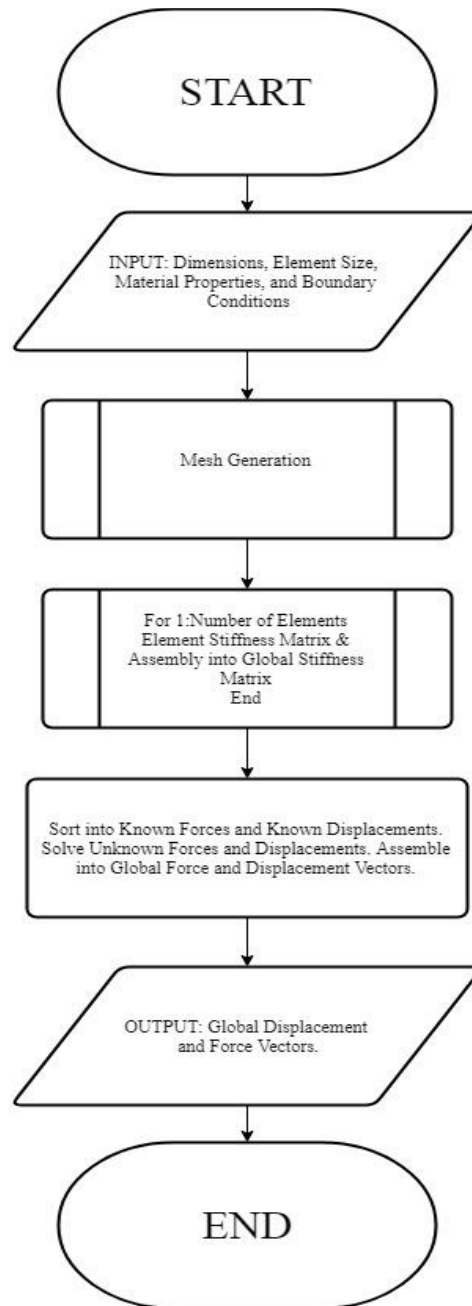


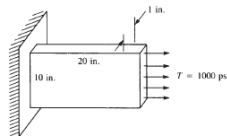
**Figure 18 Matlab Implementation Finite Element Flowchart**

## 2.8 Validation

The finite element program was validated against many benchmark problems and solutions to test the accuracy of the program. A simple example from a finite element textbook [69] is given below with the published solution on the left handside and the developed finite element program on the right. The finite element program was found to be accurate after being tested against multiple problems with accuracy increasing with number of elements. One example of validating the FEM program is given below in Figure 19.

### Solution Validation-Fixed Plate with Axial Loading

For a thin plate subjected to the surface traction shown in Figure 6-16, determine the nodal displacements and the element stresses. The plate thickness  $t = 1$  in.,  $E = 30 \times 10^6$  psi, and  $\nu = 0.30$ .



Constant Strain Triangle & Analytical Solution

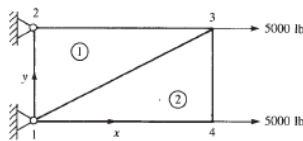


Figure 6-17 Discretized plate

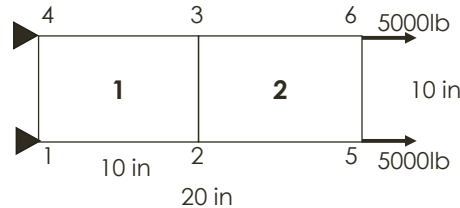
Simplifying Eq. (6.5.26), the final displacements are given by

$$\begin{Bmatrix} u_3 \\ v_3 \\ u_4 \\ v_4 \end{Bmatrix} = \begin{Bmatrix} 609.6 \\ 4.2 \\ 663.7 \\ 104.1 \end{Bmatrix} \times 10^{-6} \text{ in.} \quad (6.5.27)$$

Comparing the finite element solution to an analytical solution, as a first approximation, we have the axial displacement given by

$$\delta = \frac{PL}{AE} = \frac{(10,000)20}{10(30 \times 10^6)} = 670 \times 10^{-6} \text{ in.}$$

Author Finite Element Program Solution



$$\begin{Bmatrix} u_1 \\ v_1 \\ u_2 \\ v_2 \\ u_3 \\ v_3 \\ u_4 \\ v_4 \\ u_5 \\ v_5 \\ u_6 \\ v_6 \end{Bmatrix} = \begin{Bmatrix} 0 \\ 0 \\ .321 \\ .0589 \\ .321 \\ -.0589 \\ 0 \\ 0 \\ .656 \\ .0469 \\ .656 \\ -.0469 \end{Bmatrix}$$

Figure 19 FEM Validation Example

# CHAPTER 3: TOPOLOGY OPTIMIZATION

Exploring topology optimization of large displacement morphing structures is the motivation for this work due to its promising advantages for aerospace design and morphing structures. Chapter 3 details topology optimization approach applied to the morphing structures problem. Section 3.1 details the selection and implementation of a topology algorithm. Section 3.2 details the selection and implementation of a various strain based objective functions in place of the standard displacement based objective function. The results of the various strain based objective function are compared. Section 3.3 gives a discussion on the general application of the strain based topology optimization application as well as the behavior of the various strain based objective functions.

## 3.1 A 99 line topology optimization code written in Matlab

### 3.1.1 Numerical Derivation

The Matlab program presented in *A 99 line topology optimization code written in Matlab* was [68] chosen for two main reasons. The first being that the Matlab code presented is well known, frequently implemented, and intended for wide use in academia meaning there are many instructional resources for utilizing the program and many publications using it as the base for their topology research applications. The second reason is that the program is written efficiently and compactly with clearly defined variables and called functions which allows for simple modification and additions to the program.

The topology approach behind this program is the SIMP (Solid Isotropic Material with Penalization) approach where material properties are modeled as the relative material densities raised to a power. This approach, also called the power law approach, drives the solution to converge to values closer to one and zero than intermediate values. The topology optimization problem using the power law approach is given below in Eq. (2.12) where  $u_e$ ,  $F$  and  $f_e$  are the global and element displacement vectors and  $K$  and  $K_e$  are the global and element stiffness matrices.  $X$  is the vector of design variables, or material densities and  $x_e$  is the material density of a specific element.  $N$  is the number of elements,  $P$  is the penalization power and  $f$ , and  $volfrac$ , is

the volume fraction. Eq. (2.14),  $B_e$  represents the ratio of the element's specific strain energy density to the average strain energy density, for higher strain energy densities,  $B_e > 1$ , material is added. The given optimization problem is solved via the Optimality Criterion. Eq. (2.15) gives the sensitivity function. To ensure the existence of a solution, a mesh-independency filter, Eq. (2.16), is applied where the operator distance is defined as the distance between the centers of element  $e$  and element  $f$ . The convolution operator  $H_f$  is zero outside the filter area. The convolution operator decays linearly with the distance from element  $f$ . The convolution operator  $H_f$  is zero outside the filter area.

$$\begin{aligned}
\min_x : \quad c(x) &= U^T K U = \sum_{e=1}^N x_e^p u_e^T k_0 u_e = u^T f \\
\text{subject to:} \quad & \frac{V(x)}{V_0} = f \\
& : KU = f \\
& : 0 < x_{\min} \leq x \leq 1
\end{aligned} \tag{0.12}$$

$$\begin{aligned}
x_e^{new} = & \\
\max(x_{\min}, x_e - m) & \quad \text{if} \quad x_e B_e^n \leq \max(x_{\min}, x_e - m) \\
x_e B_e^n & \quad \text{if} \quad \max(x_{\min}, x_e - m) < x_e B_e^n < \min(1, x_e + m) \\
\min(1, x_e + m) & \quad \text{if} \quad \min(1, x_e + m) \leq x_e B_e^n
\end{aligned} \tag{0.13}$$

$$B_e = \frac{-\frac{\partial c}{\partial x_e}}{\lambda \frac{\partial V}{\partial x_e}} \tag{0.14}$$

$$\frac{\partial c}{\partial x_e} = -p(x_e)^{p-1} u_e^T k_0 u_e \tag{0.15}$$

$$\frac{\hat{\partial} c}{\partial x_e} = \frac{1}{x_e \sum_{f=1}^N \hat{H}_f} \sum_{f=1}^N \hat{H}_f x_f \frac{\partial c}{\partial x_f} \tag{0.16}$$

If optimization to multiple load cases is required, a simple addition to the compliance and sensitivity equations is implemented, summing over the number of load cases seen in Eq. (2.17).

$$c(x) = \sum_{i=1}^2 U_i^T K U_i \quad (0.17)$$

### 3.1.2 General Matlab Overview

Figure 20 gives an overview of the general process for the Matlab implementation of the topology optimization problem. Before modifying the program for strain minimization, the author's finite element program was implemented and tested against the benchmark problem given in the paper. Top.m is the original Matlab file published by Bendsoe [68]. Top\_smp.m is the topology optimization code modified to use the author's finite element code in place of the original. The solution is the same though Top\_smp.m converges slower. However, it is of note that Top.m only takes square elements from a rectangular structure that must be of the size one unit by one unit and element count can only be increased by increasing the dimensions. This is limiting and provided the motivation for the authors own finite element code.

The Benchmark problem is the solution of The Messerschmidt-Bölkow-Blohm (MBB) beam, pictured in Figure 21, using the original objective function, displacement minimization. Figure 22 shows a low element count for the problem to highlight the exact numerical consistency of the solutions. Figure 23 demonstrates the effect of increasing the number of elements. The results are from the Top\_smp.m solution are shown but are identical to the Top.m results and published benchmark results.

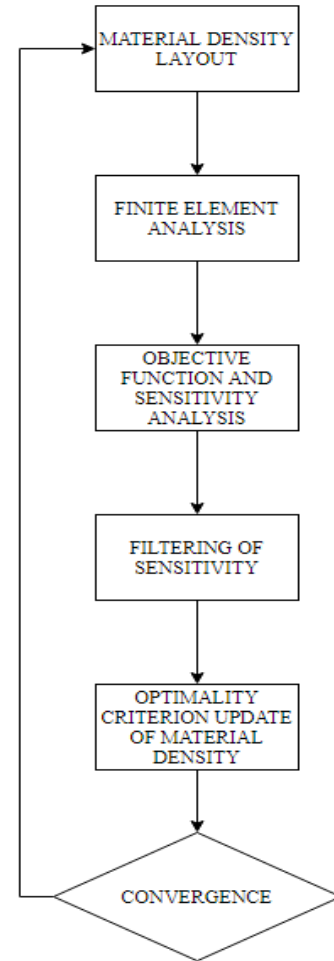


**Figure 20 Topology Optimization Algorithm Flow Chart**

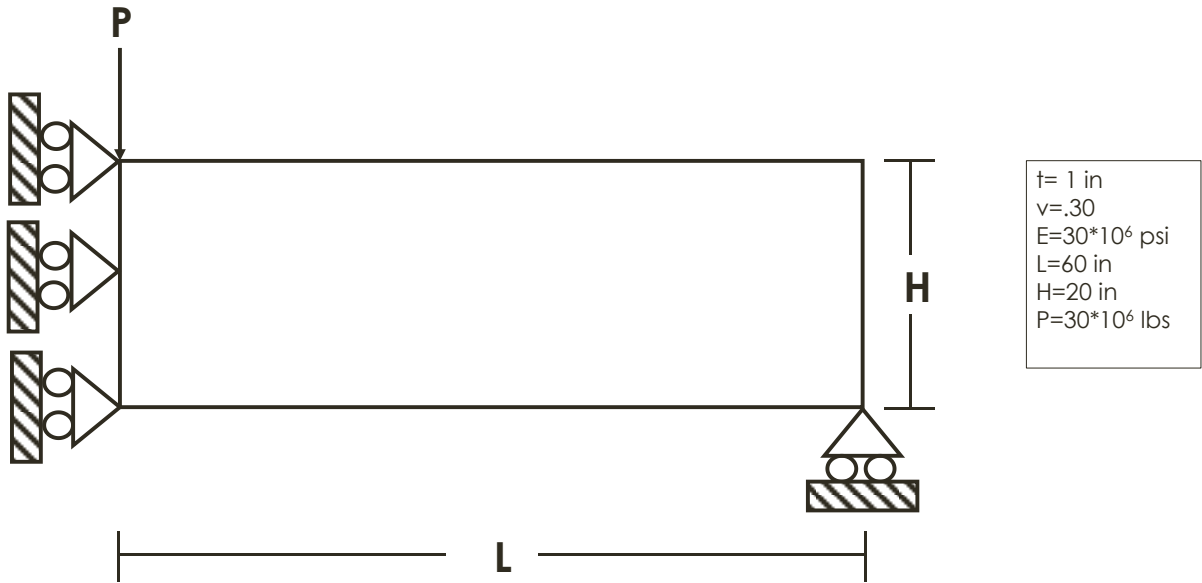


Figure 21 MBB Beam

Topology Optimization of the MBB.

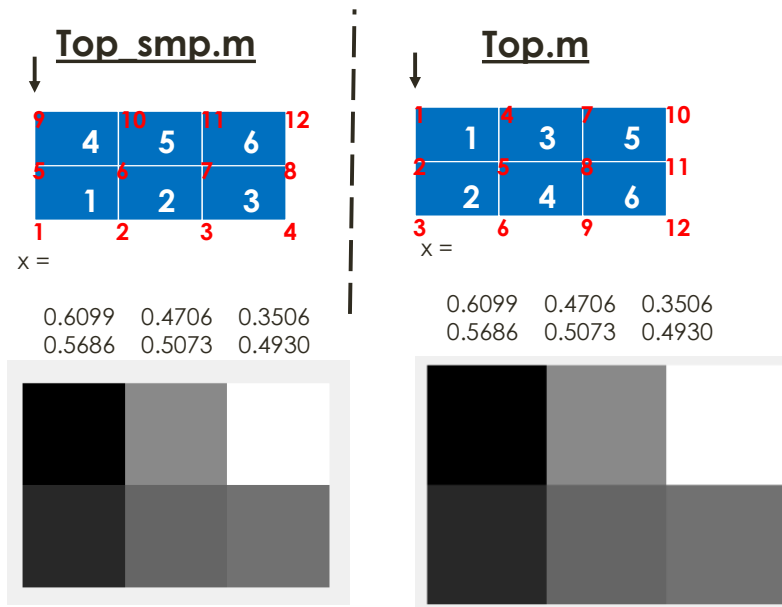
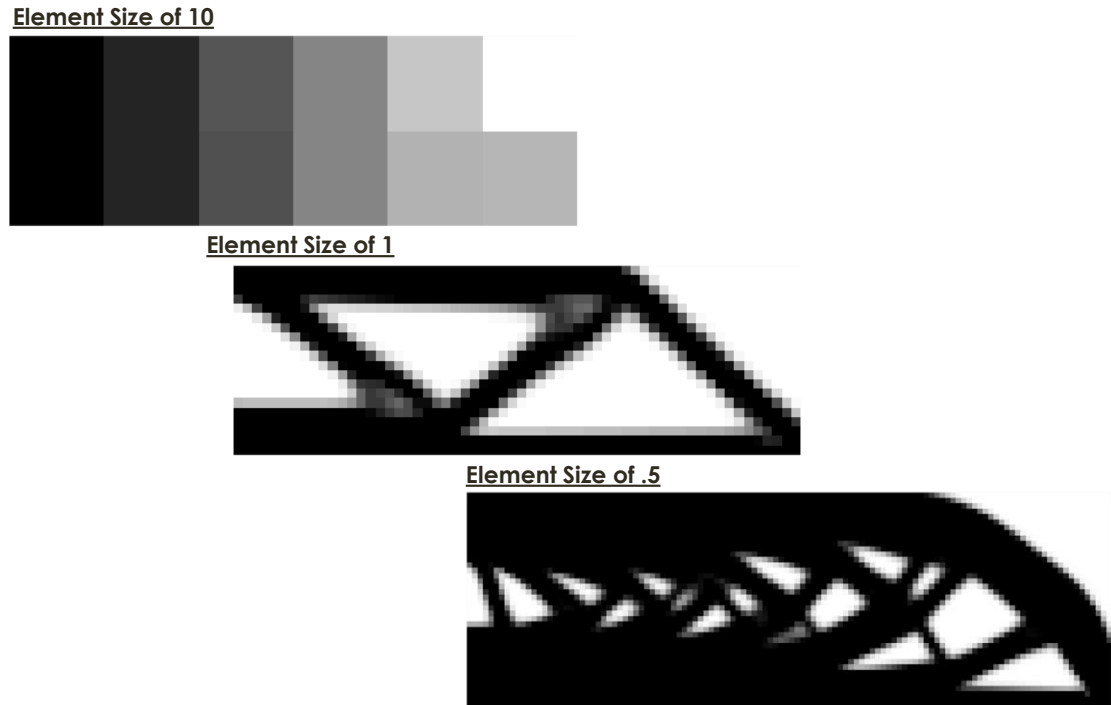


Figure 22 Low Element Count Topology Optimization of MBB Beam



**Figure 23 Increasing Element Number Solution of MBB Beam**

### 3.2 Strain Based Objective Function

In the previously described Topology Optimization approach, an optimal design is achieved by optimizing to a stiff structure via minimizing the strain energy through minimization of the displacement and stiffness matrix (Eq. (0.12)). However, due to the nature of the problem of interest in this work, which is a large displacement boundary condition problem, the standard topology problem through minimization of displacement and the stiffness matrix may not be the best approach for designing a flexible and compliant structure. Therefore in this research, a global strain function minimization approach will be employed where the objective is to minimize the strain in the structure during large displacements. The multi-objective approach minimizes a global strain instead of strain energy while maximizing compliance at specified applied location locations and is derived in [70], and results in Eq. (2.18) which replaces the objective function in the topology optimization previously described. The referenced paper uses a defined effective strain as the strain in its objective function, Eq. (2.19) where  $D_0$  represents the stress-strain matrix without the Young's Modulus and  $\phi$  which represents the applied nodal loads. It is also of interest to this work

to investigate how other types of strain in the objective functions behave. There are multiple ways to evaluate the strain in each element, taking it at the nodal points, or the gauss points, taking it at higher numbers of points, and considering principal and max shear strains. Table 1 summarizes the different strain based objective functions considered and the underlying motivation and equations for each. Section 3.2.1 provides further details on each strain objective function. Section 3.2.2 demonstrates the implementation of a strain based objective function to the MBB Benchmark problem and compares the behavior of different strain implementations.

$$\begin{aligned}
 & \text{Minimize } \sum_{i=1}^n \bar{\varepsilon}_i^2, \text{ Maximize: } U^T \Phi \\
 & \text{subject to: } \frac{V(x)}{V_0} = f \\
 & \quad : KU = f \\
 & \quad : 0 < x_{\min} \leq x \leq 1
 \end{aligned} \tag{0.18}$$

$$\bar{\varepsilon}^2 = \varepsilon^T D_0 \varepsilon^T = u_i^T C u_i = \frac{u_i^T k_i^0 u_i}{E_0} \tag{0.19}$$

**Table 1 Summary of Strain Based Objective Functions**

Objective Function	Motivation	Equation
Gauss Point Strains	To evaluate whether Gauss Point strains provide a better solution. The strains at the Gauss points may represent the highest strains or average strains.	$\bar{\varepsilon}_{GaussOnly}^2 = \varepsilon^T \varepsilon$ $\varepsilon([G_1 G_2 G_3 G_4]) = \begin{bmatrix} \varepsilon_{xx} \\ \varepsilon_{yy} \\ \gamma_{xy} \end{bmatrix}$ $[x, y] = [G_1 G_2 G_3 G_4]$
Nodal Point Strains	To evaluate whether Nodal Point strains provide a better solution. A direct substitution in the original topology approach, substituting nodal strains for nodal displacements.	$\bar{\varepsilon}_{NodalOnly}^2 = \varepsilon^T \varepsilon$ $\varepsilon(x, y) = \begin{bmatrix} \varepsilon_{xx} \\ \varepsilon_{yy} \\ \gamma_{xy} \end{bmatrix}$ $[x, y] = [N_1 N_2 N_3 N_4]$
Gauss and Nodal Point Strains	To evaluate whether a higher number of strains provide a better solution. This objective function has 8 strain points per element instead of 4.	$\bar{\varepsilon}_{GaussNodal}^2 = \varepsilon^T \varepsilon$ $\varepsilon(x, y) = \begin{bmatrix} \varepsilon_{xx} \\ \varepsilon_{yy} \\ \gamma_{xy} \end{bmatrix}$ $[x, y] = [G_1 N_1 G_2 N_2 G_3 N_3 G_4 N_4]$
X & Y Strains	To evaluate the effect X & Y Strains have on the resultant solution. X & Y strains are linear and may perform better in topology optimization.	$\bar{\varepsilon}_{XYOnly}^2 = \varepsilon^T \varepsilon$ $\varepsilon(x, y) = \begin{bmatrix} \varepsilon_{xx} \\ \varepsilon_{yy} \end{bmatrix}$ $[x, y] = [G_1 N_1 G_2 N_2 G_3 N_3 G_4 N_4]$
Shear Strains	To evaluate the effect Shear Strains have on the resultant solution. Shear strains are non-linear and may not perform well.	$\bar{\varepsilon}_{ShearOnly}^2 = \varepsilon^T \varepsilon$ $\varepsilon(x, y) = [\gamma_{xy}]$ $[x, y] = [G_1 N_1 G_2 N_2 G_3 N_3 G_4 N_4]$
Principal Strains	To evaluate whether the principal strains provide a better solution. The principal strains give the maximum and minimum strain possible for a specific point which could be a better evaluation of the strain in an element.	$\bar{\varepsilon}_{PS}^2 = \varepsilon^T \varepsilon$ $\varepsilon(x, y) = \begin{bmatrix} \varepsilon_{PS1} \\ \varepsilon_{PS2} \end{bmatrix}$ $[x, y] = [G_1 N_1 G_2 N_2 G_3 N_3 G_4 N_4]$ $\varepsilon_{PS1,PS2} = \frac{\varepsilon_{xx} + \varepsilon_{yy}}{2} \pm \sqrt{\left(\frac{\varepsilon_{xx} - \varepsilon_{yy}}{2}\right)^2 + \left(\frac{\gamma_{xy}}{2}\right)^2}$
Principal Strains and Max Shear	To evaluate whether the including the maximum shear with the principal strains provides a better solution. The maximum shear represents the maximum shear possible at a point. Combining the principal strains with the maximum shear may effectively capture the dominant strains in each element.	$\bar{\varepsilon}_{PS+MaxShear}^2 = \varepsilon^T \varepsilon$ $\varepsilon(x, y) = \begin{bmatrix} \varepsilon_{PS1} \\ \varepsilon_{PS2} \\ 2\gamma_{max} \end{bmatrix}$ $[x, y] = [G_1 G_2 G_3 G_4]$ $\frac{\gamma_{max}}{2} = \sqrt{\left(\frac{\varepsilon_{xx} - \varepsilon_{yy}}{2}\right)^2 + \left(\frac{\gamma_{xy}}{2}\right)^2}$
Effective Strains	To evaluate where the objective function from a paper (Lee and Gea 2014) will provide a better solution.	$\bar{\varepsilon}^2 = \varepsilon^T D_0 \varepsilon^T = u_i^T C u_i = \frac{u_i^T k_i^0 u_i}{E_0}$

3.2.1

**Strain Objective Function Variations**

In the original topology code, the nodal point displacements are solved for and used in the objective functions. Therefore, a direct substitution of strains at the same nodal points was one of the first strain based objective functions considered. While the solved for discretized displacements are the nodal values, the interpolating shape functions allow for finding the displacements and strains at any value within the element. Without being restricted to nodal values, it is of interest to observe strain points at other locations in the element, particularly because nodal values may not represent the highest values of the element. Therefore, the implementation of strain at the gauss points of each element was also considered. Figure 24 shows the described nodal and gauss points of each element. Equations (2.20), (2.21), and (2.22) show the objective function variations resulting from comparing strains at the nodal and gauss points. Another strain variation to consider is whether increasing the number of strains resulting in the objective function using the combined nodal and gauss points.

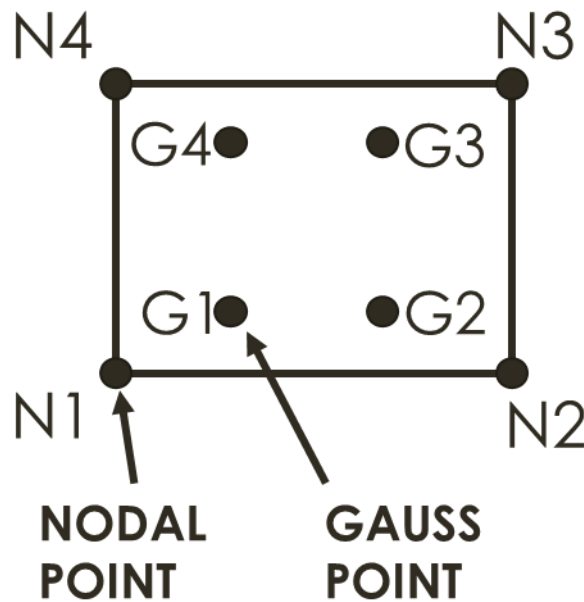


**Figure 24 Gauss and Nodal Points**

$$\bar{\varepsilon}_{GaussOnly}^2 = \varepsilon^T \varepsilon$$

$$\varepsilon([G_1 G_2 G_3 G_4]) = \begin{bmatrix} \varepsilon_{xx} \\ \varepsilon_{yy} \\ \gamma_{xy} \end{bmatrix} \quad (0.20)$$

$$[x, y] = [G_1 G_2 G_3 G_4]$$

$$\bar{\varepsilon}_{NodalOnly}^2 = \varepsilon^T \varepsilon$$

$$\varepsilon(x, y) = \begin{bmatrix} \varepsilon_{xx} \\ \varepsilon_{yy} \\ \gamma_{xy} \end{bmatrix} \quad (0.21)$$

$$[x, y] = [N_1 N_2 N_3 N_4]$$

$$\bar{\varepsilon}_{GaussNodal}^2 = \varepsilon^T \varepsilon$$

$$\varepsilon(x, y) = \begin{bmatrix} \varepsilon_{xx} \\ \varepsilon_{yy} \\ \gamma_{xy} \end{bmatrix} \quad (0.22)$$

$$[x, y] = [G_1 N_1 G_2 N_2 G_3 N_3 G_4 N_4]$$

The next variations result from comparing the behavior of the x and y strains to the shear strains. The resulting variations are found in Equations (2.23) and (2.24).

$$\bar{\varepsilon}_{XYOnly}^2 = \varepsilon^T \varepsilon$$

$$\varepsilon(x, y) = \begin{bmatrix} \varepsilon_{xx} \\ \varepsilon_{yy} \end{bmatrix} \quad (0.23)$$

$$[x, y] = [G_1 N_1 G_2 N_2 G_3 N_3 G_4 N_4]$$

$$\bar{\varepsilon}_{ShearOnly}^2 = \varepsilon^T \varepsilon$$

$$\varepsilon(x, y) = [\gamma_{xy}] \quad (0.24)$$

$$[x, y] = [G_1 N_1 G_2 N_2 G_3 N_3 G_4 N_4]$$

Finally, the Principal Strains and Max Shear Strain Equation Eq. (2.25) were implemented in Equations (2.26) and (2.27).

$$\begin{aligned}\epsilon_{PS1,PS2} &= \frac{\epsilon_{xx} + \epsilon_{yy}}{2} \pm \sqrt{\left(\frac{\epsilon_{xx} - \epsilon_{yy}}{2}\right)^2 + \left(\frac{\gamma_{xy}}{2}\right)^2} \\ \frac{\gamma_{\max}}{2} &= \sqrt{\left(\frac{\epsilon_{xx} - \epsilon_{yy}}{2}\right)^2 + \left(\frac{\gamma_{xy}}{2}\right)^2}\end{aligned}\quad (0.25)$$

$$\begin{aligned}\bar{\epsilon}_{PS}^2 &= \epsilon^T \epsilon \\ \epsilon(x, y) &= \begin{bmatrix} \epsilon_{PS1} \\ \epsilon_{PS2} \end{bmatrix} \\ [x, y] &= [G_1 N_1 G_2 N_2 G_3 N_3 G_4 N_4]\end{aligned}\quad (0.26)$$

$$\begin{aligned}\bar{\epsilon}_{PS+MaxShear}^2 &= \epsilon^T \epsilon \\ \epsilon(x, y) &= \begin{bmatrix} \epsilon_{PS1} \\ \epsilon_{PS2} \\ 2\gamma_{\max} \end{bmatrix} \\ [x, y] &= [G_1 G_2 G_3 G_4]\end{aligned}\quad (0.27)$$

### 3.2.2 Results of Strain Variation Implementation

The strain objection variations previously described were applied to the topology optimization of the MBB Beam. Figure 25 shows the initial material distribution and resultant optimization solutions from the respective strain objective functions. Figure 26 shows the effect optimizing to each strain variation has on the other objective functions, or strain variations. Figure 27 shows the convergence of the objective functions. Figure 28 show the average values of x, y, and shear strains respectively for each strain implementation.

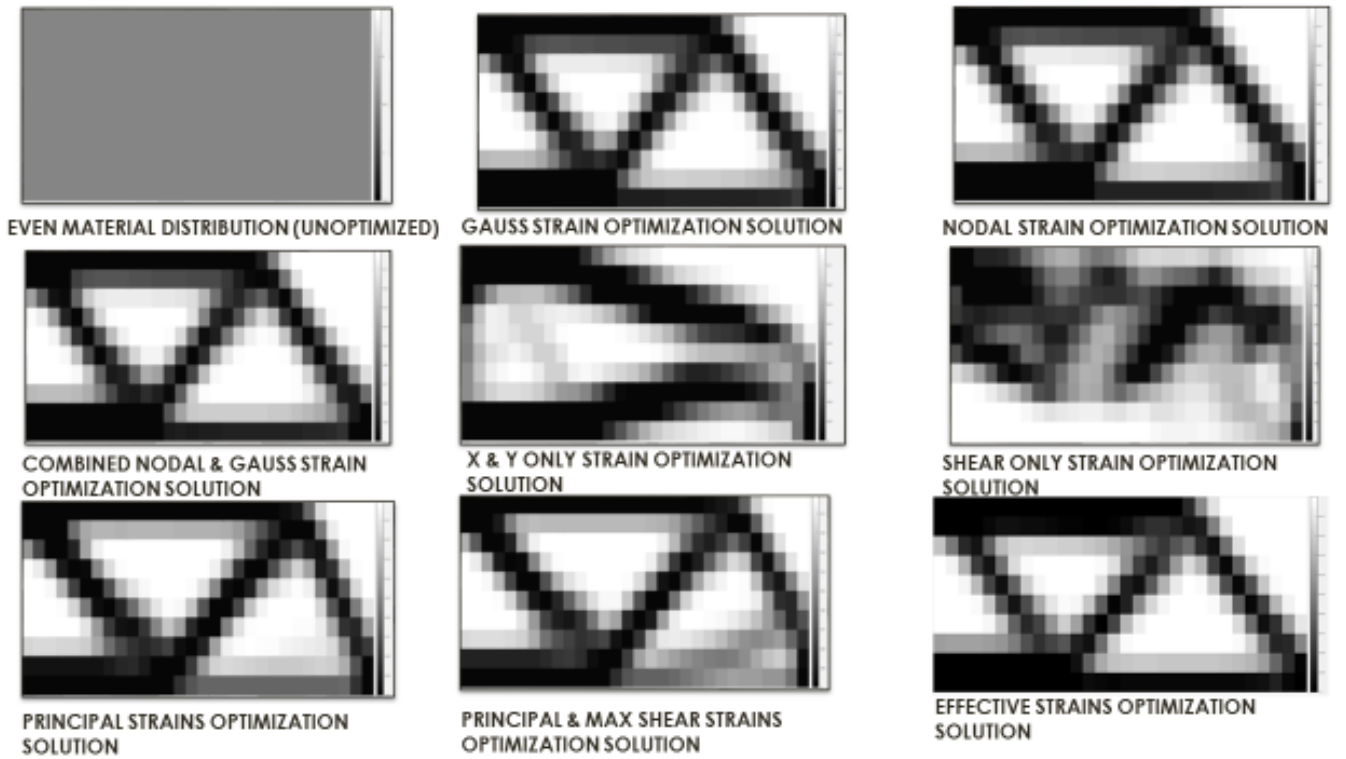


**Figure 25 Benchmark Problem Material Layout Solutions for Various Strain Implementations**

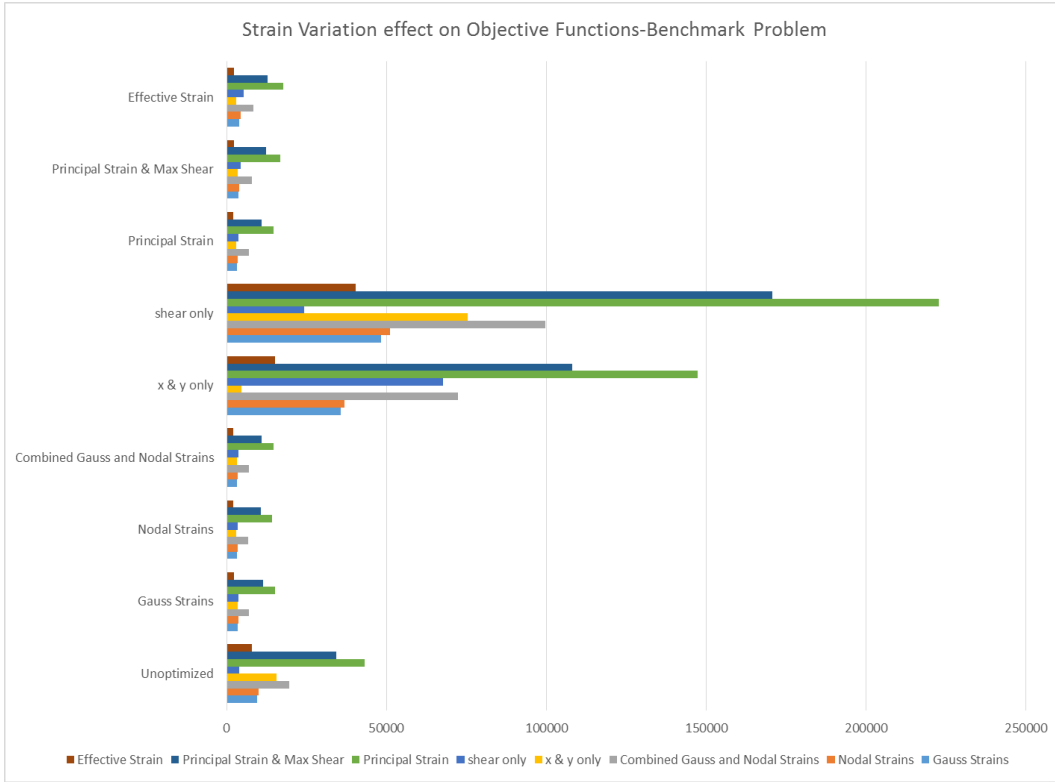


**Figure 26 Strain Objective Function Effect on other Objective Functions**

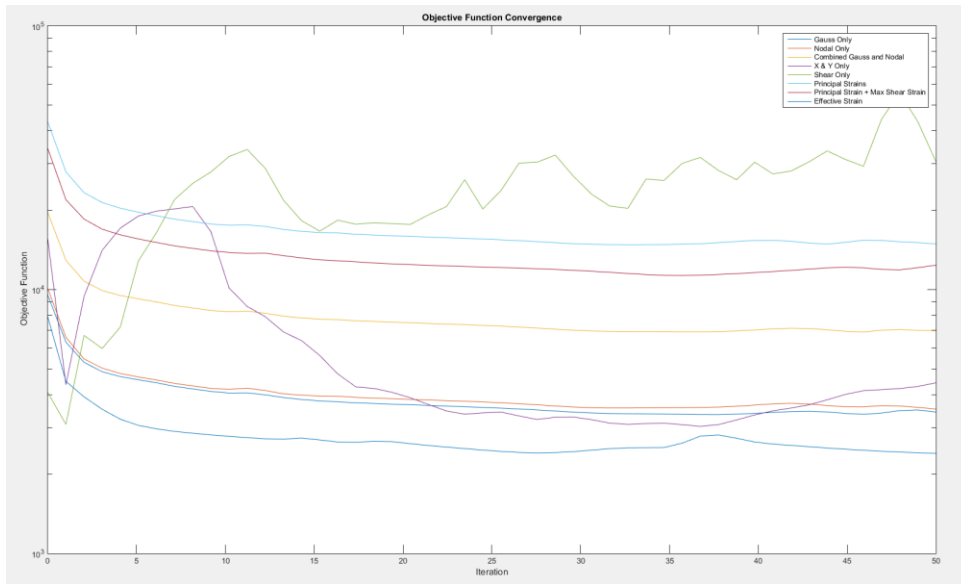


**Figure 27 Benchmark Problem Objective Function Convergence**

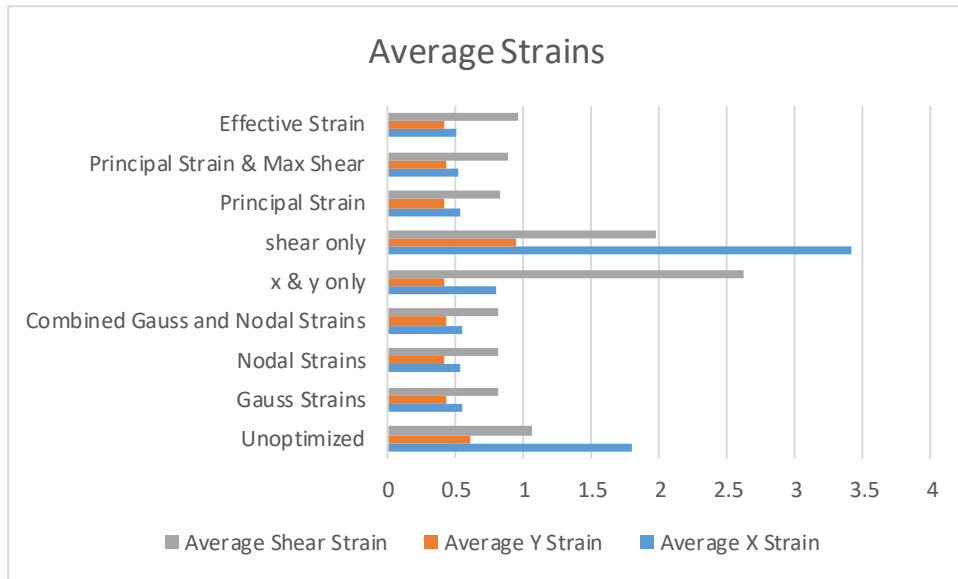


**Figure 28 Average Strain Results for the Strain Objective Functions-MBB Problem**

Figure 25 shows that the various ways of applying the relationship and combinations of the x, y, and shear strains still yields the same overall material layout. However, upon isolating the x and y strains and the shear strains, the material layout diverges from the truss structure. For the X and Y Only strain implementation, the solution converges towards a rough semi-trapezoid shape. For the Shear Only strain implementation, the solution converges towards a corrugated, diagonal pattern. The combination of the x, y, and shear strains results in the semi-trapezoidal truss shape as seen in the other strain implementations and the displacement minimization problem.

Figure 26 shows how optimizing to one type of objective function effects the others. It can be seen that except for the X and Y Only and Shear Only Strain objective functions, all objective functions behave almost identical without any performing significantly better or worse. The X and Y Only and Shear Only Strain objective functions increase, or worsen, the other objective functions.

Figure 27 shows that the Gauss Strains, Nodal Strains, Combined Gauss and Nodal, Principal Strains, Principal and Max Shear Strains, and Effective strains all effectively minimize their own Objective Function as well as the others. Figure 28 demonstrates improvements in the maximum and average x, y, and shear strains for those objective functions. Of the listed strain implementations, the Effective Strain appears to minimize the average and maximum strains the most effectively. The X & Y Strains Only minimizes its objective function but increases the

maximum and average shear strains which increases the other strain variation objective functions. The Shear Strains Only variation increases the shear strain objective function as well as the other objective functions. This indicates that a linear analysis method may not be effective for a non-linear quantity like shear strains.

### **3.3 Discussion of Results of Strain Variation Implementation**

From the results given in Section 3.2, it can be seen that strain optimization for the MBB Problem did not produce a different optimized structure, in most of the strain variation cases, from the original displacement minimization problem. However, this is not surprising for a beam problem where strain is approximately directly proportional to displacement. It is of more interest to observe the individual behaviors of the strain implementations. Furthermore, in the investigation to see if one type of strain objective function performed better than the other, for example increasing number of strains per element or using principal strains, none of the objective functions, except the isolated X and Y Only and Shear Only Strain objective functions, no objective function was found to be better performing. From the X and Y Only and Shear Only it can be seen that the linear strains, x and y, and non-linear strains, shear, have very different solutions and negatively impact the other.

It is of note that this is in this problem the x, y, and shear strains of the same magnitude and close in magnitude and the problem is not over constrained. The following section will apply the strain variation objective functions to the large displacement boundary condition and high shear strain problem.

## CHAPTER 4: PROBLEM OF INTEREST AND CORRESPONDING SOLUTION

Having established and validated a strain based topology optimization method and Matlab implementation, the next step is to apply the approach to a problem of interest. A 2D Plane Stress Problem with one end fixed and the other end subject to large displacement boundary conditions was designed to simulate the morphing trailing edge transitional surface presented in Figure 12. Figure 29 presents the proposed problem of interest subject to two opposite loading cases, upwards and downwards deflections, simulating the upward and downward deflection of a flight control being actuated. The load cases presented use enforced non-zero boundary displacements to actuate the morphing of the surface, as opposed to applying forces. Section 4.1 examines the resultant optimization behavior of the previously described strain implementations for a single load case. The problem of interest is examined as well as X Only displacement boundary conditions and Y Only displacement boundary conditions to examine the influencing behavior from each of these conditions. Sections 4.2, 4.3, and 4.4 compare starting material configurations, volume fractions, and different aspect ratios, respectively, to observe the robustness of the method and effect of the varying parameters. Section 4.5 examines the resultant optimization behavior for multiple conditions, both upwards and downwards deflection, from both Gauss and Nodal Strains and X & Y Only Objective Functions. Additionally, Y Only displacement boundary conditions are examined to observe the influencing behavior from these boundary conditions. Section 4.6 compares the optimization solutions and the un-optimized initial material layout.

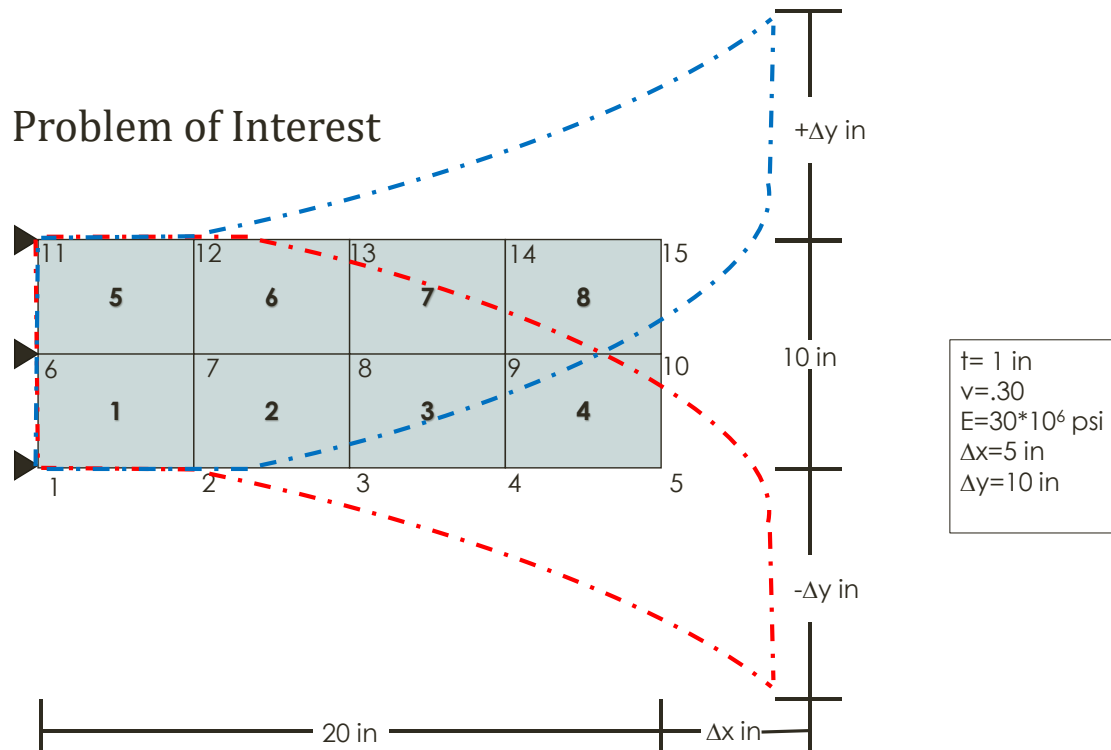
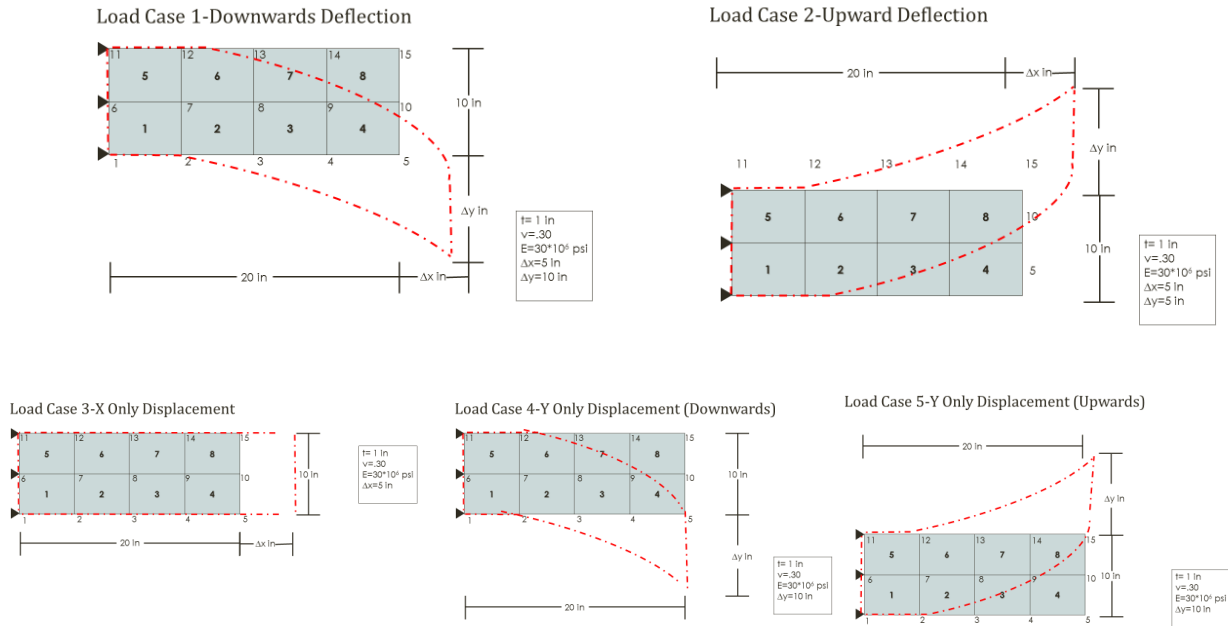


Figure 29 Defined Problem of Interest

## 4.1 Application of Strain Based Topology to Problem of Interest- Single Load Case

Before optimizing the problem of interest, or to the upward and downward deflections simultaneously, it was implemented on a single load, downwards deflection, to observe the optimization behavior of the various strain implementations. The results are given in Section 4.1.1. Note, it was not necessary to implement it individually to both load cases, both upwards and downwards deflection, due to the symmetry, opposite sign, of the problem and results. Additionally, X Displacement Only Boundary Conditions and Y Displacement Only Boundary Conditions load cases are studied in sections 4.1.2 and 4.1.3 to observe the influence of these boundary conditions. Conclusions from these results are given in 4.1.4. Figure 30 summarizes the load cases implemented.



**Figure 30 Summary of Load Cases**

### 4.1.1 Strain Implementation Variance-Load Case 1

The strain objection variations were applied to the topology optimization of Load Case 1, seen in Figure 30. Load Case 1 represents the X and (downward) Y displacement boundary conditions. While an example mesh grid is shown, a much finer grid was implemented on the work done below. The example grid shown is element size of 5 (8 elements total) while the implemented grid is of element size of 0.5 (800 elements total). Figure 31 shows the starting material distribution and resultant optimization solutions from the respective strain objective functions. Figure 32 shows the effect optimizing to each strain variation has on the other objective functions, or strain variations. Figure 33 shows how each strain objective function effects the maximum, minimum, and average values of x, y, and shear strains respectively. Figure 34 gives the strain plots for the unoptimized solution and the Combined Nodal and Gauss Strain solution for the x,y, and shear strains.

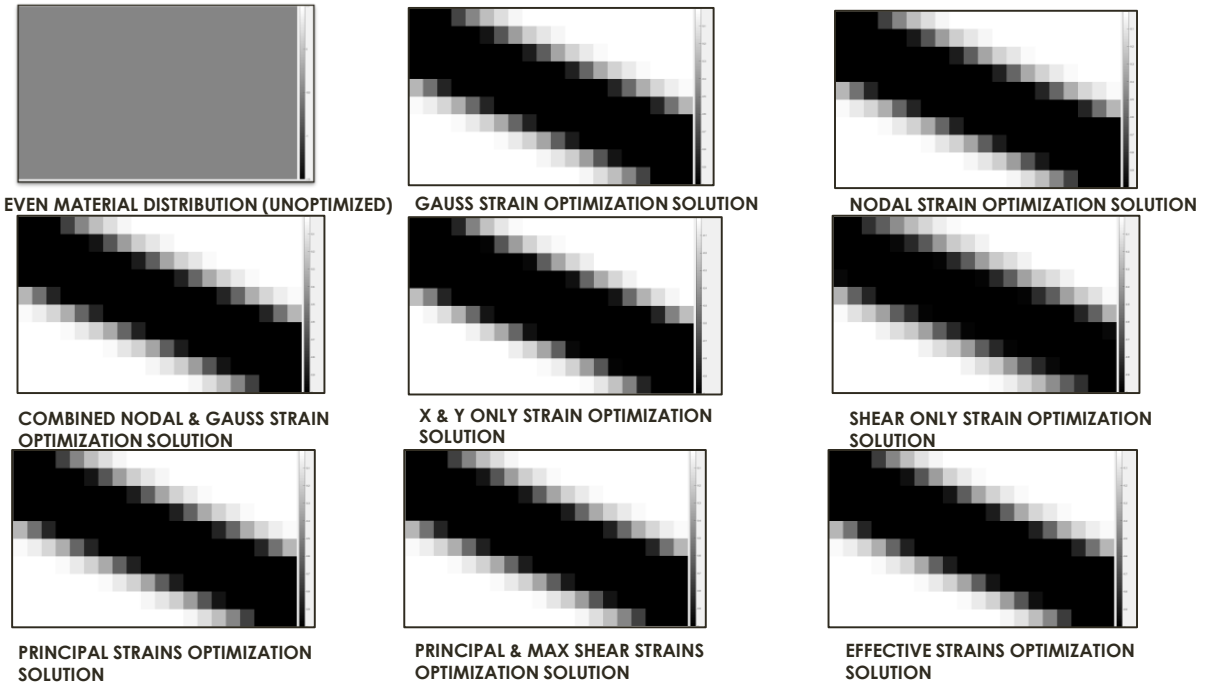


**Figure 31 Load Case 1 Material Layout Solutions for Various Strain Implementations**

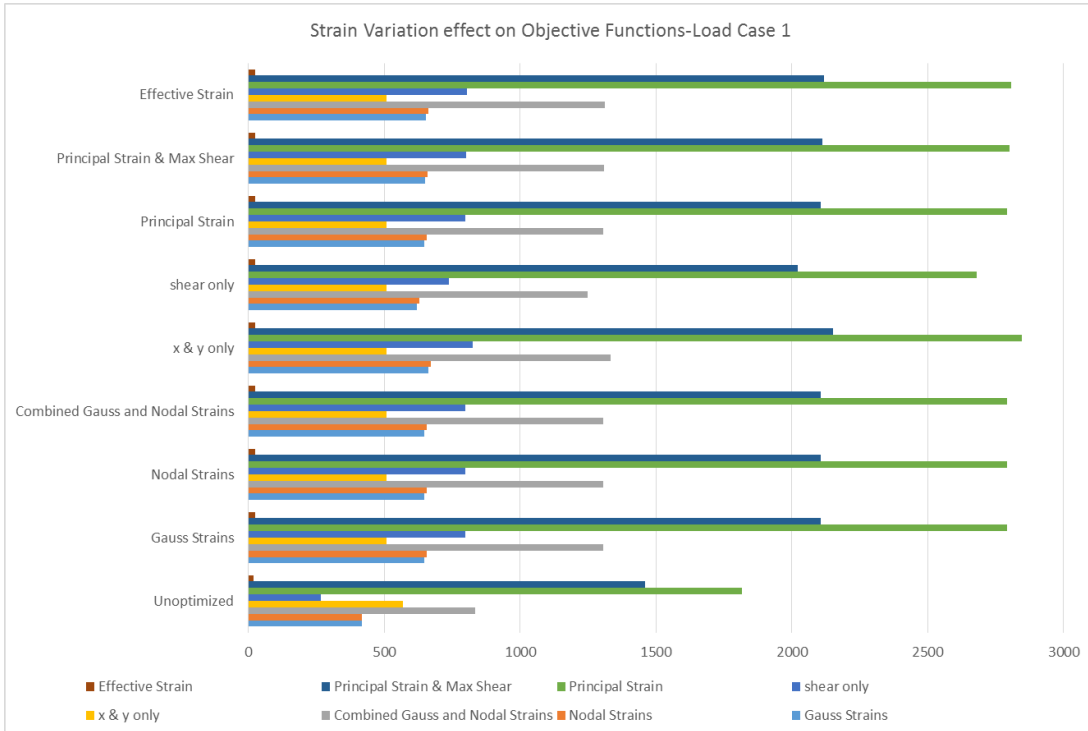


**Figure 32 Strain Variation Effect on Objective Functions-Load Case 1**

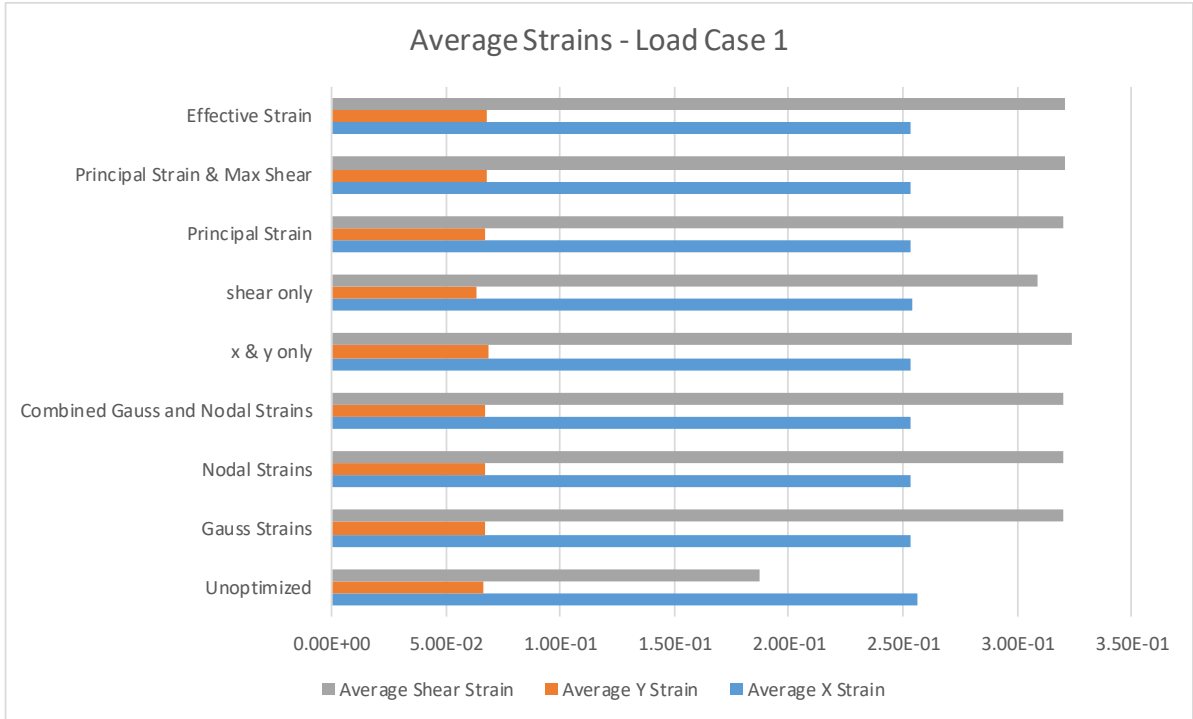


**Figure 33 Average Strains for the Strain Objective Functions - Load Case 1**

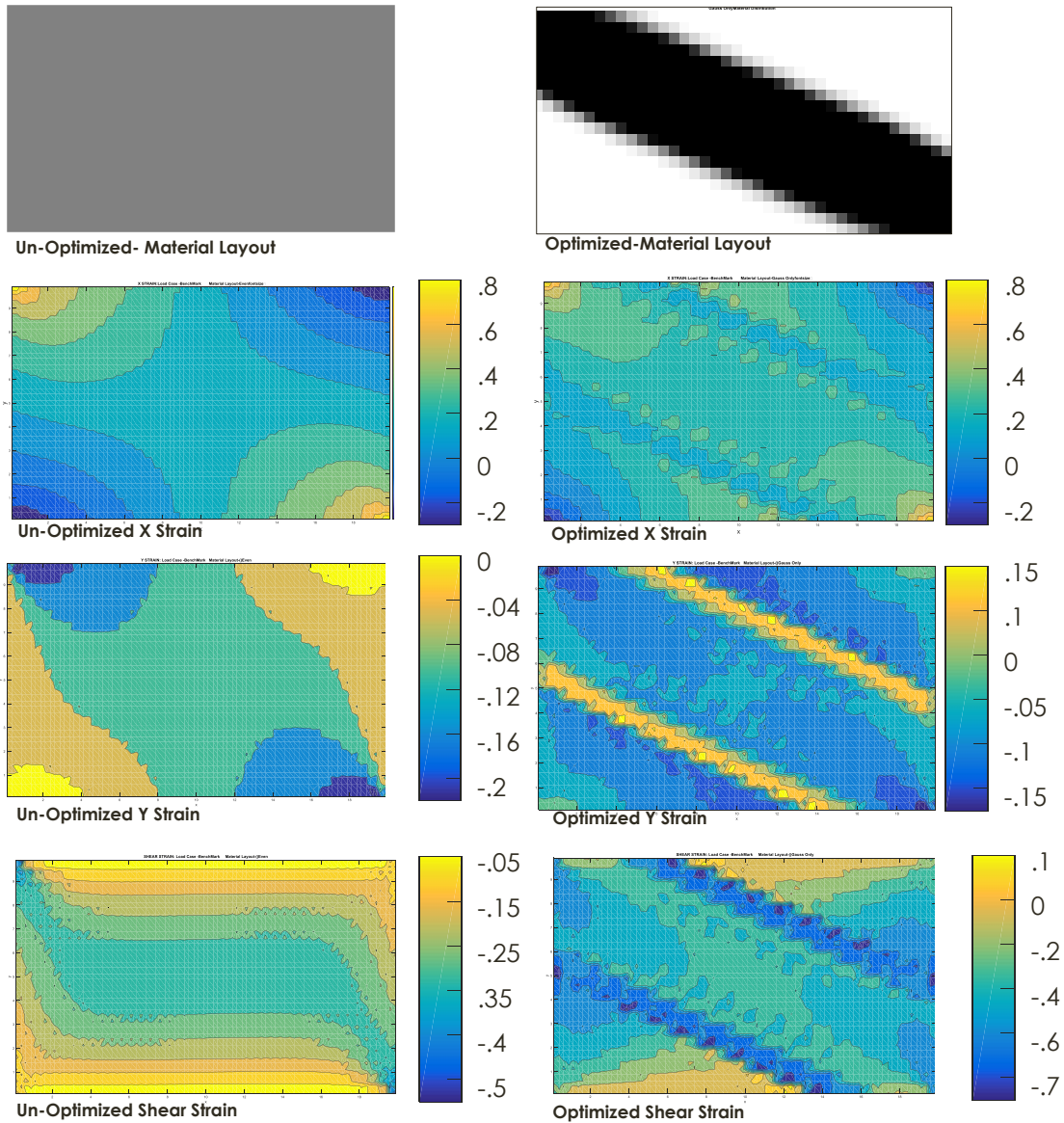


**Figure 34 Strain Plots for Load Case 1 Optimization Result**

From Figure 31, it can be observed for that the combined axial and transverse loading, Load Case 1, all strain implementations converge to the same solution. Looking at Figure 33, it can be seen that the optimized solutions have not affected the average x strains. Even optimizing to the X and Y Only Strains had little impact on the x strains. The Y Strains have similar results, where the average is unaffected. Examining the shear strains, it can be seen that the average shear strains are increased. From Figure 34 it can be the areas of lowest acting strain have been increased and the areas with higher strains have been decreased for both the x and y strains. The areas with higher relative strains, the upper left corner and lower right corner, have been reduced in surface area.

### 4.1.2 Strain Implementation Variance-Load Case 3

The strain objection variations were applied to the topology optimization of Load Case 3, seen in Figure 30. Load Case 3 represents only the X displacement boundary conditions. While an example mesh grid is shown, a much finer grid was implemented on the work done below. The example grid shown is element size of 5 (8 elements total) while the implemented grid is of element size of 0.5 (800 elements total). Figure 35 shows the starting material distribution and resultant optimization solutions from the respective strain objective functions. Figure 36 shows the effect optimizing to each strain variation has on the other objective functions, or strain variations. Figure 36 shows how each strain objective function effects the maximum, minimum, and average values of x, y, and shear strains respectively. Figure 38 gives the strain plots for the unoptimized solution and the Combined Nodal and Gauss Strain solution for the x,y, and shear strains.

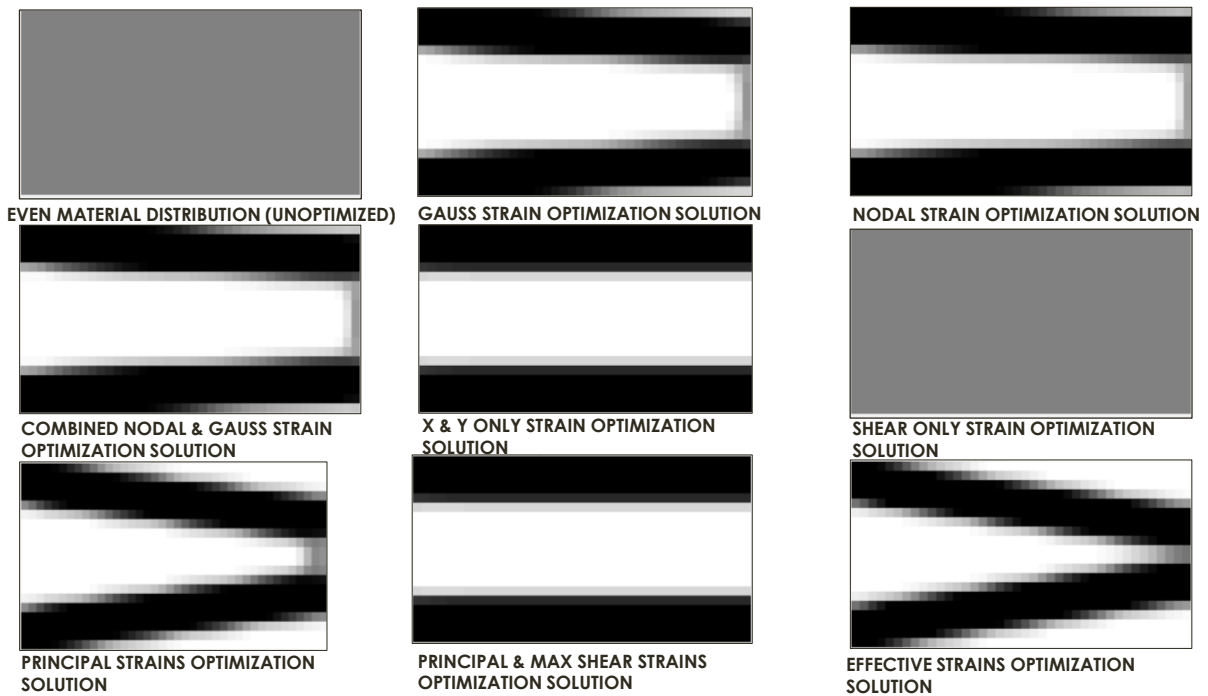
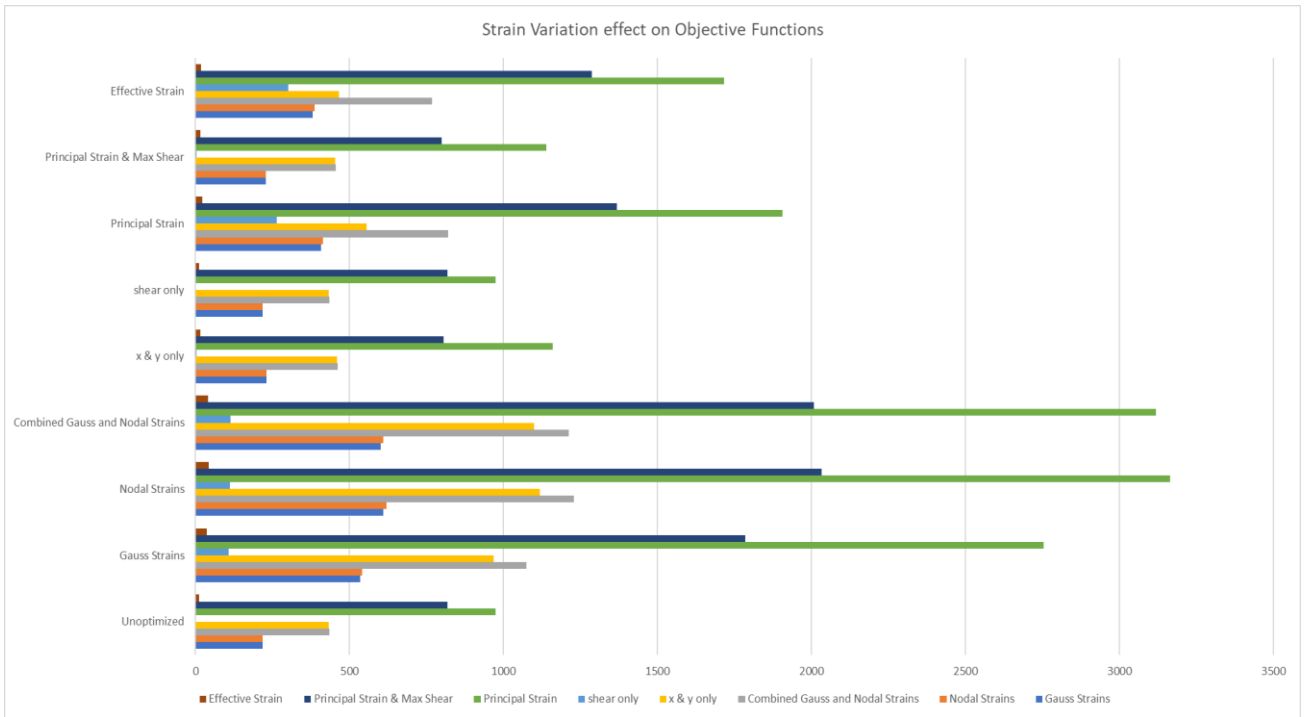
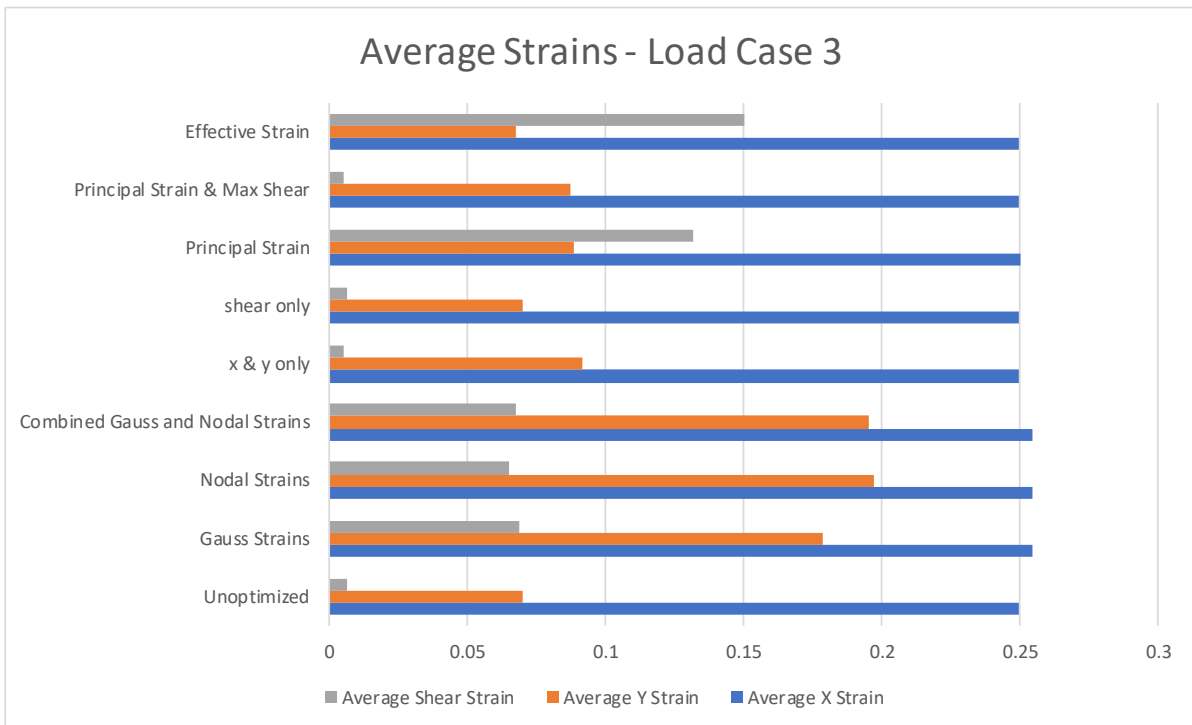


Figure 35 Load Case 3- Material Layout Solutions for Various Strain Implementations



**Figure 36 Strain Variation Effect on Objective Functions-Load Case 3**



**Figure 37 Average Strains for the Strain Objective Functions - Load Case 3**

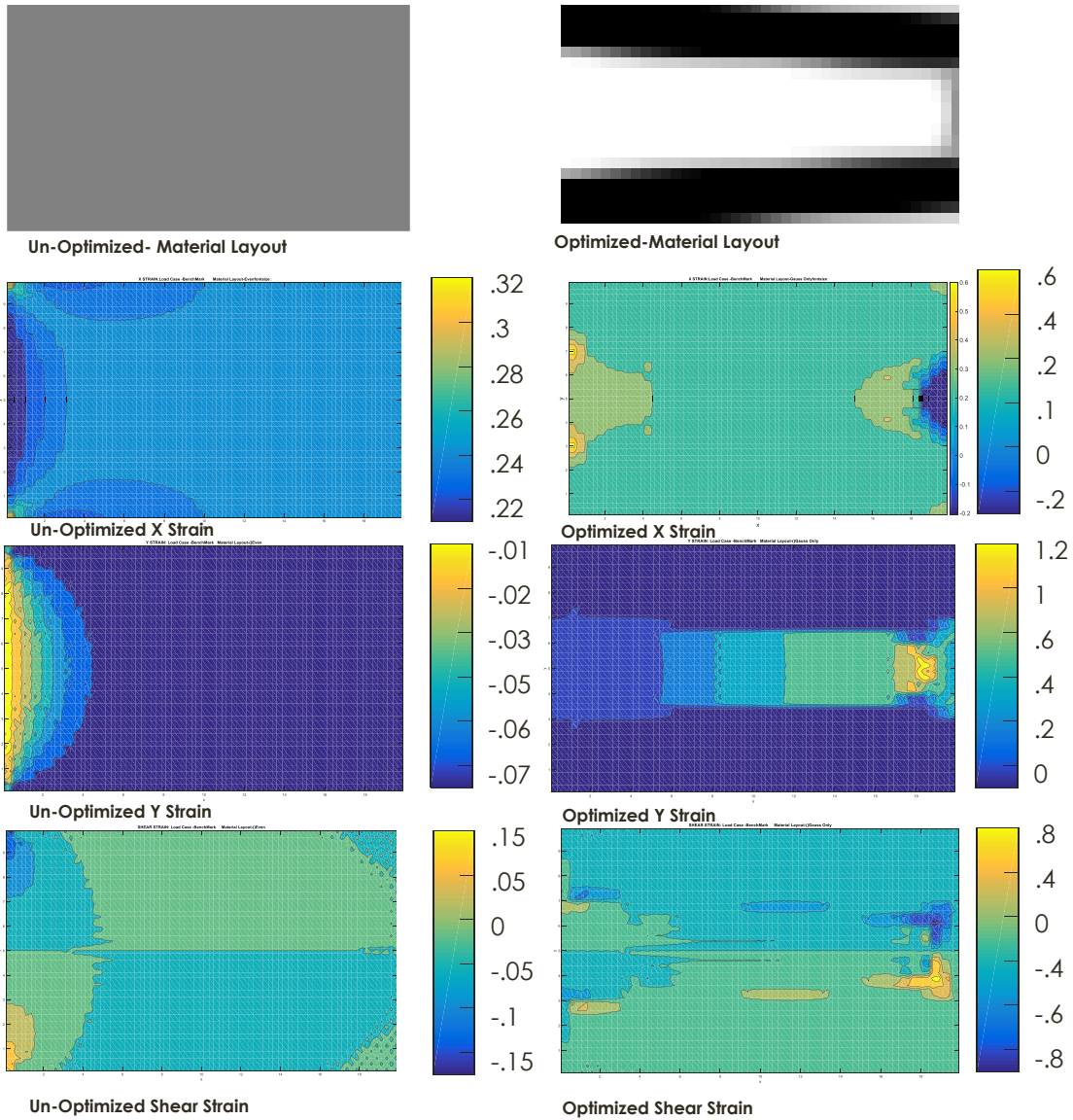


**Figure 38 Strain Plots for Load Case 3 Optimization Result**

Examining the behavior of the isolated x displacement boundary condition, Load Case 3, it can be seen that this boundary condition drives material to the top and bottom of the bar as seen in Figure 35. For this Load Case, the strain implementation results have different results. The X and Y Strains Only solution shows material distributed completely axially; however, the Shear Only Solution shows no change which is logical due to a problem with very small initial shear strains. The remaining strain variations all show some diagonalization which comes from including the shear strains, which while initially small become larger as the solution converges to the top and

bottom material concentration. Figure 37 shows that the average strains are increased. Figure 38 that for the dominant strain, the X strains, the majority of the structure has x strains between .24 to .22. The optimized solution reduces the majority of the x strains in the structure to between .2 and .1. Additionally while the maximum y strain has been increased, it can be seen that the minimum y strain, that covers a wide area, has been reduced to 0. However, the resultant shear strain has worsened.

#### **4.1.3 Strain Implementation Variance-Load Case 4**

The strain objection variations were applied to the topology optimization of Load Case 4, seen in Figure 30. Load Case 4 represents only the Y displacement boundary conditions. While an example mesh grid is shown, a much finer grid was implemented on the work done below. The example grid shown is element size of 5 (8 elements total) while the implemented grid is of element size of 0.5 (800 elements total). Figure 39 shows the starting material distribution and resultant optimization solutions from the respective strain objective functions. Figure 40 shows the effect optimizing to each strain variation has on the other objective functions, or strain variations. Figure 41 shows how each strain objective function effects the maximum, minimum, and average values of x, y, and shear strains respectively. Figure 42 gives the strain plots for the unoptimized solution and the Combined Nodal and Gauss Strain solution for the x,y, and shear strains.

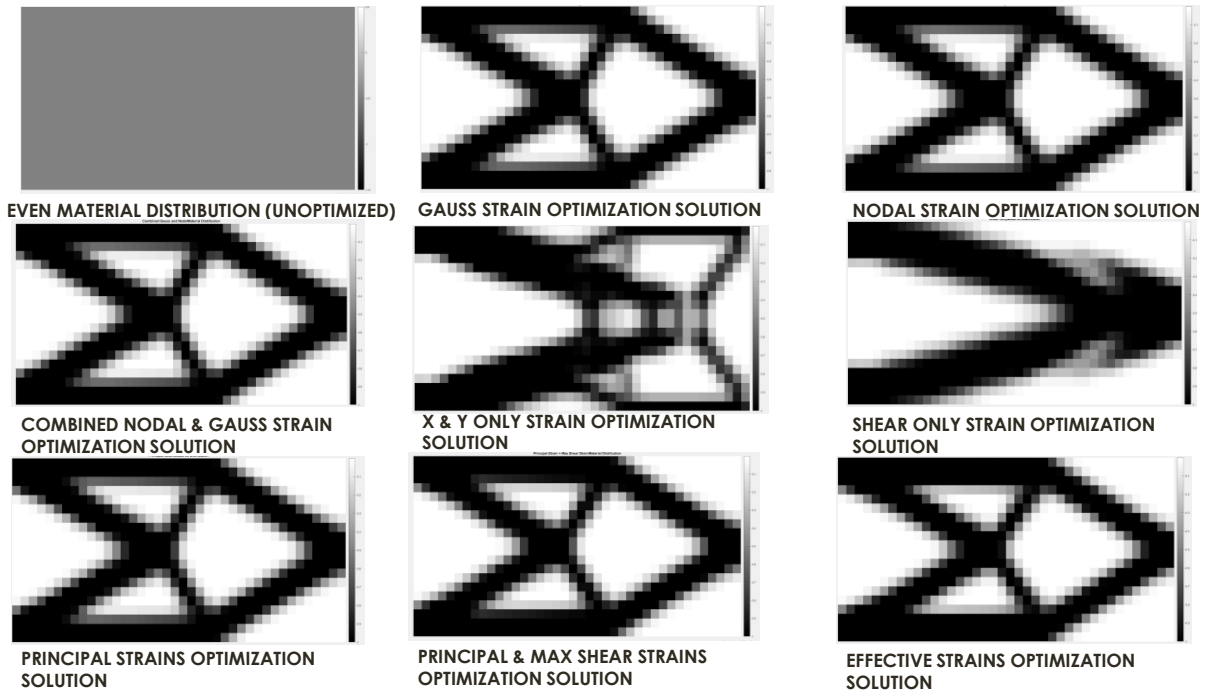


**Figure 39 Load Case 4- Material Layout Solutions for Various Strain Implementations**

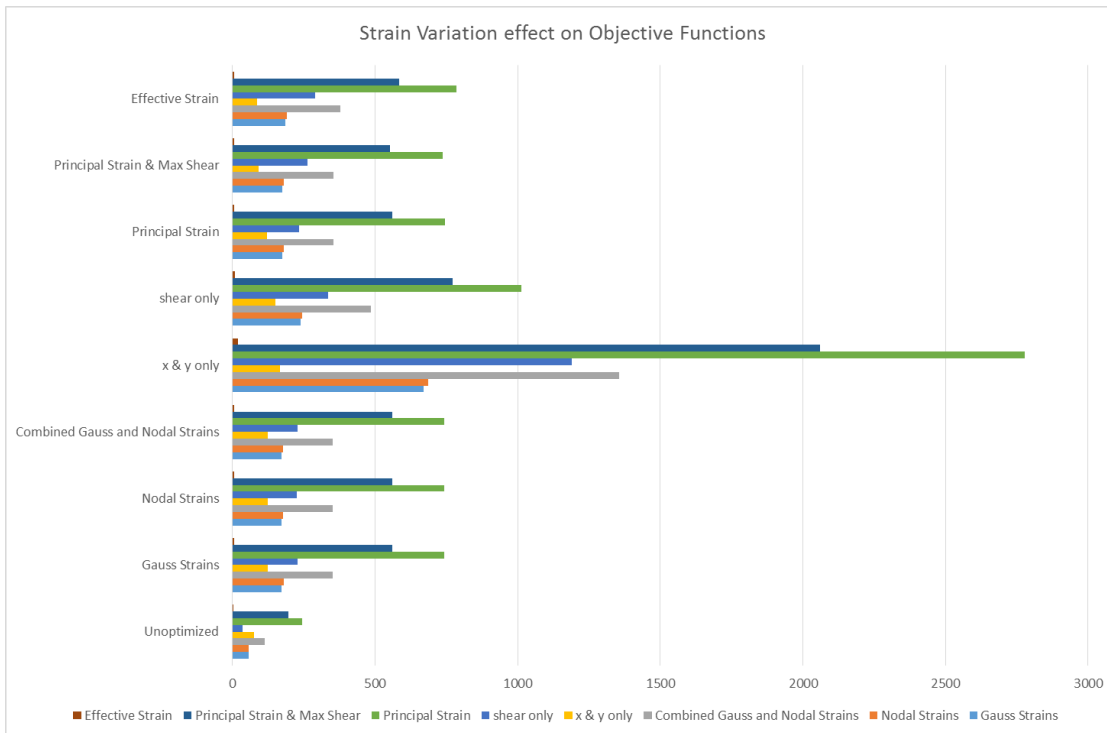


**Figure 40 Strain Variation Effect on Objective Functions-Load Case 4**

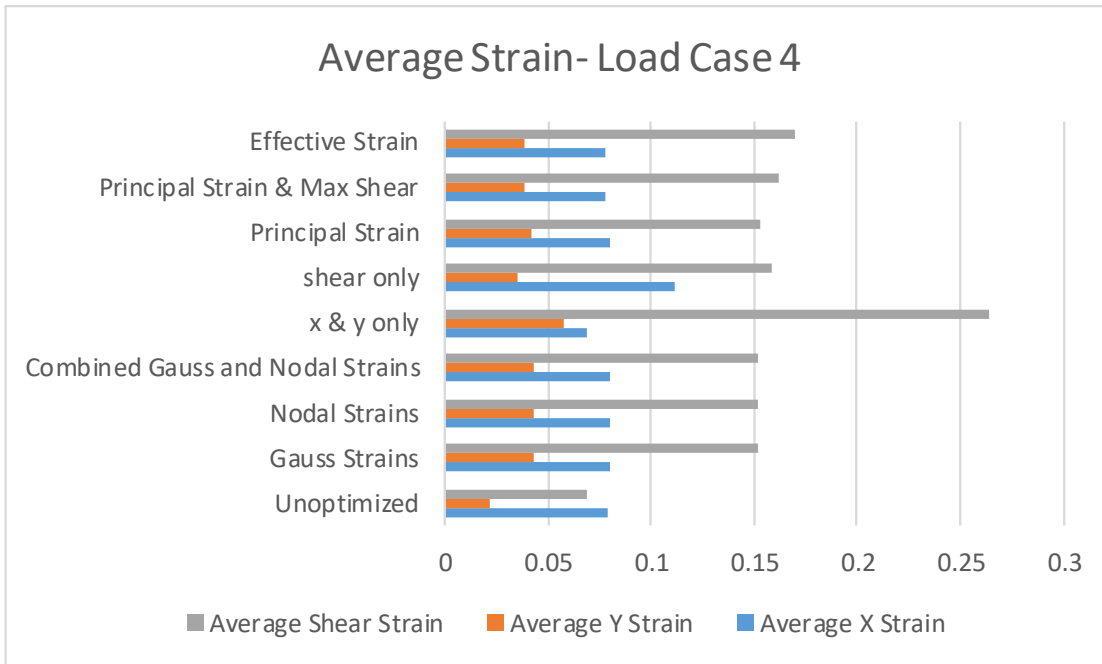


**Figure 41 Average Strains for the Strain Objective Functions - Load Case 4**

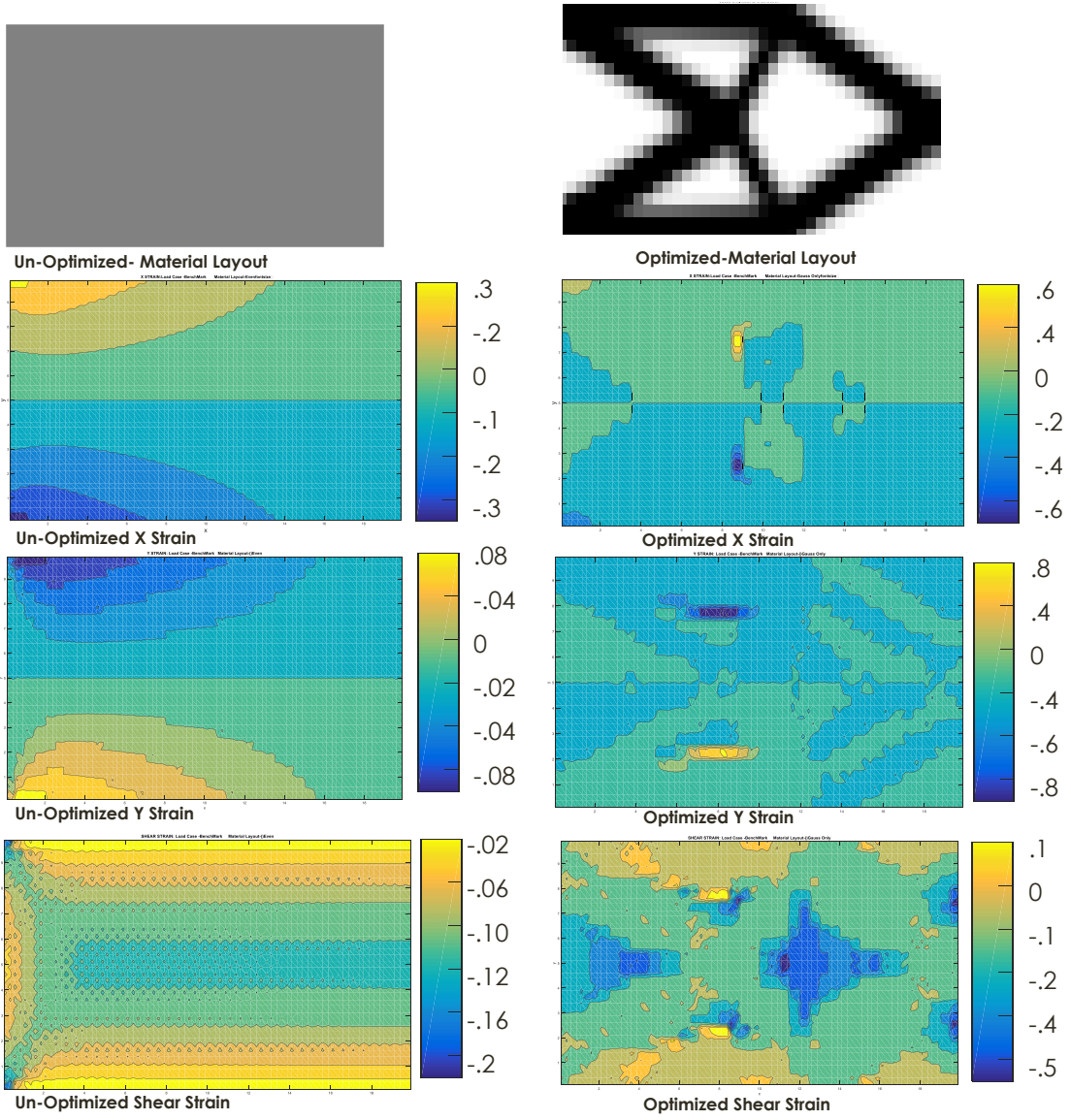


**Figure 42 Strain Plots for Load Case 4 Optimization**

Examining the behavior of the isolated y displacement boundary condition, Load Case 4, it can be seen that the transverse boundary condition drives the structure to a middle concentrated truss structure. Figure 39 shows the material solutions from the strain implementations. It can be seen that the X and Y Only Strain converges to a structure very similar to a shape typically called a force inverter. The Shear Only objective function converges to two diagonals converging to the center. The other objective functions, combinations of x, y, and shear strains, result in a truss like structure that converges to the middle. Figure 41 shows that the optimized solutions result in higher average x, y, and shear strains. Figure 42 shows that while the magnitudes of the maximum and minimum strains have increased, the optimization effect made the shapes appear to have increased the areas the lower strains are acting in and decreasing the relative higher strains found in the upper and lower left hand corners of the beam.

#### **4.1.4 Conclusions from Single Load Case Implementation**

From examining the strain variances, it can be seen that overall, no strain objective function from Table 1 was found to have any difference or improvement from the others and converged to the same material solution apart from the X and Y Only Strain objective function and the Shear Only objective function. This objective function was able to be minimized, marginally, because it did not include the shear term that worsens dramatically, driving the increase in objective function. The Shear Only objective function produced a different material solution but it did not improve any of the strains. It was decided to only use two objective functions in the following work, the Gauss and Nodal Strain objective function and the X and Y Only Strain objective function.

From looking at the X and Y combined displacements and isolating their respective influencing behavior, it can be seen that the axial displacements resolve the material the top and bottom of the bar and the transverse behavior converges to a modified force inverter, or a symmetric diagonalized truss structure. The combination of these results in a diagonalized single bar structure. While the topology for the problem of interest is able to marginally decrease the x and y strains, the shear strains are worsened for every strain variation examined, this indicates that a linear analysis approach is not effective for the non-linear shear strains. From examining the isolated x and y displacement boundary conditions, it can be seen that while optimization behavior does not

minimize the average or maximum values, it does reduce the areas the x and y strain are highest in and increases the area the lowest strains are acting in. For the x displacement only boundary condition, the magnitude of the x and y strains that act over the largest areas are reduced. For the y displacement only problem, Load Case 4, the effect is the decrease the relative strains in the right hand side upper and lower corners (which result in high strains from the fixed boundary conditions).

## 4.2 Volume Fraction Effect

The volume fraction is the total amount of material allowed across the structure. For example, a volume fraction of 0.5 means that the optimized structure will have 50% material volume of the original structure, this is standard in topology. To see if changing the volume fraction had any effect on the resultant solution, volume fraction was varied from the minimum material density, 0.001, to the maximum density of 0.99. Single Load Case Topology Optimization was applied to Load Case 1 with the Combined Nodal and Gauss Strain Objective Function and using an element size of 2.0.

Figure 43 shows the optimization solutions for the varied volume fractions. It can be seen that for the maximum amount of material, .99, there is very little change due to the limit of material being one. Per the topology method, elements with the least objective function have material density decreased and the elements with highest objective function have material increased, but with almost all elements already being at very close to one, or the maximum density, little change is needed to give the highest objective function elements a maximum material density. Similarly, for the minimum material density, 0.001, there is no change at all because the material density cannot be less than the minimum, 0.001, so no density can be decreased to increase elements with higher objective functions. Looking at intermediate densities, from 0.3 to 0.7, it can be seen that the general material trend is the same with material being first increased in the middle diagonal and creating a thicker diagonal as more material is available to add, or as the volume fraction is increased.



**Figure 43 Effect of Volume Fraction on Resultant Solution**

### **4.3 Various Material Starting Configuration Effects**

To verify that the solution is robust against the initial material layout, various material starting points were given. Single Load Case Topology Optimization was applied to Load Case 1 with the Combined Nodal and Gauss Strain Objective Function and using an element size of 1. Figure 44 shows the initial material layout and the optimized solution layout. It can be seen that the algorithm will converge to the same solution regardless of starting material layout.

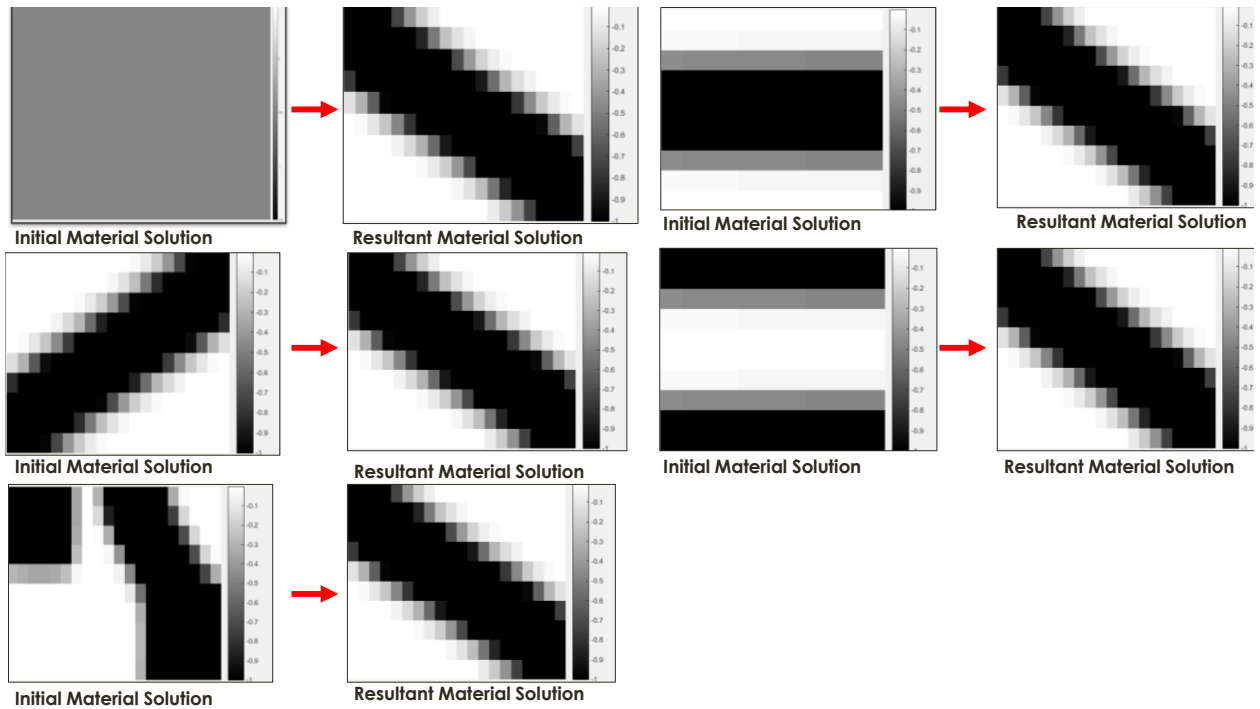


**Figure 44 Effect of Material Starting Configurations and Resultant Solution**

#### **4.4 Varying Aspect Ratio Effect on Optimization Result**

This work is interested in evaluating whether strain-based topology can provide compliant optimized solutions to morphing structures, so it is of interest to survey the results for variations of the problem of interest. Having a good understanding of the resultant solutions based on dimension of the 2D structure and the boundary conditions can provide initial insight into the design of a structure for a morphing problem. Single Load Case Topology Optimization was applied to Load Case 1 with an element size of 0.5. The dimensional aspect ratios, the ratio of the length to the height, and displacement aspect ratios, the ratio of the y displacement to the x displacement, were varied. The resultant material solutions can be seen in Figure 45. Note: due to the varying dimensions of the material solutions, the material layouts axis are squared such that they fit compactly and for comparison.

Based on the results shown in Figure 45, a few trends can be observed. Increasing the Length to Width Ratio, or have a very high length and short height, concentrates the material in the middle

of the bar while the converse, low length and large height, concentrates material in the top and bottom of the bar. For the x and y displacement ratios, a high displacement ratio, large transverse displacement compared to axial displacement, results in material being concentrated in the center, in a diagonal stair step, while the inverse, axially dominant, concentrates material on the outer portions of the bar.

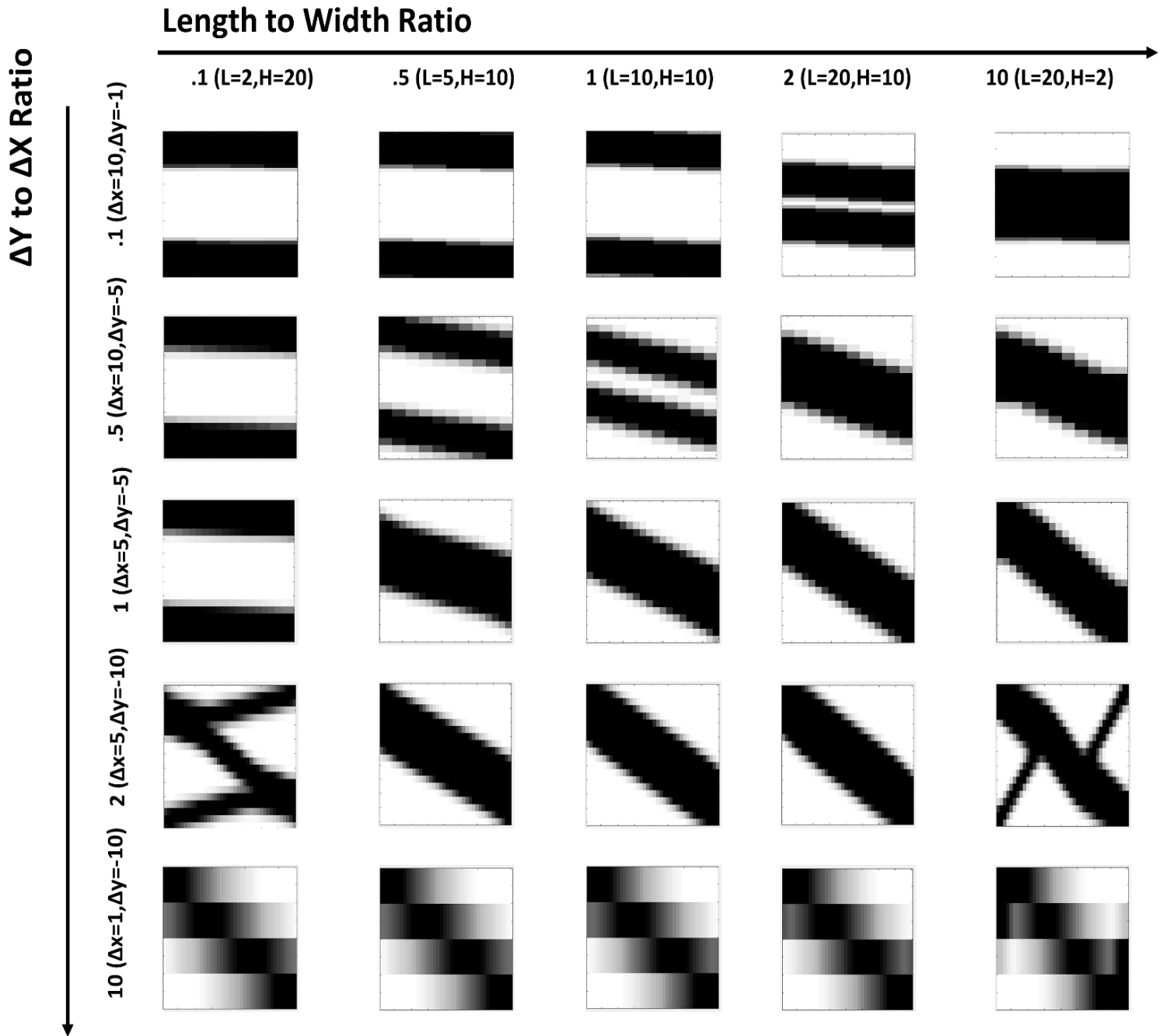


**Figure 45 Effect of Varying Aspect and Displacement Ratios on Resultant Solution**

## **4.5 Application of Strain Based Topology to Problem of Interest- Multiple Load Case**

Having observed the strain implementation behaviors on the single load case deflection and observing the dominating behavior from each the X displacements and Y Displacements, it was decided to apply only the Combined Gauss and Nodal Strains Objective Function, and X & Y Strains Only Objective Function, to the Multiple Load Case Optimization. The problem of interest was optimized subject to both Load Case 1 and Load Case 2 and the results are given in Section 4.2.1. Because X Displacement in the negative direction, or compression, was not considered due to the problem being modeled, Multi-Load Case Optimization was not applied. For the Y Displacement Only, Load Case 4 and Load Case 5 were applied, and the results are given in Section 4.2.2. Discussion of the results of the Multi Load Optimization is given in Section 4.2.3.

### **4.5.1 Multi Load Optimization for X & Y Displacement Problem**

For the Multiple Load Optimization of the problem of interest, optimized to both Load Case 1 and Load Case 2, an element size of 0.5 was used (800 elements total). Figure 46 shows the starting material distribution and resultant optimization solutions for both the Combined Gauss and Nodal Strains Objective Function and the X & Y Only Objective Function. Figure 47 shows how each strain objective function effects the average values of x, y, and shear strains respectively.

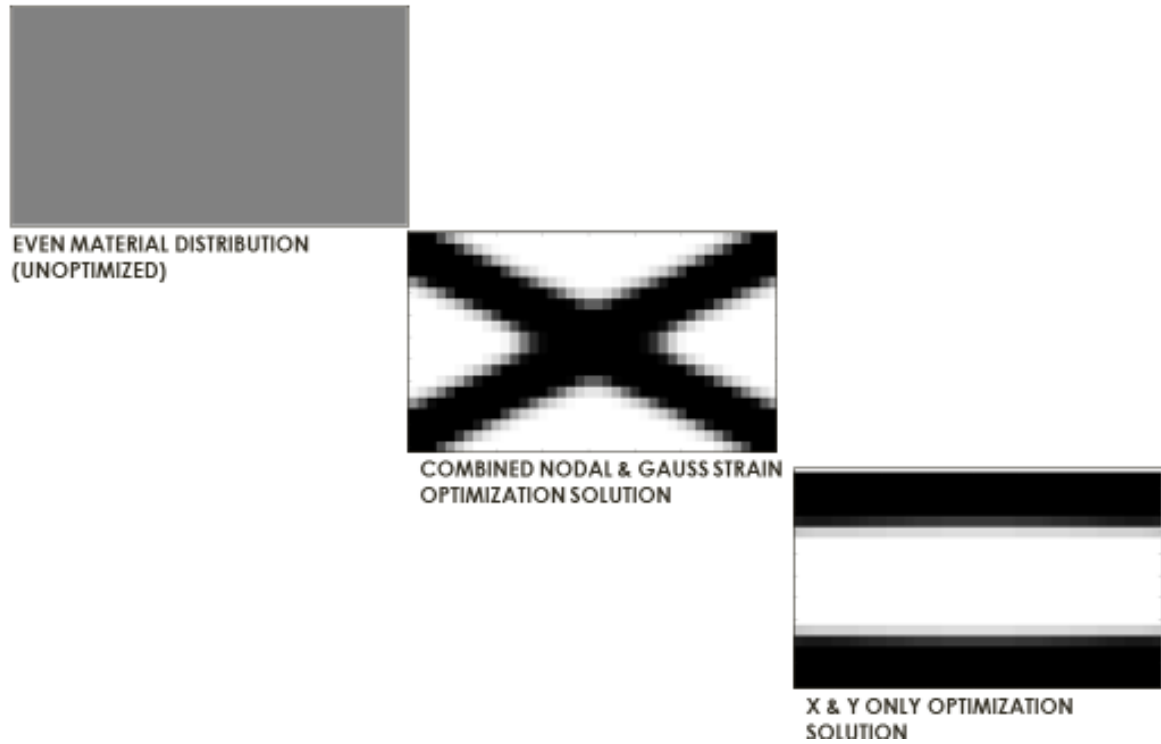


**Figure 46 Material Solutions for Multi-Load Case Optimization**

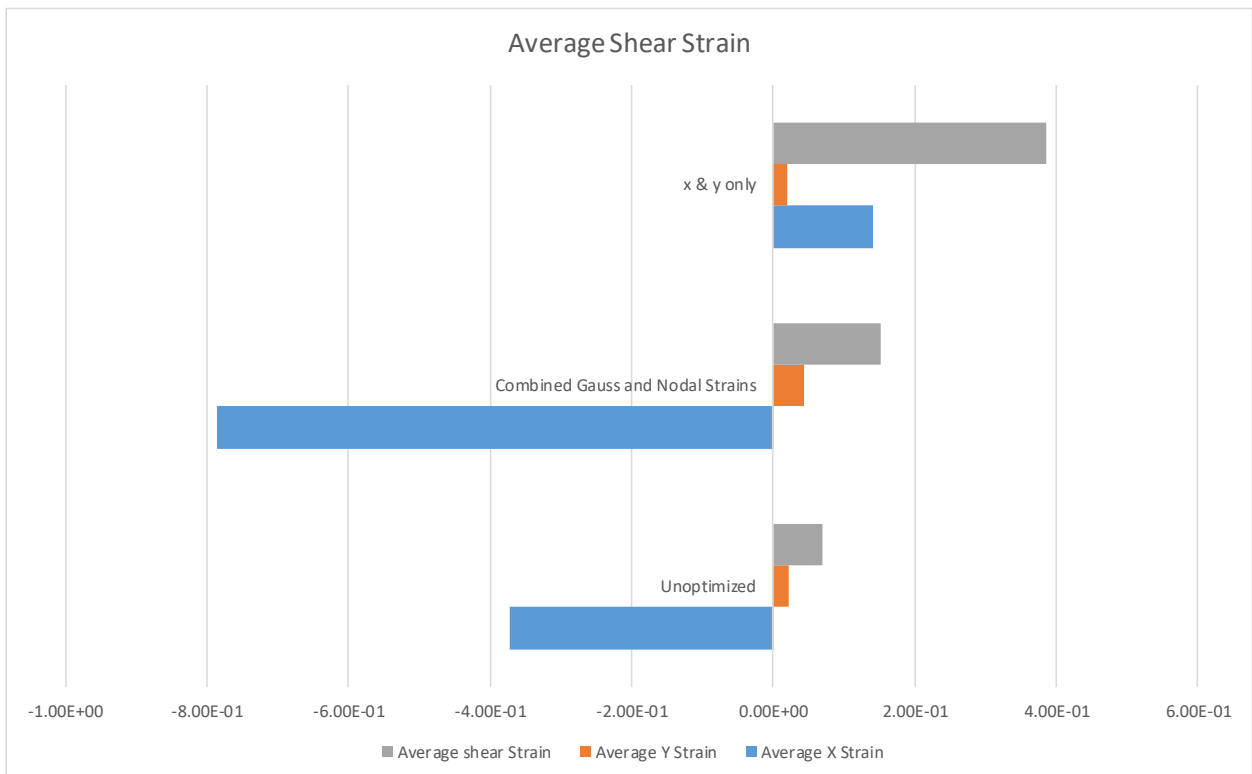


**Figure 47 Average Strains for Multi-Load Optimization- Load Case 1 & 2**

For the X and Y Displacement problem using multiple load optimization, considering both Load Case 1 and Load Case 2, the resultant material solutions can be seen in Figure 46. It can be seen that the inclusion of shear dramatically changes the results. Using the Combined Nodal and Gauss Strains, the material solution is a cross, or rather the combined solutions from the single load case solution of Load Cases 1 and 2. Optimizing to only the X and Y Strains, the optimized solution is a top and bottom material concentrated bar. For these material solutions, Figure 55 shows that the X and Y Strains Only solution decreased the average X and Y Strains, while the cross structure worsens them. However, the shear strains are worsened in both cases but more so in the X and Y Strain Only optimization solution.

#### 4.5.2 Multi Load Optimization for Y Only Displacement Problem

For the Multiple Load Optimization of the Y Only Displacement Problem, optimized to both Load Case 4 and Load Case 5, an element size of 0.5 was used (800 elements total). Figure 48 shows the starting material distribution and resultant optimization solutions for both the Combined Gauss and Nodal Strains Objective Function and the X & Y Only Objective Function. Figure 49 shows how each strain objective function effects the average values of x, y, and shear strains respectively.

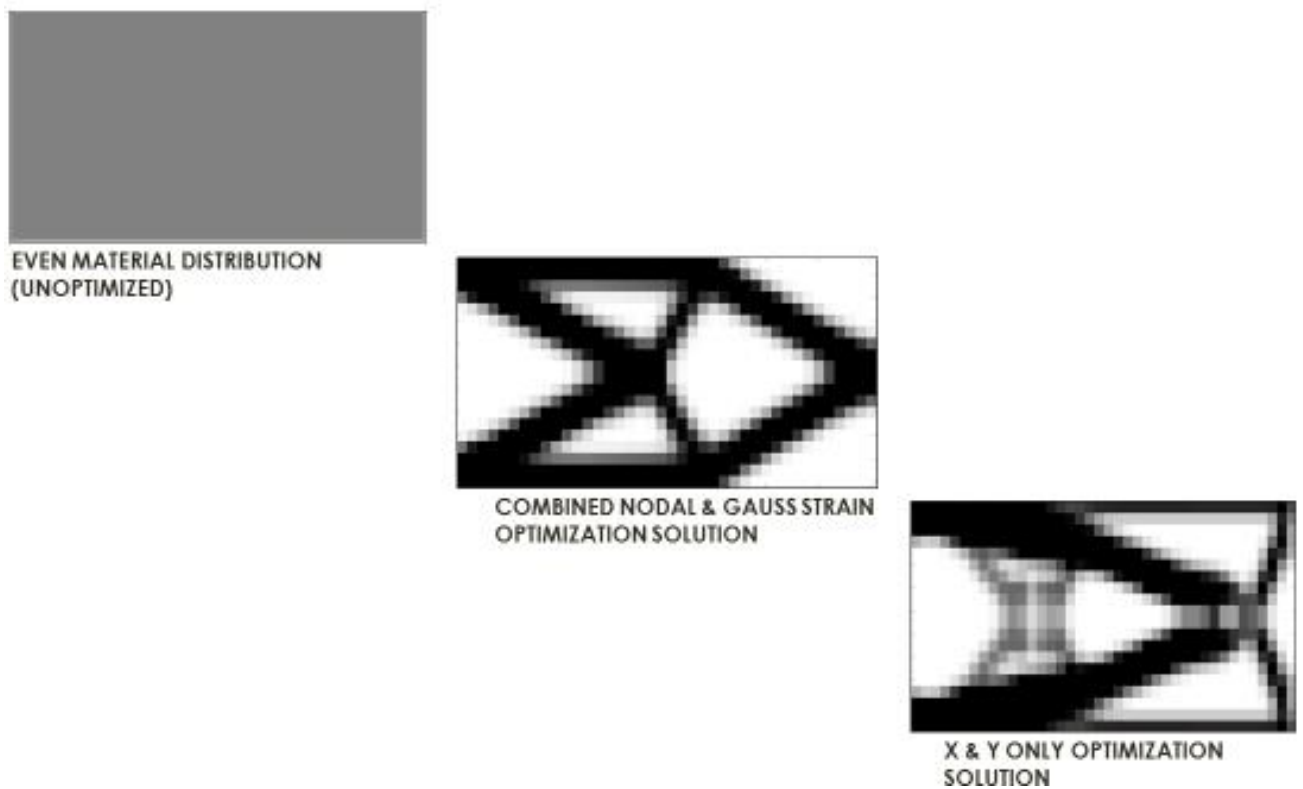


**Figure 48 Material Layout Solutions for Multiple Load Case Optimization**

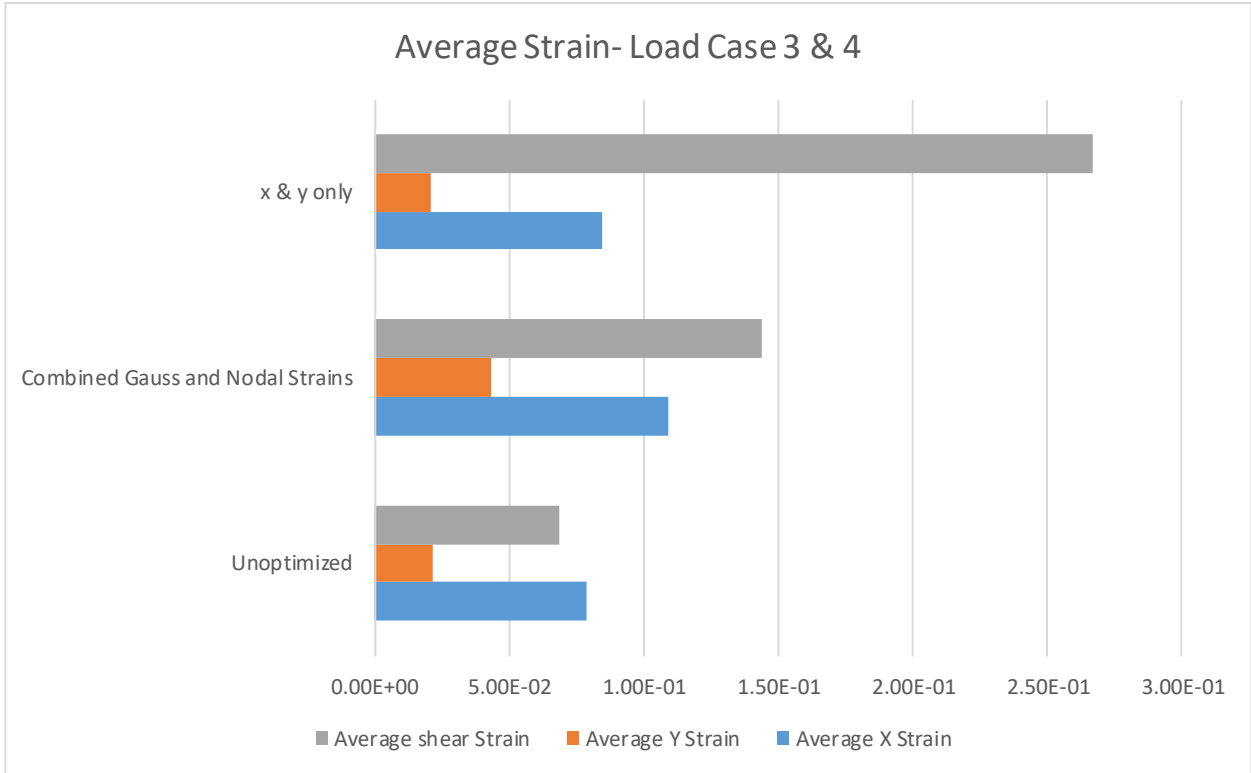


**Figure 49 Average Strains for Multi-Load Optimization- Load Case 4 & 5**

Examining the multiple load condition optimization results for the transverse, or y, displacement boundary conditions, it can be seen that it is also very similar to the single load case results. Figure 49 shows that the optimized solutions, however, increase strains across the board.

#### 4.5.3 Discussion of Multiple Load Case Implementation

Based on the multiple load case results, it can be seen that the topology optimization does a good job of optimizing to multiple load cases and converging to a solution. The worsened strains are not a function of optimizing to multiple load cases but result from the single load cases worsening strains as well. Future work that enables the strain based topology to converge and minimize objective functions for the large boundary condition, over constrained problems, for single load cases will improve the solution for the multiple load optimization solutions as well.

## 4.6 Evaluation of Optimized Solutions for Various Load Cases

After having produced the optimized solutions in the sections above, the next step was to evaluate whether the solutions are actually optimal solutions. The optimal solutions produced were evaluated against each other and against the initial un-optimized structure to compare the displacements, strains, and stress. The results are given in Section 4.6.1 and discussed in Section 4.6.2.

### 4.6.1 Results of Material Solutions Evaluation

Figure 50 shows the material solutions being evaluated for Load Cases 1-5. Figure 51- Figure 54 compares x, y, and shear strains for each material solution.

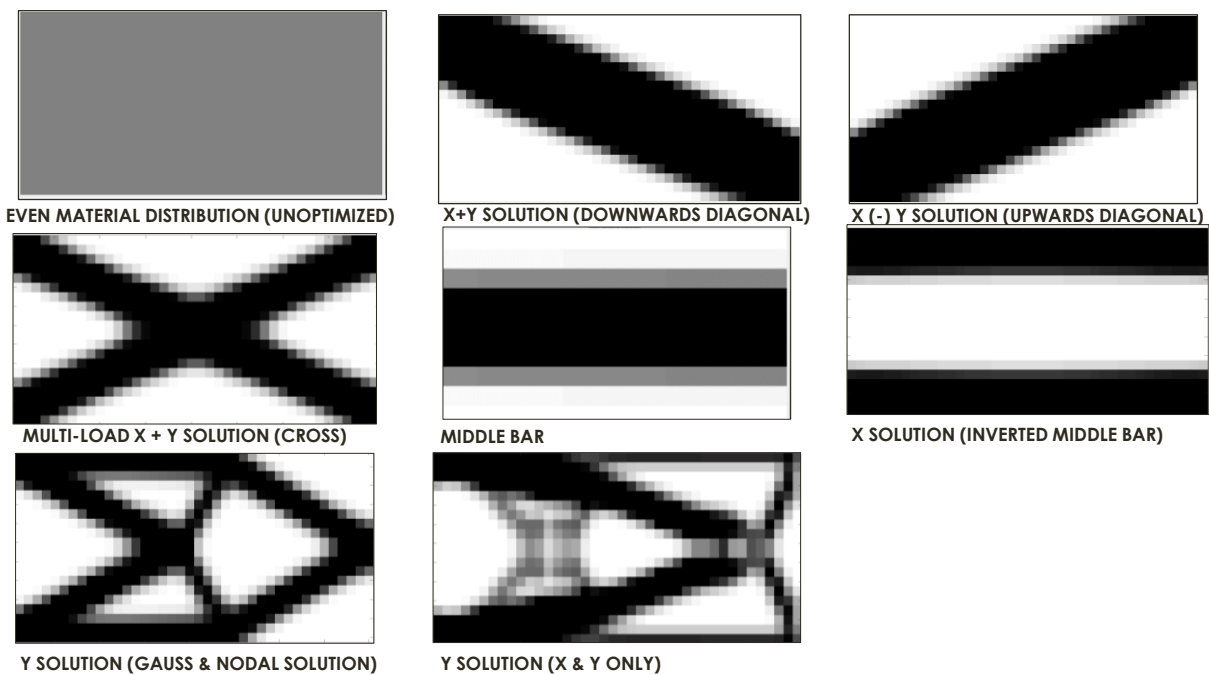


**Figure 50 Material Layouts being evaluated**

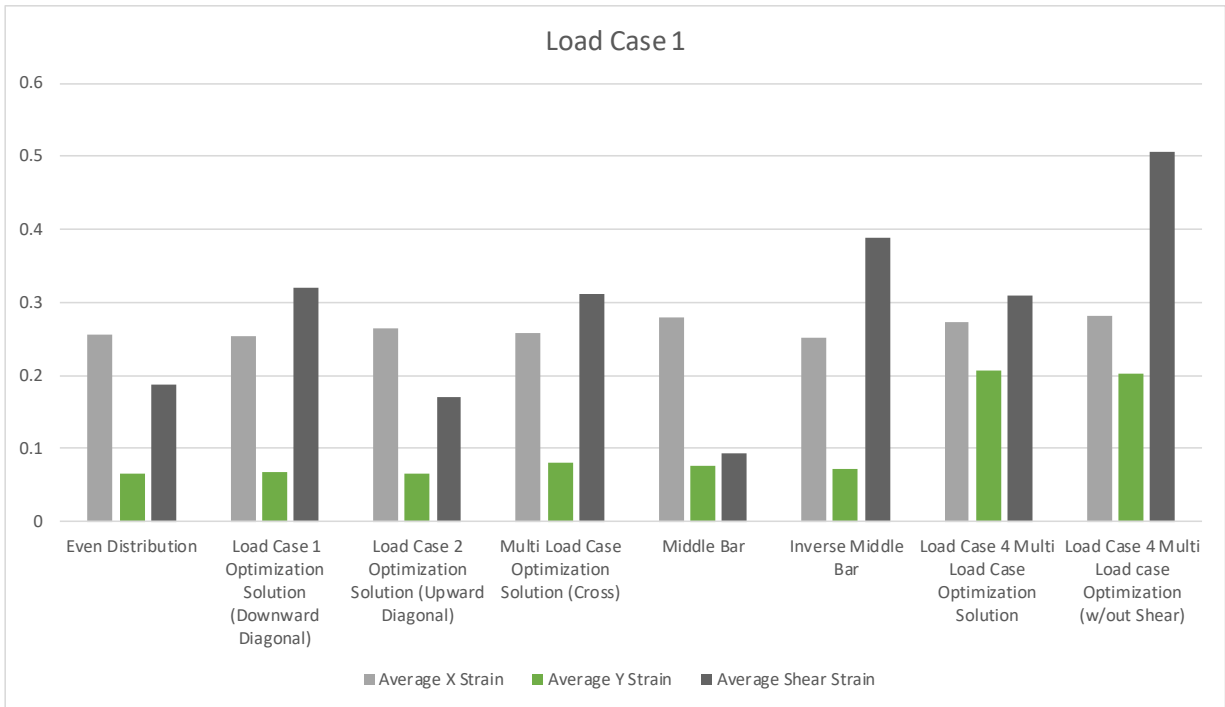


**Figure 51 Load Case 1 Strain Comparison**

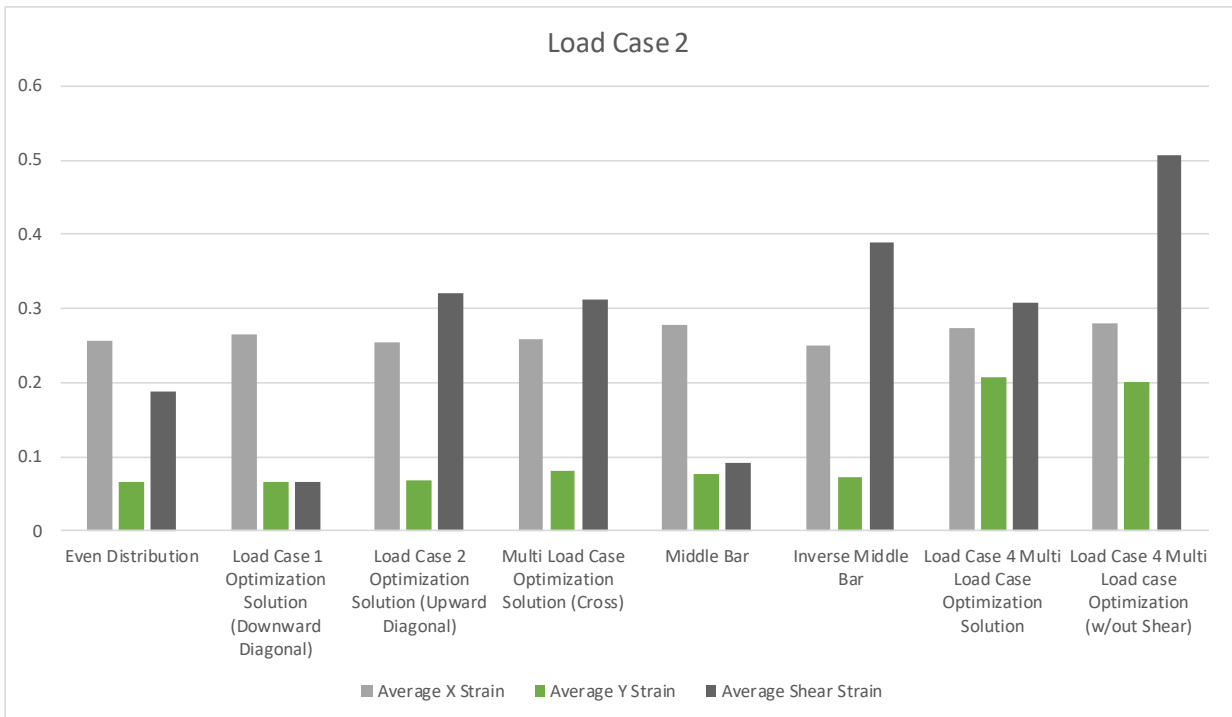


**Figure 52 Load Case 2 Strain Comparison**

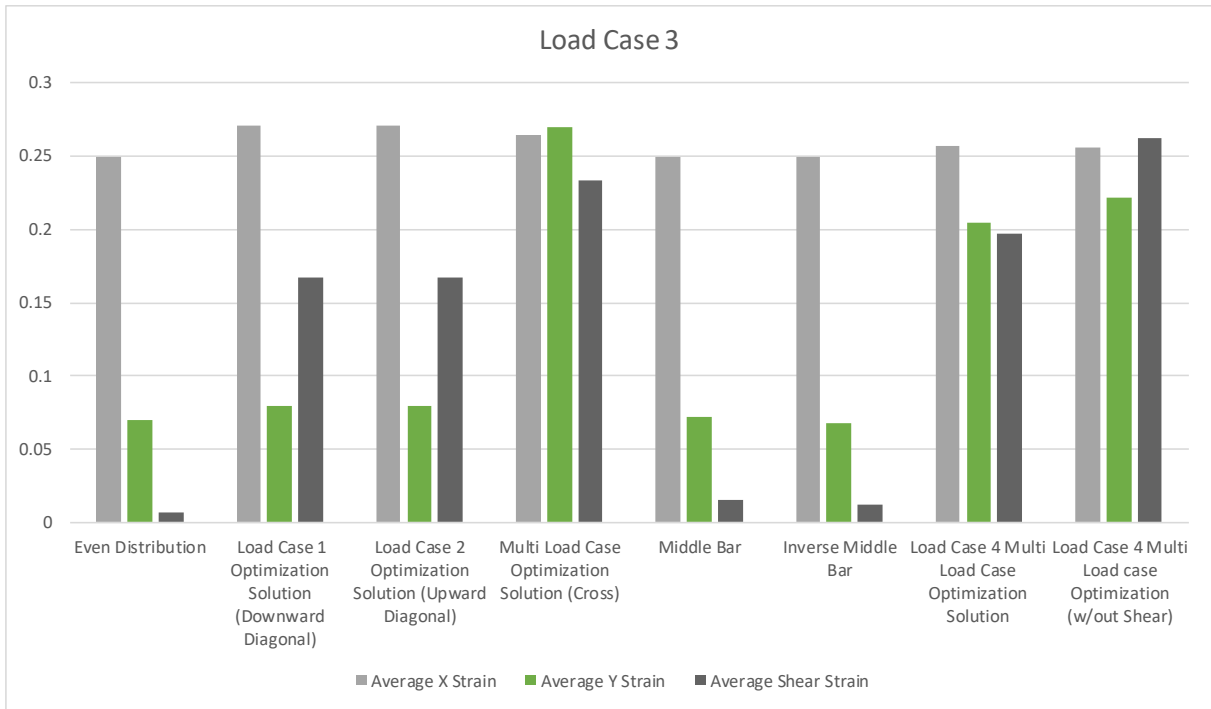


**Figure 53 Load Case 3 Strain Comparison**

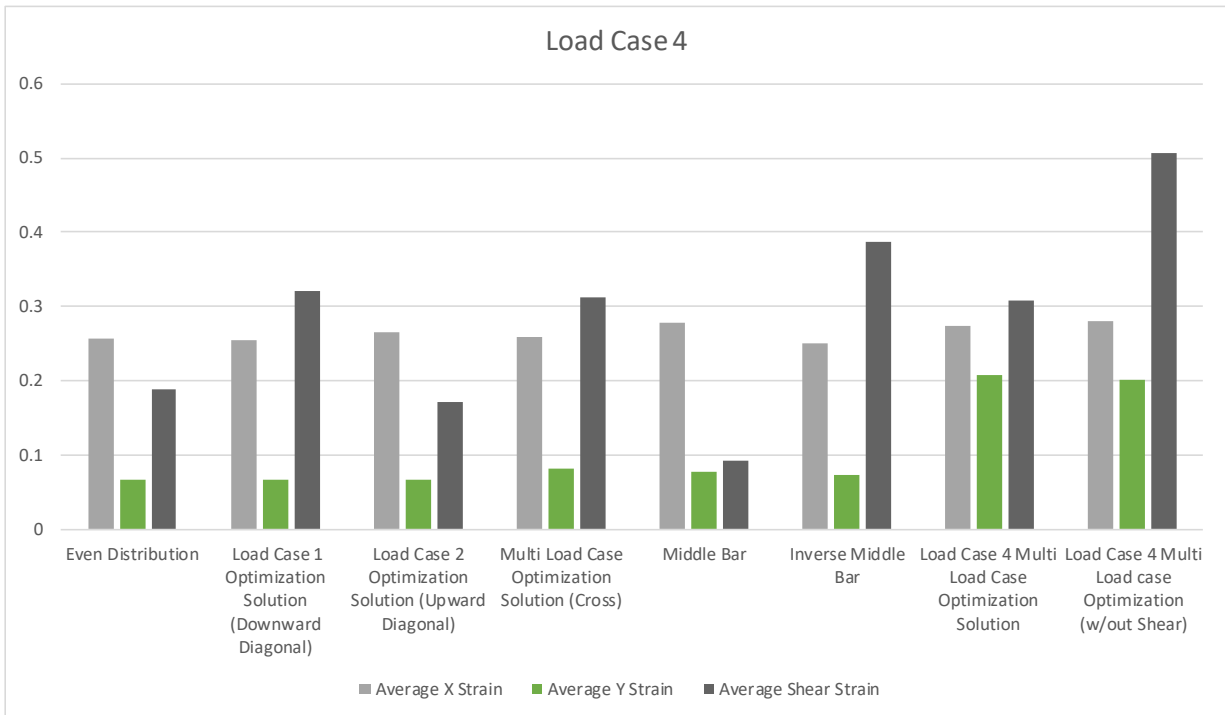


**Figure 54 Load Case 4 Strain Comparison**

**4.6.2 Discussion of Material Solutions Evaluation**

Examining the Load Case 1, results for the material layouts being tested, Downward Diagonal decreases the average x and y strains and the middle bar decreases the shear. The worst performing solutions are the multiple load cases solutions for Load Case 4 which have increased almost every variable. Load Case 2, has similar results except in place of the Downward Diagonal the Upward Diagonal performs best alongside the Middle Bar. For Load Case 3, no improvements can be seen from any of the solutions, all the other material layouts increase the strains and perform poorly. For Load Case 4, similar to Load Case 1 results, the Downward Diagonal is able to marginally decrease the x and y strains and the Middle Bar is able to decrease the average shear strain.

After comparing the optimized solutions to the un-optimized, even, material distribution, it can be seen that looking at only the strain averages, the solution does not show significant improvement compared to the initial layout.

## **4.7 Comments on Strain Based Topology Optimization of Problem of Interest**

Based on the results in Section 4.1, it can be seen that the examined strain based objective functions converged to the same material solution. The use of the original strain energy based objective function in place of a strain based objective also produced the same result. This result is consistent with the fact that for elements with constant Young's Modulus, the sum of the strain energies is the same as the sum of the strains. Similarly, the strain energy summed across the element is effectively the same when taken at the nodal and gauss points. Additionally, when examining the same resultant solution for the various strain based objective function, it can be seen that this result is consistent with the fact that strain energy is invariant with coordinate transformation such that using principal strains is the same as using the x, y, and shear strains. Further examining the optimized layout, it can be seen that an axial bar is produced as the optimal solution. Considering that the optimization problem is minimizing compliance, or minimizing strain energy or strain for this problem with constant Young's Modulus, or alternately producing the stiffest possible structure, the axial bar is the optimum stiff structure.

From these observations, several opportunities for future work on this problem can be given. First, as previously mentioned in Chapter 1, multi-material manufacturing can incorporate several materials, of varying properties such as Young's Modulus, into a single structure. This is useful for realizing topology structures but also can provide opportunity to expand topology to incorporate multiple Young's Modulus [71]. Using this, the starting material configuration could be modified to have various elemental Young's Modulus which could produce different results for strain energy and strain based objective functions. Second, it can be seen that while an optimal solution was produced for the optimization problem set up, a rigidity design problem, the optimization problem should be expanded to encompass both rigidity and flexibility design objectives. For the flexibility design, compliance is maximized at select nodal displacements, or mutual potential energy, (Eq. 2.18). Rigidity based design, as employed, minimizes the compliance, strain or strain energy, across the structure (Eq. 2.12). Future work should update the optimization problem to a multi-objective one that incorporates both the flexibility and rigidity designs, minimizing Eq. 2.12 while maximizing Eq. 2.18 [70]. Furthermore, flexibility design minimizes the actuation force at the specified nodal locations, instead of a specified displacement, so consideration should be given to the physical programming and approach to the imposed boundary conditions.

Lastly, as mentioned in Chapter 1, the Flexsys design provides a corrugated structure or "accordion-like" structure as a solution to the morphing challenge of interest. However, the optimized result is an axial bar. The structural optimization of corrugated structures for morphing applications have been studied due to its anisotropic behavior, stiff in the corrugation direction, but flexible in the transverse direction [45]. Therefore, in addition to including flexibility and rigidity design objectives, altering the problem to be a plate in bending, which was not previously assumed should also be considered to see if the resultant optimization, or the resultant structure that gives the least force required to displace the bending plate, is an "accordion-like" or corrugated structure.

# CHAPTER 5: CONCLUSIONS AND FUTURE WORK

## Thesis Overview and Summary of Conclusions

This work introduced the motivation for finding solutions to morphing problems and the interest in investigating whether a strain based topology method would produce an optimal solution, particularly now that theoretical structures produced by topology optimization can now be realized via multi-material additive manufacturing. A thorough literature review on these subjects was presented in Chapter 1. Chapter 2 gave an overview on the method of finite element analysis, gave details on the FEM program developed by the author, and provided validated of the Matlab implementation of the author's FEM program.

Topology optimization was introduced in Chapter 3. Chapter 3 also introduced new strain based objective functions for topology optimization and the results were discussed. Based on the results of Chapter 3, the implementation of a strain-based objective function for problems that are typically solved in topology optimization, like the MBB Beam, is effective. The objective functions are effectively minimized. However, moving on to problems not typically solved in topology optimization, such as the large displacement problems like the problem of interest, the topology optimization is not able to produce solutions that effectively minimize the objective functions, this is seen in Chapter 4. Based on the lack of convergence across the many strain variations tested, this is likely a result of the linear strain-displacement relationship of the  $x$  and  $y$  strains. The large strains are linearly related to the large displacements that are unable to be minimized due to the fact that they are boundary conditions. Additionally, the shear strains, which are non-linear, are not able to be solved either, most likely due to the linear analysis approach of this problem and the non-linear nature of shear strains.

Chapter 4 applied the strain based topology optimization to the discussed problem of interest and discussed the results. Aside from the non-convergence of this type of problem, it was found that transverse displacement conditions drive a symmetric truss like shape that converges to the middle of the displaced end. The axial displacement conditions drive a top and bottom material concentration bar. It was found that the combined axial and transverse displacements drive diagonalized bar. It was found that the  $x$  and  $y$  strains for these problems could be marginally improved but the shear strains increased significantly. Furthermore it was found that the inclusion

of shear strains in the objective function greatly changes the shape for the isolated axial and transverse displacement conditions. It was found that for strain based topology optimization applied to a morphing problem, the magnitudes of the maximum and average strains are not improved but the stress concentrations are reduced. In Section 4.2 it was found that the general shape is not affected by the volume fraction except when limited to maximum material density and minimum material density. Section 4.3 found that the approach is robust to starting material configuration and will converge to the same solution. Aspect ratio and displacement aspect ratio were shown in Section 4.4 and found that increasing aspect ratio changes the shape from an inverted middle bar to a middle bar and that increasing displacement aspect ratio diagonalizes the material layout to the direction of the applied transverse loading.

In Section 4.5, it was found that the approach effectively does find optimized solutions for multiple load cases, though the overall increase in objective function found in the single load cases optimization was also found in the multiple load case optimization. The overall performance of the material solutions found in the previously mentioned sections was evaluated in Section 4.6. It was found that while some variables, such as maximum x strain or average y strains, were able to be decreased in some of the load cases, an optimal solution decreasing all the strains in all load cases was not obtained.

In Section 4.7, the application of a strain based topology to the problem of interest was discussed. The various strain based objective functions and the original strain energy objective function were found to converge to the same material solution due to invariance among coordinate transform and uniform Young's Modulus. Additionally, the resultant material solution, an axial bar, was discussed to be the "stiffest" or most rigid design which is consistent with the optimization problem set up based on a rigidity design objective.

## **Future Work and Conclusion**

Based on these conclusions, strain based topology is a good approach in typical topology problems. However, the types of problems of interest in this work, the large displacement boundary conditions, are able to reduce the relative stress concentrations but not the objective functions, or average strains, via topology optimization. As discussed in Section 4.7, several changes to the optimization problem should be considered for future work. The incorporation of non-uniform Young's Modulus in the starting material configuration should be considered to see if this produces a difference in strain energy versus strain based objective function results. The optimization

problem should be extended to include both rigidity and flexibility design objectives. Additionally, the problem should be set up to include a plate in bending. Further work should also investigate non-linear analysis for the updating scheme to see if another approach could reduce the magnitude of the strains. Additionally, many factors were not investigated thoroughly in the topology approach. Future work should investigate whether removing or refining the sensitivity filter will improve the results and still converge to a stable solution. Future work should also explore the effect on the penalty number has on strain based topology optimization. The penalty number, typically 3, for the topology method has been extensively explored and validated for the displacement minimization problem; however, it may have different results for the strain minimization problem. Other future work considerations should include applying different material properties, Young's modulus and Poisson's ratio, and distributed loading to simulate aerodynamic forces.

While this work did not find that the current topology approaches with modifications to the objective function effectively solved the problem of interest with respect to reducing the magnitude of the strains, it did successfully implement in typically topology problems and reduce the relative stress concentrations in the morphing problems. Additionally, this work validated and showed consistent with the expected results for a rigidity based design objective, an axial bar, with constant Young's Modulus. However, it also provided motivation for the necessity in pursuing compliant, or rigidity and flexibility based designs, mechanism design for this type of problem since the resultant optimal structure produces stiff and increased strain objective functions results. Furthermore, interest in morphing structures will only increase with increasing performance demand for aircraft. Therefore motivation for finding optimal solutions to morphing structures is still as relevant as ever. Further pursuit and implementation of future work to the strain based topology method could yield the desired optimal solution.

## BIBLIOGRAPHY

1. Gibbs-Smith, C.H., *Clément Ader: his flight-claims and his place in history*. 1968: HMSO.
2. NASA, *Airplane Parts and Function*, in <https://www.grc.nasa.gov/www/k-12/airplane/airplane.html>. NASA: [www.grc.nasa.gov](http://www.grc.nasa.gov).
3. Kota, S., P. Flick, and F.S. Collier. *Flight Testing of FlexFloil™ Adaptive Compliant Trailing Edge*. in *54th AIAA Aerospace Sciences Meeting*. 2016.
4. Thill, C., et al., *Morphing skins*. The aeronautical journal, 2008. **112**(1129): p. 117-139.
5. Precup, N., M. Mor, and E. Livne. *The design, construction, and tests of a concept aeroelastic wind tunnel model of a high-lift variable camber continuous trailing edge flap (HL-VCCTEF) wing configuration*. in *56th AIAA/ASCE/AHS/ASC Structures, Structural Dynamics, and Materials Conference*. 2015.
6. Rodriguez, A.R. *Morphing aircraft technology survey*. in *45th AIAA aerospace sciences meeting and exhibit*. 2007.
7. Barbarino, S., et al., *A review of morphing aircraft*. Journal of Intelligent Material Systems and Structures, 2011. **22**(9): p. 823-877.
8. Love, M., et al., *Impact of actuation concepts on morphing aircraft structures*. AIAA Paper, 2004. **1724**: p. 2004.
9. Jha, A.K. and J.N. Kudva. *Morphing aircraft concepts, classifications, and challenges*. in *Smart structures and materials*. 2004. International Society for Optics and Photonics.
10. Kota, S., et al. *Design and application of compliant mechanisms for morphing aircraft structures*. 2003.
11. Kudva, J.N., et al. *Overview of the DARPA/AFRL/NASA smart wing program*. in *Smart structures and materials 1999: industrial and commercial applications of smart structures technologies*. 1999. International Society for Optics and Photonics.
12. Campbell, I., D. Bourell, and I. Gibson, *Additive manufacturing: rapid prototyping comes of age*. Rapid prototyping journal, 2012. **18**(4): p. 255-258.

13. Lyons, B., *Additive manufacturing in aerospace: Examples and research outlook*. The Bridge, 2014. **44**(3).
14. Brackett, D., I. Ashcroft, and R. Hague. *Topology optimization for additive manufacturing*. in *Proceedings of the solid freeform fabrication symposium, Austin, TX*. 2011. S.
15. Ader, C., *Military Aviation*. 2003, AIR UNIV PRESS MAXWELL AFB AL.
16. Weisshaar, T.A., *Morphing aircraft systems: historical perspectives and future challenges*. Journal of Aircraft, 2013.
17. Lang, J.M., *Hinge structure for aircraft surfaces*. 1949, Google Patents.
18. Davey, F.H., *Aerofoil*. 1928, Google Patents.
19. Parker, H., *The parker variable camber wing*. 1920.
20. Burnelli, V., J., 1933, *Aircraft*. US Patent, (1,917,428).
21. Gallaudet, E.F., *Aeroplane*. 1916, Google Patents.
22. Perry, R. *Variable Sweep: A Case Study of Multiple Re-innovation*. in *AIAA 3rd Annual Meeting*. 1966.
23. Stevenson, J.P., *Grumman F-14" Tomcat"*. 1975: Aero Publishers.
24. Leone, D. *U.S. Navy's Last F-14 Tomcat Flight, On This Day, In 2006*. 2013 [cited 2018 march 11].
25. Wlezien, R., et al. *The aircraft morphing program*. in *39th AIAA/ASME/ASCE/AHS/ASC Structures, Structural Dynamics, and Materials Conference and Exhibit*. 1998.
26. Wax, S., G. Fischer, and R. Sands, *The past, present, and future of DARPA's investment strategy in smart materials*. JOM, 2003. **55**(12): p. 17-23.
27. Suleman, A., et al. *Novel air vehicle configurations: from fluttering wings to morphing flight*. in *World Congress on Computational Mechanics (WCCM XI)*. 2014. Barcelona.
28. Prakash, T. and R.S. Pant. *Studies in telescopic span morphing of HALE UAV*. in *Mechanical and Aerospace Engineering (ICMAE), 2017 8th International Conference on*. 2017. IEEE.

29. Wang, X., W. Zhou, and Z. Wu, *Feedback tracking control for dynamic morphing of piezocomposite actuated flexible wings*. Journal of Sound and Vibration, 2018. **416**: p. 17-28.
30. Sun, J., et al., *Active inflatable auxetic honeycomb structural concept for morphing wingtips*. Smart Materials and Structures, 2014. **23**(12): p. 125023.
31. Doepke, E.B., M.K. Philen, and R.L. West. *Design and optimization of a morphing aileron control surface using FMC actuators*. in *Sensors and Smart Structures Technologies for Civil, Mechanical, and Aerospace Systems 2014*. 2014. International Society for Optics and Photonics.
32. Meng, X.G., L. Xu, and M. Sun, *Aerodynamic effects of corrugation in flapping insect wings in hovering flight*. Journal of Experimental Biology, 2011. **214**(3): p. 432-444.
33. Chen, Y., et al., *Structural design and analysis of morphing skin embedded with pneumatic muscle fibers*. Smart Materials and Structures, 2011. **20**(8): p. 085033.
34. Zhang, Z. and M. Philen, *Pressurized artificial muscles*. Journal of Intelligent Material Systems and Structures, 2012. **23**(3): p. 255-268.
35. Peel, L.D., et al., *Development of a simple morphing wing using elastomeric composites as skins and actuators*. Journal of Mechanical Design, 2009. **131**(9): p. 091003.
36. Georges, T., et al., *Design of shape memory alloy actuators for morphing laminar wing with flexible extradors*. Journal of Mechanical Design, 2009. **131**(9): p. 091006.
37. Barbarino, S., W.G. Dettmer, and M.I. Friswell. *Morphing trailing edges with shape memory alloy rods*. in *Proceedings of 21st international conference on adaptive structures and technologies (ICAST)*. 2010.
38. Olympio, K.R. and F. Gandhi, *Zero Poisson's Ratio Cellular Honeycombs for Flex Skins Undergoing One-Dimensional Morphing*. Journal of Intelligent Material Systems and Structures, 2010. **21**(17): p. 1737-1753.
39. Olympio, K.R. and F. Gandhi, *Flexible skins for morphing aircraft using cellular honeycomb cores*. Journal of intelligent material systems and structures, 2010. **21**(17): p. 1719-1735.
40. Bubert, E.A., et al., *Design and fabrication of a passive 1D morphing aircraft skin*. Journal of Intelligent Material Systems and Structures, 2010. **21**(17): p. 1699-1717.

41. Airoidi, A., et al., *Design and manufacturing of skins based on composite corrugated laminates for morphing aerodynamic surfaces*. Smart Materials and Structures, 2017. **26**(4): p. 045024.
42. Airoidi, A., et al., *Composite Corrugated Laminates for Morphing Applications*, in *Morphing Wing Technologies*. 2018, Elsevier. p. 247-276.
43. Bai, J., et al., *A corrugated flexible composite skin for morphing applications*. Composites Part B: Engineering, 2017. **131**: p. 134-143.
44. Dayyani, I., et al., *The mechanics of composite corrugated structures: A review with applications in morphing aircraft*. Composite Structures, 2015. **133**: p. 358-380.
45. Ermakova, A. and I. Dayyani, *Shape optimisation of composite corrugated morphing skins*. Composites Part B: Engineering, 2017. **115**: p. 87-101.
46. Gong, X., et al., *Variable stiffness corrugated composite structure with shape memory polymer for morphing skin applications*. Smart Materials and Structures, 2017. **26**(3): p. 035052.
47. Thill, C., et al., *Composite corrugated structures for morphing wing skin applications*. Smart Materials and Structures, 2010. **19**(12): p. 124009.
48. Thurnherr, C., et al., *Stiffness analysis of corrugated laminates under large deformation*. Composite Structures, 2017. **160**: p. 457-467.
49. Singh, K. and R.K. Kapania. *Optimal Design of Tow-Steered Composite Laminates with Curvilinear Stiffeners*. in *2018 AIAA/ASCE/AHS/ASC Structures, Structural Dynamics, and Materials Conference*. 2018.
50. Akhavan, H. and P. Ribeiro, *Geometrically non-linear periodic forced vibrations of imperfect laminates with curved fibres by the shooting method*. Composites Part B: Engineering, 2017. **109**: p. 286-296.
51. Bowen, C.R., et al., *Morphing and Shape Control using Unsymmetrical Composites*. Journal of Intelligent Material Systems and Structures, 2007. **18**(1): p. 89-98.
52. Passos, A. and M. Luersen, *Multiobjective optimization of laminated composite parts with curvilinear fibers using Kriging-based approaches*. Structural and Multidisciplinary Optimization, 2017: p. 1-13.

53. Chintapalli, S., et al., *The development of a preliminary structural design optimization method of an aircraft wing-box skin-stringer panels*. Aerospace Science and Technology, 2010. **14**(3): p. 188-198.
54. Choi, W.-h., J.-m. Kim, and G.-J. Park, *Comparison study of some commercial structural optimization software systems*. Structural and Multidisciplinary Optimization, 2016. **54**(3): p. 685-699.
55. Grihon, S., L. Krog, and D. Bassir, *Numerical optimization applied to structure sizing at AIRBUS: a multi-step process*. International Journal for Simulation and Multidisciplinary Design Optimization, 2009. **3**(4): p. 432-442.
56. Hansen, L.U. and P. Horst, *Multilevel optimization in aircraft structural design evaluation*. Computers & structures, 2008. **86**(1-2): p. 104-118.
57. Kroo, I., et al., *Multidisciplinary optimization methods for aircraft preliminary design*. AIAA paper, 1994. **4325**: p. 1994.
58. Moored, K.W. and H. Bart-Smith, *The Analysis of Tensegrity Structures for the Design of a Morphing Wing*. Journal of Applied Mechanics, 2006. **74**(4): p. 668-676.
59. Vitali, R., et al., *Structural optimization of a hat-stiffened panel using response surfaces*. Journal of aircraft, 2002. **39**(1): p. 158-166.
60. Bendsoe, M.P. and O. Sigmund, *Material interpolation schemes in topology optimization*. Archive of applied mechanics, 1999. **69**(9-10): p. 635-654.
61. Eschenauer, H.A. and N. Olhoff, *Topology optimization of continuum structures: A review\**. Applied Mechanics Reviews, 2001. **54**(4): p. 331-390.
62. Bendsoe, M.P. and O. Sigmund, *Topology optimization: theory, methods, and applications*. 2013: Springer Science & Business Media.
63. Bourell, D.L., D.W. Rosen, and M.C. Leu, *The roadmap for additive manufacturing and its impact*. 3D Printing and Additive Manufacturing, 2014. **1**(1): p. 6-9.
64. Guo, N. and M.C. Leu, *Additive manufacturing: technology, applications and research needs*. Frontiers of Mechanical Engineering, 2013. **8**(3): p. 215-243.
65. *Boeing to develop AM standardization*. 2018 [cited 2018 March 11]; Available from: <https://www.materialstoday.com/additive-manufacturing/news/boeing-to-develop-am-standardization/>.

66. *GE Additive appoints new CEO*. 2018 [cited 2018 March 11]; Available from: <https://www.materialstoday.com/additive-manufacturing/news/ge-additive-appoints-new-ceo/>.
67. Machi, V. *Defense Industry Moves Toward Multi-Material 3D Printing*. 2017 [cited 2018 March 11]; Available from: <http://www.nationaldefensemagazine.org/articles/2017/10/30/defense-industry-moves-toward-multi-material-3d-printing>.
68. Sigmund, O., *A 99 line topology optimization code written in Matlab*. Structural and multidisciplinary optimization, 2001. **21**(2): p. 120-127.
69. Logan, D.L., *A first course in the finite element method*. 2011: Cengage Learning.
70. Lee, E. and H.C. Gea, *A strain based topology optimization method for compliant mechanism design*. Structural and Multidisciplinary Optimization, 2014. **49**(2): p. 199-207.
71. Hvejsel, C.F. and E. Lund, *Material interpolation schemes for unified topology and multi-material optimization*. Structural and Multidisciplinary Optimization, 2011. **43**(6): p. 811-825.

# Appendix

## Appendix A-Finite Element Code

### Main FEM Code

```
function [U, FORCE] =
fem_smp_func(nelx, nely, z, v, E, FORCE, BC, NODE, ELEMENT, LtGMM, x, penal);
%Self-Coded Finite Element Code-Shawn M Parsons
%Inputs:
    %nelx-number of x elements
    %nely-number of y elements
    %z-thickness
    %v-poisson's ration
    %E-young's modulus
    %FORCE-column vector (2*number of nodes) of the force in each direction
at each node
    %BC-column vector of given boundary conditions
    %ELEMENT-reference of the element and nodes it contains
    %LtGMM-Local to Global Mapping Matrix
    %x-"Density" of each element (nely x nelx matrix)
    %penal-penalization factor
%-----

%% Import Data
    [numb_element, m] = size(ELEMENT);
    [numb_node, m] = size(NODE);
    [numb_BC, m] = size(BC);

%Setting Up Global Stiffness
    Global_K = sparse(2*numb_node, 2*numb_node);
    displacement = zeros(2*numb_node, 1);

%X for each element-Updating the Density from the Optimized Results
    x0 = 0;
    for i = 1:nely
```

```

        for j=1:nelx
            x_el(x0+j)=x(nely+1-i,j);
        end
        x0=nelx*i;
    end

%% Shape Functions & Global Stiffness Matrix Assemblage
    %Sort Element Coordinates
    for i=1:numb_element;
        for j=1:4
            coord(j,1)=NODE(ELEMENT(i,1+j),2); %x Column
            coord(j,2)=NODE(ELEMENT(i,1+j),3); %y Column
        end

        [K_element,~]=el_stiff( coord,E,v,x_el(i),penal,z );

    %Global Assemblage
        Global_K_temp=zeros(2*numb_node,2*numb_node);
        Global_K_temp([LtGMM(i,:),[LtGMM(i,:)])=K_element([1 2 3 4 5 6
7 8],[1 2 3 4 5 6 7 8]);
        Global_K=Global_K+Global_K_temp;
    end

%% Boundary Conditions/Sorting into Unknown Displacements/Unknown Forces
    %Creating an Index of whether or not there are boundary conditions at
    %each node in each direction
    U=zeros(2*numb_node,1);
    BC=sortrows(BC);%Ordered BC
    A=zeros(2*numb_node,1);
    for i=1:length(BC)
        A(BC(i))=1; %A=1 represents the boundary conditions or known
displacements
    end

```

```

    unknowndisp=find(A==0);
    [numbdisp,n]=size(unknowndisp);
    unknownforce=find(A==1);
    [numbforce,n]=size(unknownforce);
    order=[find(A==0);find(A==1)]; %Ordered based on known force/unknown
force or unknown displacement known displacement
    GKS=Global_K([order],[order]);

    %Setting Up Known and Unknown Force and Displacement Vectors
    U([unknownforce])=[BC(:,2)]; %in global order, added in known
displacements
    F([unknowndisp],:)=FORCE([unknowndisp]); %in global order, added in known
forces; don't think this is necessary

%%
% %Getting the relevant vectors
    N_star=GKS*U([order]);

% %Solving
    F_star=FORCE([order]);
    F_star=F_star([1:numbdisp]);
    U_soln(:,1)=GKS([1:numbdisp],[1:numbdisp])\ (F_star-
N_star([1:numbdisp]));
    F_soln=N_star([1+numbdisp:numbdisp+numbforce]);

%Adding Back in Globally
    U([unknowndisp])=U_soln;
    FSOLN=zeros(numb_node,1);
    FSOLN([order])=GKS*U([order]);
    FORCE([unknownforce])=FSOLN([unknownforce]);

end

```

## Function: Element Shape Functions

```
1
2
3 function [Nmat,Bmat] = shapefunc( coord );
4 %NOTE: This is set up to generate stiffness function of an order as seen
5 %below such that the numbering system should be set up to call in the same
6 %order (BLH, BRH,TRH,TLH)
7 %
8 % 4*-----*3
9 % | |
10 % | |
11 % 1*-----*2
12
13
14
15 x1=coord(1,1);x2=coord(2,1);x4=coord(4,1);x3=coord(3,1);
16 y1=coord(1,2);y2=coord(2,2);y4=coord(4,2);y3=coord(3,2);
17
18
19 syms x y
20 N1=(x-x2)*(y-y4)/((x1-x2)*(y1-y4));
21 N2=(x-x1)*(y-y3)/((x2-x1)*(y2-y3));
22 N3=(x-x4)*(y-y2)/((x3-x4)*(y3-y2));
23 N4=(x-x3)*(y-y1)/((x4-x3)*(y4-y1));
24 Nmat=[N1,N2,N3,N4];
25 Bmat=[diff(N1,x),0,diff(N2,x),0,diff(N3,x),0,diff(N4,x),0;0,diff(N1,y),0,diff(N2,y),0,diff(N3,y),0,diff(N4,y),0];
26 end
27
28
29
30
31
32
```

## Function: Element Stiffness

```
1 function [K_element,B]=el_stiff( coord,E,v,x,penal,z )
2 %% Shape Functions & Global Stiffness Matrix Assemblage
3
4 %ShapeFunction
```

```

4         [N,B]= shapefunc( coord );
5
6         %Calculation of Element Constitutive Relations Matrix
7         D=(E/(1-(v^2)))*[1 v 0; v 1 0; 0 0, .5*(1-v)];
8
9         %Calculate Stiffness Matrix for each Element using Gaussian Quadrature
10        %Integration
11        K_prime=[B']*[D]*[B];
12        K=matlabFunction(K_prime); %Transform from Symbolic
13        K_element=(x^penal)*z*gaussquad(K,coord(1,1),coord(2,1),coord(1,2),coord(3,1));
14        B=matlabFunction(B);
15
16    end
17
18
19

```

## Function: Gauss Quadrature

```

1    function [soln] = gaussquad(f,a,b,c,d);
2    %Approximates Integral of a function using Gauss Quadrature of two points
3    %test inputs to debug
4    %f=@(x,y) x*y; test=gaussquad(f,0,5,3,7);
5    x_i=[0.5773502691896257,-0.5773502691896257];
6    c_i=[1,1];
7
8    x_x=.5*((b-a)*x_i+(b+a)*[1,1]);
9    c_x=.5*(b-a)*c_i;
10   x_y=.5*((d-c)*x_i+(d+c)*[1,1]);
11   c_y=.5*(d-c)*c_i;
12
13   sum=0;

```

```

12
13
14 for i=1:2
15     for j=1:2
16         sum=sum+c_x(i)*c_y(j)*f(x_x(i),x_y(j));
17     end
18 end
19 soln=sum;
20
21 end
22
23
24

```

## FEM-Initial Processing and Mesh Generation

```

1 function [NODE,ELEMENT,FORCE,LtGMM,BC] = fem_processing(xdim,ydim,z,elsz,FORCE_IN,
2 %% In-Processing
3     %Create Node and Elements
4         nelx=xdim/elsz;
5         nely=ydim/elsz;
6         numb_node=(nelx+1)*(nely+1);
7         NODE=zeros(numb_node,4);
8         ELEMENT=zeros(nelx*nely,7);
9         FORCE=zeros(2*(nelx+1)*(nely+1),1);
10        numb_element=nelx*nely;
11
12        %Creating Nodes
13        x0=0;
14        for i= 1:(nely+1)
15            for j= 1:(nelx+1)
16                NODE_num= x0+j;
17                NODE(NODE_num,1)=NODE_num;
18                NODE(NODE_num,2)=(j-1)*elsz;

```

```

16         NODE(NODE_num, 3) = (i-1) * elsz;
17         NODE(NODE_num, 4) = z;
18     end
19     x0 = i * (nelx+1);
20     end
21     %Creating Elements
22     x0 = 0;
23     y0 = 0;
24     for i = 1:nely
25         for j = 1:nelx
26             BLH = x0 + j;
27             BRH = x0 + j + 1;
28             TLH = BLH + (nelx+1);
29             TRH = BRH + (nelx+1);
30             ELEMENT(y0+j, 1) = y0+j;
31             ELEMENT(y0+j, 2) = BLH;
32             ELEMENT(y0+j, 3) = BRH;
33             ELEMENT(y0+j, 4) = TRH;
34             ELEMENT(y0+j, 5) = TLH;
35             ELEMENT(y0+j, 6) = v;
36             ELEMENT(y0+j, 7) = E;
37         end
38     end
39     x0 = (nelx+1) * i;
40     y0 = nelx * i;
41     end
42     %Mapping of Grid
43     for k = 1:numb_element
44         for l = 1:4
45             xx(l) = NODE(ELEMENT(k, l+1), 2);
46             y(l) = NODE(ELEMENT(k, l+1), 3);
47         end
48     end
49     scatter(xx, y)
50     hold on

```

```

47     line(xx,y)
48     hold on
49
50     for l=1:4
51         text(xx(1),y(1),num2str(ELEMENT(k,l+1)),'Color','blue','FontSize',18)
52     end
53
54     avgx=.5*(xx(2)-xx(1))+xx(1);
55     avgy=.5*(y(4)-y(1))+y(1);
56
57     text(avgx,avgy,num2str(ELEMENT(k,1)),'Color','red','FontSize',32);
58     end
59     figure
60
61     % Adding Forces in
62     [szF,temp]=size(FORCE_IN);
63     for i=1:szF
64         k=find(NODE(:,2)==FORCE_IN(i,1));
65         tempind=NODE([k,:]);
66         nodeloc=find(tempind(:,3)==FORCE_IN(i,2));
67         nodeloc=tempind(nodeloc,1);
68         if FORCE_IN(i,3)==1
69             FORCE(2*nodeloc-1,1)=FORCE_IN(i,4);
70         elseif FORCE_IN(i,3)==2
71             FORCE(2*nodeloc,1)=FORCE_IN(i,4);
72         end
73     end
74
75     % Boundary Condition Generater
76     %BC_IN=[all (1) or single value (2), x(1) or y(2) if all/xcoord if single,va
77     [szBC,temp]=size(BC_IN);
78     ind_BC=1;
79     if szBC==0
80         BC=[];

```

```

78         end
79     for i=1:szBC
80
81         %All at this boundary condition
82         if BC_IN(i,1) ==1
83             %All at X Location
84             if BC_IN(i,2) ==1
85                 %Find all the nodes that have this x coordinate
86                 k=find(NODE(:,2)==BC_IN(i,3));
87                 for j=1:length(k)
88                     if BC_IN(i,4)==1 %if it is a u displacement value
89                         BC(ind_BC,1)=2*NODE(k(j),1)-1; %location in global sys
90                     elseif BC_IN(i,4)==2 %if it is a v displacement value
91                         BC(ind_BC,1)=2*NODE(k(j),1); %location in global sy
92                     end
93                     BC(ind_BC,2)=BC_IN(i,5); %actual value
94                     ind_BC=ind_BC+1;
95                 end
96             %All at Y Location
97             elseif BC_IN(i,2) ==2
98                 %Find all the nodes that have this y coordinate
99                 k=find(NODE(:,3)==BC_IN(i,3));
100                for j=1:length(k)
101                    if BC_IN(i,4)==1 %if it is a u displacement value
102                        BC(ind_BC,1)=2*NODE(k(j),1)-1; %location in global sys
103                    elseif BC_IN(i,4)==2 %if it is a v displacement value
104                        BC(ind_BC,1)=2*NODE(k(j),1); %location in global sy
105                    end
106                    BC(ind_BC,2)=BC_IN(i,5); %actual value
107                    ind_BC=ind_BC+1;
108                end
109            end
110        end
111        elseif BC_IN(i,1) ==2 %for a single boundary condition
112            k=find(NODE(:,2)==BC_IN(i,2)); %finding the matching x coordinate
113            for j=1:length(k)
114                if NODE(k(j),3)==BC_IN(i,3) %checking to see if it is the proper
115                    BC(ind_BC,1)=2*NODE(k(j),1);

```

```

109         if BC_IN(i,4)==1 %if it is a u displacement value
110             BC(ind_BC,1)=2*NODE(k(j),1)-1;%location in global system
111         elseif BC_IN(i,4)==2 %if it is a v displacement value
112             BC(ind_BC,1)=2*NODE(k(j),1);%location in global system
113         end
114         BC(ind_BC,2)=BC_IN(i,5);%actual value
115         ind_BC=ind_BC+1;
116         break
117     end
118
119     break
120 end
121
122
123 %Sizing of Grid Elements/Nodes
124 [numb_element,m]=size(ELEMENT);
125 [numb_node,m]=size(NODE);
126
127
128 %Local-to-Global-Mapping-Matrix (LtGMM)
129 LtGMM=zeros(numb_element,8);
130 for i=1:numb_element
131     for j=1:4
132         LtGMM(i,2*j-1)=(2*ELEMENT(i,j+1))-1;
133         LtGMM(i,2*j)=2*ELEMENT(i,j+1);
134     end
135 end
136 end

```

## Appendix B-Topology Optimization

## Single Load Case Topology Optimization

```
%% A 99 LINE TOPOLOGY OPTIMIZATION CODE BY OLE SIGMUND, JANUARY 2000 %%
%% CODE MODIFIED FOR INCREASED SPEED, September 2002, BY OLE SIGMUND %%

%Shawn M. Parsons
%Modified 99 Line Topology Optimization CODE

function [x, loop, objfunc, vol] =
top_smp(xdim, ydim, v, E, FORCE, BC, NODE, ELEMENT, LtGMM, volfrac, penal, rmin, z, elsz, C
ompVal);

% INITIALIZE
    nelx=xdim/elsz;
    nely=ydim/elsz;
    x(1:nely,1:nelx) = volfrac;
    loop = 0;
    change = 1.;
    c=0;

%%
% START ITERATION
while (change > .001 & loop < 50)
    loop = loop + 1;
    xold = x;

% FE-ANALYSIS
    [U, F] = fem_smp_func(nelx, nely, z, v, E, FORCE, BC, NODE, ELEMENT, LtGMM, x, penal);

% OBJECTIVE FUNCTION AND SENSITIVITY ANALYSIS
    c = 0.;
    x0=0;
    c_s1=0;
```

```

c_s2=0;
c_s3=0;
c_s4=0;
c_s5=0;
c_s6=0;
c_s7=0;
c_s8=0;

for ely = 1:nely
    for elx = 1:nelx

        %Location Index for Element
        disp_el=LtGMM(x0+elx,:);
        gamma_ind=disp_el(2:2:end)/2;

        %Values for Element
        Ue=U(disp_el,1);
        x_el=x(nely+1-ely,elx);

        for j=1:4
            coord(j,1)=NODE(ELEMENT(x0+elx,1+j),2);    %x Column
            coord(j,2)=NODE(ELEMENT(x0+elx,1+j),3);    %y Column
        end

        %Original Element
        [KE,B]=el_stiff( coord,E,v,1,1,z);
        [gausscoord]=gaussquad_points(coord(1,1),coord(2,1),coord(1,2),coord
(3,2));
        effective_strain=(Ue'*KE*Ue)/E;

        for j=1:4
            B_el_gauss=B(gausscoord(j,1),gausscoord(j,2));
            B_el_node=B(coord(j,1),coord(j,2));
            strain_temp_node=B_el_node*Ue;
            strain_temp_gauss=B_el_gauss*Ue;

```

```

%All 3 Gauss Strains Only
s1(3*j-2,1)=strain_temp_gauss(1);
s1(3*j-1,1)=strain_temp_gauss(2);
s1(3*j,1)=strain_temp_gauss(3);

```

```

%All 3 Nodal Strains Only
s2(3*j-2,1)=strain_temp_node(1);
s2(3*j-1,1)=strain_temp_node(2);
s2(3*j,1)=strain_temp_node(3);

```

```

%Combined Node and Gauss Strains
s3(6*j-5,1)=strain_temp_gauss(1);
s3(6*j-4,1)=strain_temp_gauss(2);
s3(6*j-3,1)=strain_temp_gauss(3);
s3(6*j-2,1)=strain_temp_node(1);
s3(6*j-1,1)=strain_temp_node(2);
s3(6*j,1)=strain_temp_node(3);

```

```

%x and y strains only
s4(4*j-3,1)=strain_temp_gauss(1);
s4(4*j-2,1)=strain_temp_gauss(2);
s4(4*j-1,1)=strain_temp_node(1);
s4(4*j,1)=strain_temp_node(2);

```

```

%Shear Strain ONLY
s5(2*j-1,1)=strain_temp_gauss(3);
s5(2*j,1)=strain_temp_node(3);

```

```

%Principal Strain (Gauss and Nodal)
s6(4*j-3,1)=.5*(strain_temp_gauss(1) +strain_temp_gauss(2))+
sqrt((strain_temp_gauss(1) - strain_temp_gauss(2))^2+ strain_temp_gauss(3)^2);

s6(4*j-2,1)=.5*(strain_temp_gauss(1)+strain_temp_gauss(2))-
sqrt((strain_temp_gauss(1) -strain_temp_gauss(2))^2 +strain_temp_gauss(3)^2);

```

```

s6(4*j-1,1)=.5*(strain_temp_node(1)+strain_temp_node(2))+
sqrt((strain_temp_node(1)+ strain_temp_node(2))^2+strain_temp_node(3)^2);

s6(4*j,1)=.5*(strain_temp_node(1)+strain_temp_node(2))-
sqrt((strain_temp_node(1)+strain_temp_node(2))^2+strain_temp_node(3)^2);

%Principal + Max Shear (Gauss Points)
s7(3*j-2,1)=.5*(strain_temp_gauss(1)+ strain_temp_gauss(2))+
sqrt((strain_temp_gauss(1)-strain_temp_gauss(2))^2+ strain_temp_gauss(3)^2);

s7(3*j-1,1)=.5*(strain_temp_gauss(1)+strain_temp_gauss(2))-
sqrt((strain_temp_gauss(1)-strain_temp_gauss(2))^2+ strain_temp_gauss(3)^2);

s7(3*j,1)=sqrt((strain_temp_gauss(1)+strain_temp_gauss(2))^2+
strain_temp_gauss(3)^2);

end

obj_el_s1=s1'*s1;
obj_el_s2=s2'*s2;
obj_el_s3=s3'*s3;
obj_el_s4=s4'*s4;
obj_el_s5=s5'*s5;
obj_el_s6=s6'*s6;
obj_el_s7=s7'*s7;
%obj_el_s8=s8'*s8;
obj_el_s8=effective_strain;

%Compliance

c_s1=c_s1+obj_el_s1;
c_s2=c_s2+obj_el_s2;
c_s3=c_s3+obj_el_s3;
c_s4=c_s4+obj_el_s4;
c_s5=c_s5+obj_el_s5;

```

```

c_s6=c_s6+obj_el_s6;
c_s7=c_s7+obj_el_s7;
c_s8=c_s8+obj_el_s8;

dc_s1(nely+1-ely,elx) =( -penal*x_el^(penal-1))*obj_el_s1;
dc_s2(nely+1-ely,elx) =( -penal*x_el^(penal-1))*obj_el_s2;
dc_s3(nely+1-ely,elx) =( -penal*x_el^(penal-1))*obj_el_s3;
dc_s4(nely+1-ely,elx) =( -penal*x_el^(penal-1))*obj_el_s4;
dc_s5(nely+1-ely,elx) =( -penal*x_el^(penal-1))*obj_el_s5;
dc_s6(nely+1-ely,elx) =( -penal*x_el^(penal-1))*obj_el_s6;
dc_s7(nely+1-ely,elx) =( -penal*x_el^(penal-1))*obj_el_s7;
dc_s8(nely+1-ely,elx) =( -penal*x_el^(penal-1))*obj_el_s8;

c_s1_el(nely+1-ely,elx)=obj_el_s1;
c_s2_el(nely+1-ely,elx)=obj_el_s2;
c_s3_el(nely+1-ely,elx)=obj_el_s3;
c_s4_el(nely+1-ely,elx)=obj_el_s4;
c_s5_el(nely+1-ely,elx)=obj_el_s5;
c_s6_el(nely+1-ely,elx)=obj_el_s6;
c_s7_el(nely+1-ely,elx)=obj_el_s7;
c_s8_el(nely+1-ely,elx)=obj_el_s8;

end
x0=(ely)*nelx;
end

objfunc(loop,1)=c_s1;
objfunc(loop,2)=c_s2;
objfunc(loop,3)=c_s3;
objfunc(loop,4)=c_s4;
objfunc(loop,5)=c_s5;
objfunc(loop,6)=c_s6;
objfunc(loop,7)=c_s7;
objfunc(loop,8)=c_s8;

```

```

if CompVal==1
    c=c_s1;
    dc=dc_s1;
elseif CompVal==2
    c=c_s2;
    dc=dc_s2;
elseif CompVal==3
    c=c_s3;
    dc=dc_s3;
elseif CompVal==4
    c=c_s4;
    dc=dc_s4;
elseif CompVal==5
    c=c_s5;
    dc=dc_s5;
elseif CompVal==6
    c=c_s6;
    dc=dc_s6;
elseif CompVal==7
    c=c_s7;
    dc=dc_s7;
elseif CompVal==8
    c=c_s8;
    dc=dc_s8;
end

% FILTERING OF SENSITIVITIES
[dc] = check(nelx,nely,rmin,x,dc);
% DESIGN UPDATE BY THE OPTIMALITY CRITERIA METHOD
[x] = OC(nelx,nely,x,volfrac,dc);
% PRINT RESULTS
change = max(max(abs(x-xold)));
disp([' It.: ' sprintf('%4i',loop) ' Obj.: ' sprintf('%10.4f',c) ...
      ' Vol.: ' sprintf('%6.3f',sum(sum(x))/(nelx*nely)) ...
      ' ch.: ' sprintf('%6.3f',change )])
vol(loop,1)=sum(sum(x))/(nelx*nely);
% PLOT DENSITIES
colormap(gray);

```

```

        imagesc(-x); axis tight; axis off;pause(1e-6);colorbar;
end

%%%%%%%%%%%%%%%%%%%%%%%%%%%%%%%%%%%%%%%%%%%%%%%%%%%%%%%%%%%%%%%%%%%%%%%%%% OPTIMALITY CRITERIA UPDATE %%%%%%%%%%%%%%%%%%%%%%%%%%%%%%%%%%%%%%%%%%%%%%%%%%%%%%%%%%%%%%%%%%%%%%%%%%%
function [xnew]=OC(nelx,nely,x,volfrac,dc)
l1 = 0; l2 =100000; move = 0.2;
while (l2-l1)/(l2+l1) > 1e-4 & l2> 1e-40
    lmid = 0.5*(l2+l1);
    xnew = max(0.001,max(x-move,min(1.,min(x+move,x.*sqrt(-dc./lmid)))));
    xnew      =      max(0.001,max(x-move,min(1.,min(x+move,x.*(max(1e-10,-
dc./lmid)).^0.3))));

    if sum(sum(xnew)) - volfrac*nelx*nely > 0;
        l1 = lmid;

    else
        l2 = lmid;

    end
end
end

%%%%%%%%%%%%%%%%%%%%%%%%%%%%%%%%%%%%%%%%%%%%%%%%%%%%%%%%%%%%%%%%%%%%%%%%%% MESH-INDEPENDENCY FILTER %%%%%%%%%%%%%%%%%%%%%%%%%%%%%%%%%%%%%%%%%%%%%%%%%%%%%%%%%%%%%%%%%%%%%%%%%%%
function [dcn]=check(nelx,nely,rmin,x,dc)
dcn=zeros(nely,nelx);
for i = 1:nelx
    for j = 1:nely
        sum=0.0;
        for k = max(i-floor(rmin),1):min(i+floor(rmin),nelx)
            for l = max(j-floor(rmin),1):min(j+floor(rmin),nely)
                fac = rmin-sqrt((i-k)^2+(j-l)^2);
                sum = sum+max(0,fac);
                dcn(j,i) = dcn(j,i) + max(0,fac)*x(l,k)*dc(l,k);
            end
        end
        dcn(j,i) = dcn(j,i)/(x(j,i)*sum);
    end
end
end
end

```

```

%%
%-----
%%%%%%%%%%%%%%%%%%%%%%%%%%%%%%%%%%%%%%%%%%%%%%%%%%%%%%%%%%%%%%%%%%%%%%%%
%
% This Matlab code was written by Ole Sigmund, Department of Solid      %
% Mechanics, Technical University of Denmark, DK-2800 Lyngby, Denmark.  %
% Please sent your comments to the author: sigmund@fam.dtu.dk          %
%
%
% The code is intended for educational purposes and theoretical details  %
% are discussed in the paper                                           %
% "A 99 line topology optimization code written in Matlab"            %
% by Ole Sigmund (2001), Structural and Multidisciplinary Optimization, %
% Vol 21, pp. 120--127.                                              %
%
%
% The code as well as a postscript version of the paper can be        %
% downloaded from the web-site: http://www.topopt.dtu.dk %
%
%
% Disclaimer:                                                            %
% The author reserves all rights but does not guaranty that the code is %
% free from errors. Furthermore, he shall not be liable in any event   %
% caused by the use of the program.                                    %
%%%%%%%%%%%%%%%%%%%%%%%%%%%%%%%%%%%%%%%%%%%%%%%%%%%%%%%%%%%%%%%%%%%%%%%%
%

```

## Multiple Load Case Topology Optimization

```

%%% A 99 LINE TOPOLOGY OPTIMIZATION CODE BY OLE SIGMUND, JANUARY 2000 %%%
%%% CODE MODIFIED FOR INCREASED SPEED, September 2002, BY OLE SIGMUND %%%

```

```

%Shawn M. Parsons
%Modified 99 Line Topology Optimization CODE

```

```

function[x,loop,objfunc,vol]=
top_smp_ML(xdim,ydim,v,E,FORCE1,BC1,FORCE2,BC2,NODE,ELEMENT,LtGMM,volfrac,penal,rmin,z,elsz);

% INITIALIZE
nelx=xdim/elsz;
nely=ydim/elsz;
x(1:nely,1:nelx) = volfrac;
loop = 0;
change = 1.;

%%
% START ITERATION
while (change > .001 & loop < 50 )
loop = loop + 1;
xold = x;

c_disp=0;
c2star=0;
c1star=0;
c=0;
x0=0;
% FE-ANALYSIS
[U1,F1]
=fem_smp_func(nelx,nely,z,v,E,FORCE1,BC1,NODE,ELEMENT,LtGMM,x,penal);
[U2,F2]
=fem_smp_func(nelx,nely,z,v,E,FORCE2,BC2,NODE,ELEMENT,LtGMM,x,penal);

% OBJECTIVE FUNCTION AND SENSITIVITY ANALYSIS

```

```

for ely = 1:nely
    for elx = 1:nelx

        %Location Index for Element
        disp_el=LtGMM(x0+elx,:);

        %Values for Element
        Ue1=U1(disp_el,1);
        Ue2=U2(disp_el,1);
        x_el=x(nely+1-ely,elx);

        for j=1:4
            coord(j,1)=NODE(ELEMENT(x0+elx,1+j),2);    %x Column
            coord(j,2)=NODE(ELEMENT(x0+elx,1+j),3);

        end

        [KE,B]=el_stiff( coord,E,v,1,1,z);
        [gausscoord]
gaussquad_points(coord(1,1),coord(2,1),coord(1,2),coord(3,2));

        for j=1:4
            %Load Case 1
            B_el_gauss=B(gausscoord(j,1),gausscoord(j,2));
            B_el_node=B(coord(j,1),coord(j,2));
            strain_temp_node=B_el_node*Ue1;
            strain_temp_gauss=B_el_gauss*Ue1;

            %Combined Node and Gauss Strains
            s1(6*j-5,1)=strain_temp_gauss(1);
            s1(6*j-4,1)=strain_temp_gauss(2);
            s1(6*j-3,1)=strain_temp_gauss(3);
            %s1(6*j-3,1)=0;
            s1(6*j-2,1)=strain_temp_node(1);
            s1(6*j-1,1)=strain_temp_node(2);
            s1(6*j,1)=strain_temp_node(3);

```

```

    %s1(6*j,1)=0;

    %Load Case 2
    strain_temp_node=B_el_node*Ue2;
    strain_temp_gauss=B_el_gauss*Ue2;

    %Combined Node and Gauss Strains
    s2(6*j-5,1)=strain_temp_gauss(1);
    s2(6*j-4,1)=strain_temp_gauss(2);
    s2(6*j-3,1)=strain_temp_gauss(3);
    s2(6*j-3,1)=0;
    s2(6*j-2,1)=strain_temp_node(1);
    s2(6*j-1,1)=strain_temp_node(2);
    s2(6*j,1)=strain_temp_node(3);
    s2(6*j,1)=0;

end

%Compliance

c=c+s1'*s1+s2'*s2;
dc_s1(nely+1-ely,elx) =(-penal*x_el^(penal-1))*(s1'*s1);
dc_s2(nely+1-ely,elx) =(-penal*x_el^(penal-1))*(s2'*s2);
dc(nely+1-ely,elx)=dc_s1(nely+1-ely,elx)+dc_s2(nely+1-ely,elx);

end
x0=(ely)*nelx;
end
objfunc(loop,1)=c;
% FILTERING OF SENSITIVITIES
[dc] = check(nelx,nely,rmin,x,dc);

```

```

% DESIGN UPDATE BY THE OPTIMALITY CRITERIA METHOD
[x] = OC(nelx,nely,x,volfrac,dc);
% PRINT RESULTS
change = max(max(abs(x-xold)));
disp([' It.: ' sprintf('%4i',loop) ' Obj.: ' sprintf('%10.4f',c) ...
      ' Vol.: ' sprintf('%6.3f',sum(sum(x))/(nelx*nely)) ...
      ' ch.: ' sprintf('%6.3f',change )])
vol(loop,1)=sum(sum(x))/(nelx*nely);
% PLOT DENSITIES
colormap(gray);
imagesc(-x); axis tight; axis off;pause(1e-6);colorbar;
end

%%%%%%%%%%%%%%%%%%%%%%%%%%%%%%%%%%%%%%%%%%%%%%%%%%%%%%%%%%%%%%%%%%%%%%%%%%%%%%
function [xnew]=OC(nelx,nely,x,volfrac,dc)
l1 = 0; l2 =100000000; move = 0.15;
while (l2-l1 > 1e-4)
    lmid = 0.5*(l2+l1);
    xnew = max(0.001,max(x-move,min(1.,min(x+move,x.*sqrt(-dc./lmid)))));

    if sum(sum(xnew)) - volfrac*nelx*nely > 0;
        l1 = lmid;

    else
        l2 = lmid;

    end

end

%%%%%%%%%%%%%%%%%%%%%%%%%%%%%%%%%%%%%%%%%%%%%%%%%%%%%%%%%%%%%%%%%%%%%%%%%%%%%%
function [dcn]=check(nelx,nely,rmin,x,dc)
dcn=zeros(nely,nelx);
for i = 1:nelx
    for j = 1:nely
        sum=0.0;
        for k = max(i-floor(rmin),1):min(i+floor(rmin),nelx)
            for l = max(j-floor(rmin),1):min(j+floor(rmin),nely)

```

```

        fac = rmin-sqrt((i-k)^2+(j-1)^2);
        sum = sum+max(0,fac);
        dcn(j,i) = dcn(j,i) + max(0,fac)*x(l,k)*dc(l,k);
    end
end
dcn(j,i) = dcn(j,i)/(x(j,i)*sum);
end
end
%%

%-----

%%%%%%%%%%%%%%%%%%%%%%%%%%%%%%%%%%%%%%%%%%%%%%%%%%%%%%%%%%%%%%%%%%%%%%%%

%
% This Matlab code was written by Ole Sigmund, Department of Solid      %
% Mechanics, Technical University of Denmark, DK-2800 Lyngby, Denmark.  %
% Please sent your comments to the author: sigmund@fam.dtu.dk          %
%
%
% The code is intended for educational purposes and theoretical details  %
% are discussed in the paper                                           %
% "A 99 line topology optimization code written in Matlab"             %
% by Ole Sigmund (2001), Structural and Multidisciplinary Optimization, %
% Vol 21, pp. 120--127.                                               %
%
%
% The code as well as a postscript version of the paper can be        %
% downloaded from the web-site: http://www.topopt.dtu.dk %
%
%
% Disclaimer:                                                            %
% The author reserves all rights but does not guaranty that the code is %
% free from errors. Furthermore, he shall not be liable in any event   %
% caused by the use of the program.                                     %
%%%%%%%%%%%%%%%%%%%%%%%%%%%%%%%%%%%%%%%%%%%%%%%%%%%%%%%%%%%%%%%%%%%%%%%%

%

```